Experiments on a Hybrid Composite Beam for Bridge Applications

Stephen Van Nosdall

Thesis submitted to the faculty of the Virginia Polytechnic Institute and State University
in partial fulfillment of the requirements for the degree of

Master of Science
In
Civil Engineering

Cristopher D. Moen, Committee Chair
Finley A. Charney
Carin L. Roberts-Wollmann

May 6, 2013
Blacksburg, VA

Keywords: Hybrid-Composite Beam, FRP, Force Distribution

Experiments on a Hybrid Composite Beam for Bridge Applications

Stephen Van Nosdall

ABSTRACT

This thesis details a study of the structural behavior of Hybrid-Composite Beams (HCB) consisting of a fiber reinforced polymer (FRP) shell with a concrete arch tied with steel prestressing strands. The HCB offers advantages in life cycle costs through reduced transportation weight and increased corrosion resistance. By better understanding the system behavior, the proportion of load in each component can be determined, and each component can be designed for the appropriate forces. A long term outcome of this research will be a general structural analysis framework that can be used by DOTs to design HCBs as rapidly constructible bridge components. This study focuses on identifying the load paths and load sharing between the arch and FRP shell.

Testing was performed by applying point loads on simple span beams (before placing the bridge deck) and a three beam skewed composite bridge system. Curvature from strain data is used to find internal bending forces, and the proportion of load within the arch is found. Additionally, a stress integration method is used to confirm the internal force contributions. The tied arch carries about 80% of the total load for the non-composite case without a bridge deck. When composite with a bridge deck, the arch has a minimal contribution to the HCB stiffness and strength as it is below the neutral axis. For this composite case the FRP shell and prestressing strands resist about 85% of the applied load while the bridge deck carries the remaining 15% to the end diaphragms and bearings.

Acknowledgements

I'd like to thank my committee members, Dr. Moen, Dr. Wollmann, and Dr. Charney for making sure I got through the thesis process and made something that would be helpful to the structural engineering community. I could not have finished without their guidance and, more importantly, their confidence in me. I also owe a great deal of thanks to Dr. Cousins and Dr. Leon for advice on testing, and editing my manuscript. All of my professors here at Virginia Tech have been wonderful as well, and have given me the skills I need to be a great structural engineer. At the lab Brett Farmer, Dennis Huffman, and Dave Mokarem were essential for helping to prepare the set-up and give advice on the tests performed on the beams. Mike Zicko and John Hillman of the HCBridge company have also given me a lot of help with any inquiries we had about the beams. I'm happy to have worked on a project that is so different and that I love to tell people about so much, and wish them luck in future projects. I would have never made it here without my amazing professors at Bucknell University either, particularly Dr. Buonopane, Dr. Salyards, and Dr. Ziemian.

Getting the tests completed was a real team effort between myself, Sasha Bajzak, Maggie Mascaro, and our amazing leader Shainur Ahsan. They were all great partners and even greater friends. The help from everyone else at the lab for our deck placement and other intensive construction tasks is also greatly appreciated.

I could not have possibly kept going without the great friends I have made here in Blacksburg. Whether it was help on schoolwork, weekend trips, playing overly complicated board games, or encouraging me to overindulge on steak on a weekly basis, they have made Blacksburg a home. In particular, thank you Brad, Eric, Alison, Doug, Hannah, Charles, John, Kevin, Megan, Frank, Nora, Luc, Sam, Jon, Erin, Jordan, Dillenbeck, Paul, Carmen, Vince, Luke, and Christine. You guys rock, and have helped me more than you can ever imagine. While these people made Blacksburg great, Dan Treppel always made sure I remembered I had to graduate eventually, and has continued to be a great friend, and I've had plenty of support from Becky, Sidney, Jasna and Justin.

On the homefront, my entire extended family has been very supportive of all my academic efforts. My parents, Tom and Donna, and sisters, Becky and Sarah, have seen much less of me since I came down here, but have always sent their love and encouragement.

Professors, friends, and family- I am very blessed to have you all!

Table of Contents

Appendices

List of Tables

List of Figures

Attribution

The manuscript appearing as Chapter 3, "Experiments on a Hybrid-Composite Beam for Bridge Applications" was co-authored with Dr. Cristopher Moen, Dr. Carin Roberts-Wollmann, and Dr. Thomas Cousins. It was originally presented at the 92nd Annual Meeting of the Transportation Research Board, January 2013, Washington, D.C., and accepted for publication in the 2013 series of the *Transportation Research Record: Journal of the Transportation Research Board* (forthcoming). This material is being reproduced with permission of the Transportation Research Board. This does not imply endorsement by the Transportation Research Board of any product, method, practice, or policy.

1 Introduction

This research investigates the distribution of forces among the components of a relatively new hybrid-composite beam. As the country's infrastructure continues to age new alternatives to traditional steel and concrete bridge girders are emerging. The hybrid-composite beam created by John Hillman uses glass fiber reinforced polymers in conjunction with steel prestressing strands and a concrete arch in a system. This beam has several advantages over traditional girders, including a lighter shipping weight, faster construction, and increased corrosion resistance. While installations have already been made in several states, refinements in the design process are still possible and can lead to wider usage of the member. This research examines the load path through the beam to better understand its behavior and improve the design process.

1.1 Hillman Hybrid-Composite Beam

The Hybrid-Composite Beam (HCB) examined in this study contains three main structural components: a glass fiber reinforced polymer (FRP) box girder that acts as an external shell, a concrete arch providing compression forces, and steel prestressing strands providing tension reinforcement. These parts can be seen in Figure 1-1.

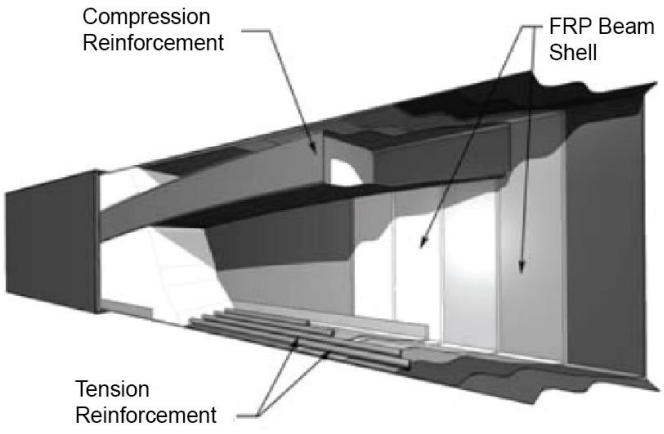

Figure 1-1 Internal View with Three Main Components of the HCB (Hillman, 2008)

The FRP box girder that acts as an external shell for the beam, seen in Figure 1-2, uses layers of glass fibers infused into a vinylester resin matrix to create a box girder. The shell is constructed out of two separate pieces; the main piece contains the bottom flange and two webs, while the top is a separately formed lid that also includes "wing flanges." The main piece also contains the steel prestressing strands, a foam material and FRP cross-ties. The steel strands are infused in the bottom flange's resin matrix, and will be further discussed below. Foam fills the shell's interior, with space cut out to be later filled with the concrete that forms the arch. Strips of FRP are also placed above the bottom layer of foam that connect the FRP webs to increase the shell stiffness during the placement of the arch. Finally, there are additional layers of FRP surrounding the conduit at midspan to aid the shell during arch placement. The lid covers the box as well as containing a "wing flange" on either side of the beam's main body. These flanges contribute to the shell stiffness and also act as stay-in-place formwork for the placement of a concrete deck.

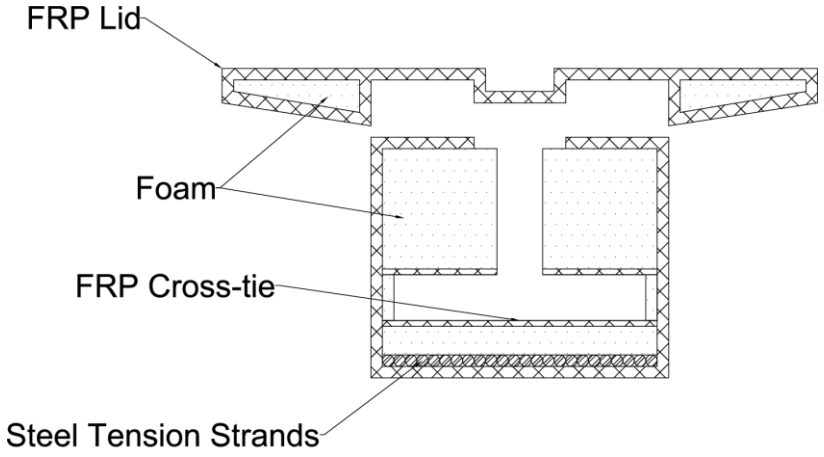

Figure 1-2 FRP Cross Section

The compression forces in the beam are provided by a parabolic concrete arch formed with self-consolidating concrete. At either end of the beam the concrete forms a block used for anchoring the tension reinforcement. A "shear fin" of concrete extends from the top of the arch to

the top of the beam, containing mild reinforcing steel used as shear connectors for composite action with a deck. These pieces of reinforcing steel are tied on to prestressing strands in the center of the arch. A representative arch cross-section can be seen in Figure 1-3. The arch can be placed either in the field or before shipment of the beams.

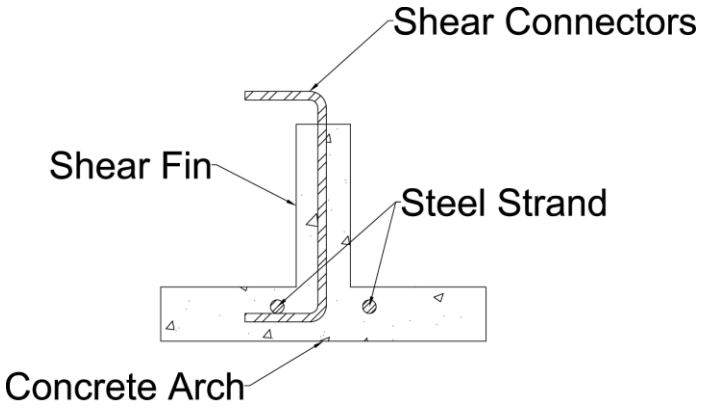

Figure 1-3 Concrete Arch Cross-Section

The tension reinforcement is provided by steel prestressing strands infused in the bottom FRP flange. These strands have no prestressing force, but extend into the blocks at the end of the beam, creating a tied arch system. A view of the end of the beam can be seen in Figure 1-4, and Figure 1-5 shows a cross section view with all components of the assembled beam.

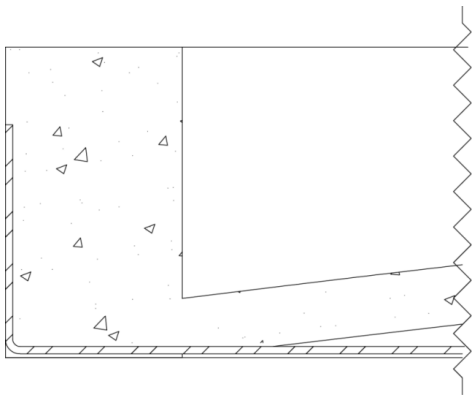

Figure 1-4 Detail View of Beam End

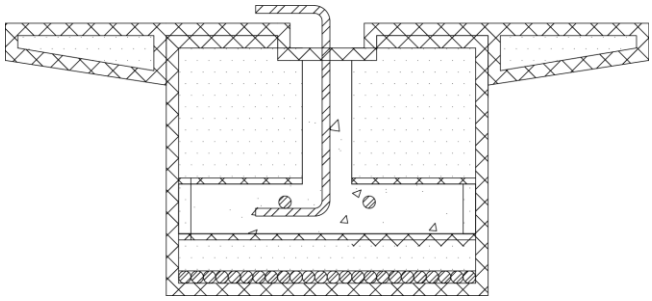

Figure 1-5 Fully Assembled Beam Cross-Section

1.2 Construction Process

Fabrication of the HCB shells is performed by Harbor Technologies in Brunswick, ME. Layers of fiberglass and the steel strands are laid out within a mold. The foam pieces are then placed within the mold, with an air filled bag ensuring that the space needed to pour the arch remains empty. After both the main piece and lid have been formed they are connected using epoxy and self-tapping screws. The placement of the lid for the tested beams can be seen in Figure 1-6.

Figure 1-6 Placement of Lid onto FRP Shell

Shear connectors are placed by inserting mild reinforcing steel through holes in the lid and holding them in place with a loose strand within the cavity. The self-consolidating concrete can then be placed within the shell, either before or after placing the beams into their final positions. Setting the beams into place first allows smaller equipment to be used and an overall easier construction process. However, if it is desired for beams to immediately have full strength in the field, the arch can be placed earlier and allowed to gain strength. Regardless of when it is placed, the process is performed by pumping concrete into holes at different points in the top flange. The procedure begins at a hole at a quarter point, where the concrete flows to the end of the beam. The other end of the beam is then filled, followed by the midspan of the beam. As the concrete reaches the top of the beam each hole is closed with a plywood cap.

2 Literature Review

2.1 FRP in Bridge Design

This section reviews information from Hollaway's 2010 publication on the history and current uses of Fiber Reinforced Polymers in civil engineering (Hollaway 2010). While traditional materials like steel and concrete still dominate the construction industry, since the 1980s research institutes and consultants have shown interest in polymer composite materials. These materials utilize high strength fibers protected by a polymer resin, and are referred to as FRPs in civil engineering applications. Properties of FRPs depend on many different factors, including the individual component properties, fiber and resin surface interaction, proportions of polymer and fiber, manufacturing method, type of loading, and environment. Manufacturing can be performed using three different general methods: manual, semi-automatic, and automatic. Automated methods have a high degree of control, and result in better properties and durability.

Since FRP is not as well-known as traditional materials, engineers have various concerns about how it will perform while in service. Performance during fires is the single greatest barrier to widespread use, and despite research there is still much to study and limited information available. Temperatures greater than 570°F will cause polymer decomposition and produce toxic gasses, while temperatures as low as 210°F will make composites soften, creep and distort, reducing material strength and causing concerns over buckling failure modes. Consequently, FRP is neglected when evaluating fire performance of composite systems and focus is on strength of steel or concrete. Liquid penetration depends on the fiber to polymer strength ratio, with carbon fiber reinforced polymers (CFRP) having better performance than glass fiber reinforced polymer (GFRP). Coupling agents also have been developed to help materials resist liquids in wet environments.

Civil engineering use of GFRP began in the 1950s but generally GFRP was not understood by the inexperienced fabricators. During the 1970s larger fabricating firms who had FRP experience from other industries became involved with buildings. Manual fabrication methods were used for early structures, but during the 1980s the desire for new materials with high strength, stiffness and durability that could replace traditional materials in hostile environments led to the rise of automated methods. FRP pedestrian bridges made use of the lightweight materials and ease of installation to construct bridges in remote areas without heavy equipment. The ease of construction can also allow labor and traffic closure savings that can offset higher material costs.

While pure FRP structures can be useful, greater benefits appeared with its use in hybrid systems, especially in structural rehabilitation applications. Hybrid examples include external FRP plate bonding on reinforced concrete, rehabilitation of steel beams, retrofitting concrete columns, and FRP reinforcement. While analysis and design of these hybrids is generally understood there are other issues, such as the previously mentioned uncertainty of material durability. Another issue is the variety of materials that fall under the general label of "FRP" coupled with varying additives that all lead to different material properties. Between the lack of a general database of material information, codes, or specifications it can be difficult for engineers to move to FRP from more familiar materials.

Hybrid systems utilizing FRP with concrete and steel in optimal combinations is currently a large focus in new construction. For these to be successful, three criteria need to be met: cost effectiveness when looking at lifetime cost compared to quality and performance, use of FRP in tension as much as possible, and that the FRP can be neglected in scenarios involving fire. Bridge components in particular have received a lot of attention, with universities in the US, UK, China, and Switzerland studying new systems, including concrete-filled FRP tubes used as columns and

FRP/concrete beams. An example of optimizing material use is in concrete beams, where any material in tension is inefficient since its strength is neglected- substituting FRP in this region reduces the weight of the member and uses materials more efficiently, with other advantages from its corrosion resistance. The future of FRP seems tied to use in conjunction with traditional materials.

2.2 Long-term Use of FRP (Durability and Creep)

Durability of FRP is of great concern to engineers, both from an environmental degradation and creep perspective. As previously discussed, there is no simple answer concerning FRP's creep performance due to the large number of variables within the construction of the composites (e.g., fibers, resin type, processing method). These factors prevent easy use of material performance studies from other disciplines. For example, while FRP has been used in a number of water related applications such as marine vessels and piping, it is not completely water resistant. The effects of sea-water on FRP on these polyester based resins may be minimal, but the performance of vinylester resins (which are regularly used in civil engineering applications, including the HCB) in these environments is not as well known (Karbhari 2003).

Nevertheless, there have been some studies on FRP's long-term behavior in civil engineering applications. A review of technical literature was published by Scott, et al that looked at both theoretical models for predicting behavior and experimental results (Scott, et al 1995). A power law model developed by Findley is popular among researchers, and also was recommended for use in analysis in the ASCE Structural Plastics Design Manual (ASCE 1984). The model has the general form

$$\varepsilon(t) = \varepsilon_0' + \varepsilon_t t^n \qquad \text{(Eq. 1)}$$

where $\varepsilon(t)$ is the time dependent creep strain, ε_0 is initial elastic strain, ε_t is a stress-dependent coefficient, n is a material constant, and t is the time after loading (Findley 1987). While the review noted that there are varied results among different investigations due to a lack of uniformity, in general creep behavior depends on the fiber orientation- when loaded along the direction of the fiber, fiber properties have the greatest effect on creep, whereas the overall matrix will dominate in off-axis loading.

While not performed with regard to civil engineering applications, Wu and Hahn did perform an analysis on the properties of glass fibers encased in vinylester fabricated with Vacuum Assisted Resin Transfer Molding (VARTM), the materials and fabrication method used in the HCB (Wu and Hahn 1997). Material properties were comparable to other glass/polymer composites, though fiber orientation had a large impact on strengths. Samples were also exposed to moisture and high temperatures, with minimal impacts on overall mechanical properties.

Another literature study by Sá, et al. reported on investigations after the 1994 review was published, focusing particularly on creep in pultruded members (Sá, et al. 2011). Studies performed using flexural tests on pultruded GFRP specimens for civil engineering applications showed that the most important aspect of the design that affects creep is the resin that encases the fibers (Sá 2011). FRPs that use vinylester have been repeatedly shown to have better creep properties than FRPs that use a polyester agent. Additionally, creep has not been a problem for glass FRPs whose stress levels are only 25-30% of the ultimate stress (Karbhari 2003). Coupled with the fact that in civil engineering FRP is generally designed for serviceability rather than strength and will have a large factor of safety due to the brittle failure mode, creep's effects will be limited.

2.3 Past Papers on Composite Members

In 2003 Nordin and Täljsten investigated the performance of hybrid FRP beams composed of a GFRP I-beam with CFRP on the tension flange and a block of concrete attached to the compression flange (Nordin and Täljsten 2004). The beam takes advantage of the tensile strength of the CFRP, the lower cost of the GFRP, and the compressive strength of the concrete. Three different cross-sections were investigated- one with no concrete topping (as a control), one with steel shear connectors, and one with epoxy bonding, seen in Figure 2-1.

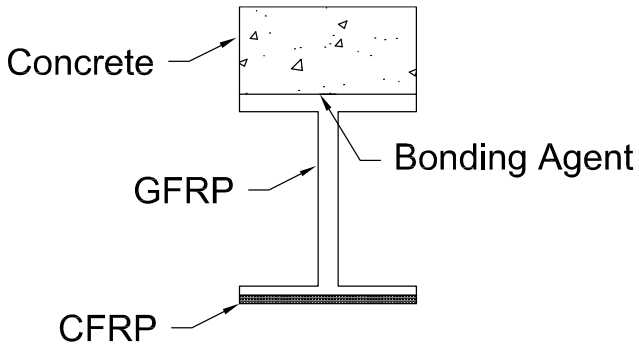

Figure 2-1 Nordin and Täljsten's hybrid FRP I-beam

Tests were performed using a four-point bending load with strain gages on the top and bottom flanges and rosette gages on the webs. Failure occurred in beam stability for the FRP-only cross-section and due to concrete deck failure in the latter two specimens. The bending stiffness *EI* was calculated for each beam from the measured midspan deflections. Theoretical *EI* values were also calculated using a transformed area method where the CFRP and concrete is turned into equivalent areas of GFRP. Theoretical displacement calculations include both a flexure component and a shear component for the GFRP web. The transformed moment of inertia was used to calculate theoretical stresses. The theoretical stiffness matched well with tests, though the test stiffness values were slightly higher. Final conclusions were that beams of this type can be useful,

but concrete in the compression zone is necessary to achieve sufficient stiffness and better GFRP cross sections (such as double webs) could help improve performance.

In 2005 Hejll, et al. investigated large scale hybrid composite girders composed of four individual GFRP rectangles bonded together with CFRP on the top and bottom flanges and a full GFRP deck (Hejll et al. 2005). The beam cross section can be seen in Figure 2-2.

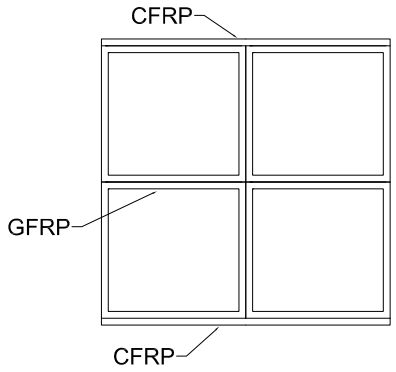

Figure 2-2 Girder of Four FRP Rectangles

Two beams, one without the CFRP on the flanges, were tested in four point bending. Failure occurred suddenly in both tests due to buckling of the top flange at approximately the same load, though strains were much lower in the beam with CFRP. The results of these tests were compared to a theoretical derivation that assumed linear elastic behavior in the CFRP and full composite action between the FRP and CFRP. Transformed moments of inertias were calculated and displacements were calculated using classical Bernoulli beam theory. A finite element model was also used to verify the theoretical equations. Comparing tests, theory, and a numerical model showed that the theory accurately predicted strains. Deflection predictions were close to test values, but the tested beam had slightly higher deflections.

In 2009 Honickman and Fam studied the bond between concrete and GFRP stay-in-place forms (Honickman and Fam 2009). Eight slabs were fabricated and tested to investigate the effects of different bond systems (six with adhesive bonds and two with stud connectors) and GFRP ratios.

A model was made to predict the flexural behavior of the adhesively bonded slabs, incorporating failure criteria for flexural tension or compression failure, concrete shear failure, and bond failure. A moment curvature response based on equilibrium of forces and strain compatibility was assumed, and then an initial strain on the tension side and neutral axis were assumed. Strains are turned into stresses and forces are found, and if equilibrium is not met a new neutral axis location is assumed. Once the section has equilibrium the forces are summed about the neutral axis to calculate the moment capacity of the section. The model was shown to be accurate at predicting the failure of the tested slabs. Of the six adhesively bonded slabs, two had concrete shear failure and four had bond failure.

In 2012 Karimi, et al. published a paper on the analytical modeling of FRP encased steel-concrete composite columns (Karimi et al. 2012). Six of these columns, made of a steel I-beam encased in a concrete cylinder that is confined by an FRP tube (seen in Figure 2-3), were made and tested in axial compression.

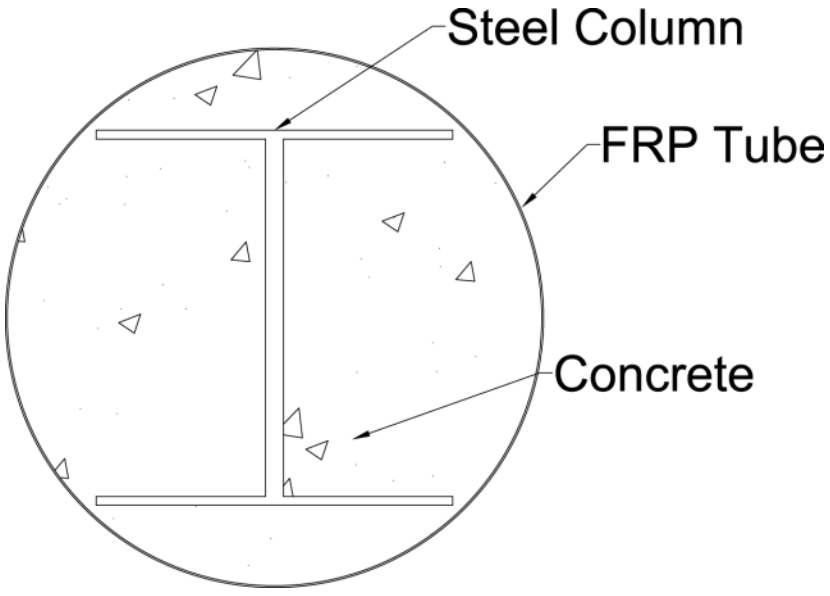

Figure 2-3 FRP Encased Steel-Concrete Composite Column

To analytically model the behavior, the Euler buckling load is evaluated based on column stiffness at different strain levels and compared to the compressive load capacity to classify it as a long or short column. The cross-sectional load capacity is found by superimposing the contributions of the three different materials by multiplying the cross sectional areas by the stress in each material. The steel is treated as an elastic-plastic material and FRP behavior was assumed to be elastic. The ultimate failure mode is rupture of the FRP tube, which is evaluated by assuming strain compatibility between the FRP and concrete. The analytical model resulted in values close to those seen during testing.

2.4 Accelerated Bridge Construction

Aging infrastructure and increasing congestion requires both the construction of brand new and replacement bridges and plans to maintain aging structures. The total cost of a bridge should include not only materials and labor but also user costs, including increased wait times, traveling longer routes to avoid construction zones, inefficient movement of goods, and lost commerce at local businesses. In light of these costs, accelerated bridge construction (ABC) has become a topic of interest, leading to an increase in prefabricated bridge components. Still, user costs are often neglected when examining bridge alternatives and traditional construction methods may be used due to familiarity. As ABC becomes more common, costs will continue to decline and contractors will gain experience and greater willingness to use new techniques. In the US, the level of prefabrication can vary from just a few pieces to entire bridges, and guidelines are in place from the Federal Highway Administration to assist in design and decision making (FWHA 2009). Steel or prestressed girders are common, with prefabricated decks appearing less often. Self-propelled modular transports have also been used to move preassembled bridges weighing several thousand tons into place (Hällmark et al. 2012).

The rapid deployment bridge system most comparable to the HCB is the "Bridge-in-a-Backpack" (BIAB) initiative introduced in 2001 by the University of Maine's AEWC Advanced Structures and Composites Center. Hollow FRP composite tube arches are filled with self-consolidating concrete and secured in concrete abutments at the ends of a span. Arches are covered with either a light or heavy decking which in turn is covered but the roadway. In 2008 the first of these bridges was constructed for public use in Pittsfield, Maine. The bridge uses 23 arches and was completed in just two weeks thanks to the light weight and ease of construction. Additionally the FRP provides the bridges corrosion resistance, though they do have the downside of having brittle failures. Eight roadway bridges have been erected with this technology so far, and have shown acceptable performance (Fleck and Kuzy 2012).

A more traditional alternative is the northeast extreme tee (NEXT) beam, a precast concrete double tee section inspired by members developed for railroads. Various fillers and adjustable side-forms allow the dimensions of these beams to be altered in accordance with the requirements of the bridge without a large increase in cost, and the space within the double tee provides accommodation for under-bridge utilities. The top flange also provides a surface used as formwork for casting a deck, allowing for accelerated construction. Shipping weight is still a concern, as the beam is effectively two stringers tied together, and therefore twice the weight of a normal beam. Using lightweight concrete in the members can reduce shipping costs and possibly increase available span lengths (Culmo and Seraderian 2010).

Another use for accelerated bridge construction is use within military applications, where bridges may need to be constructed quickly for movement of heavy equipment. The current system used by American military is the US Army Rapidly Emplaced Bridge System (REBS). The bridge is an aluminum structure comprised of two tread-ways in two halves that can load on to a transport

vehicle. This vehicle is capable of moving the pieces into position to assemble and then place over a gap, spanning up to 43 ft. The transport vehicle is also capable of retrieving the bridge for reuse (US Army 2006).

An army prototype examined in 2006 used a system involving a truss of hollow aluminum tubes and stay in place FRP formwork to span 48 ft. The truss could be preassembled and folded for deployment, then quickly expand for construction. FRP decking and reinforcement was used for its light weight, and the deck itself is concrete procured and placed in-theater. Design and optimization were performed by consulting both military and civilian codes, generally obtaining loads from the Army materials and checking strength limit states with design manuals from the Aluminum Association and American Concrete Institute. This prototype could represent significant weight savings compared to the REBS (Hanus et al. 2006).

2.5 Past Work on Hillman Composite Beam

In 2008 a report was published detailing the fabrication and testing of a prototype HCB. Lessons learned from manufacturing the beams were incorporated into the fabrication process, followed by making eight 30 ft (9.1 m) beams to test as a railroad bridge. Concerns of bridge engineers regarding the unfamiliar FRP, such as durability and fire resistance were brought up but require further investigation. The field test found that "the stresses, strains, and deflections proved to be predictable and within the code specified limits (Hillman 2008)."

In 2009, a report came out of the University of Maine summarizing tests of a 70 ft (21.3 m) HCB representative of those used in a Maine Department of Transportation project. Overall, the beam was found adequate for all required loads but some suggestions for improvements were made. For better performance while the concrete arch is curing, recommendations were made to stiffen the box with wings on both sides of the beam, make the top flange and wings one segment

and provide more cross ties within the box (all of which have been incorporated for current tests). Calculations were found to under-predict the required camber since both the self-weight of the beam and effects of concrete shrinkage had been neglected. Static tests showed linear load-deflection behavior within service level loading and no fatigue degradation of flexural stiffness during cyclical loading. The FRP materials properly resisted weathering caused by UV treatments and exposure to humidity, with limited effect to the outer surface that actually improved material performance. After a successful test up to the design load of 135 kips, the beam was tested to failure. The beam failed after holding a load of 209 kips when the tension reinforcement broke free at one end of the beam. This is a brittle failure mode, but these beams are designed with excess capacity (Snape and Lindyberg 2009).

Data for the research presented herein came from tests performed by Ahsan for his thesis, "Evaluation of Hybrid-Composite Beam for Use in Tide Mill Bridge" (Ahsan 2012). A full-scale model was constructed to investigate the effects of a skew angle on a bridge system using the beams. Instrumentation plans were created based on previous work analyzed as part of the literature review, focusing on the report on the Knickerbocker Bridge. Multiple gages were employed to create strain profiles for the full height of the beam, with all the materials instrumented to allow the force distribution to be examined. Further description of the gages relevant to this research are found in Appendix A1.

After completing tests on both the individual beams and a full bridge system, the forces within the beams were analyzed by examining the strain profiles. The findings on the force distribution among the beam components were submitted to the Transportation Research Board and accepted for presentation in January 2013 and publication in the 2013 edition of the

Transportation Research Record, the TRB's journal. The published manuscript follows as Chapter 3.

3 Transportation Research Record Paper

Experiments on a Hybrid-Composite Beam for Bridge Applications

Word Count: 4483
Number of Figures and Tables: 11

Stephen Van Nosdall, EIT
Via Scholar, Graduate Research Assistant
Via Department of Civil and Environmental Engineering
Virginia Tech
200 Patton Hall, Blacksburg, VA 24060
Tel.: (732)-616-8943
E-mail: spvn001@vt.edu

Cristopher D. Moen, PhD, PE
Assistant Professor
Via Department of Civil and Environmental Engineering
Virginia Tech
200 Patton Hall, Blacksburg, VA 24060
Tel.: (540) 231-6072
E-mail: cmoen@vt.edu

Thomas E. Cousins, PhD, PE
Professor
Via Department of Civil and Environmental Engineering
Virginia Tech
200 Patton Hall, Blacksburg, VA 24060
Tel.: (540) 231-6753
E-mail: tcousins@vt.edu

Carin L. Roberts-Wollmann, PhD, PE
Professor
Via Department of Civil and Environmental Engineering
Virginia Tech
200 Patton Hall, Blacksburg, VA 24060
Tel.: (540) 231-2052
E-mail: wollmann@vt.edu

March 15, 2013

3.1 Abstract

This paper details a study of the structural behavior of Hybrid-Composite Beams (HCB) consisting of a fiber reinforced polymer (FRP) shell with a tied concrete arch. The HCB offers advantages in life cycle costs through reduced transportation weight and increased corrosion resistance. By better understanding the system behavior, the proportion of load in each component can be determined, and each component can be designed for the appropriate forces. A long term outcome of this research will be a general structural analysis framework that can be used by DOTs to design HCBs as rapidly constructible bridge components. This study focuses on identifying the load paths and load sharing between the arch and FRP shell in an HCB and testing an HCB with a composite bridge deck. Testing was performed by applying point loads on simple span beams (before placing the bridge deck) and a three beam skewed composite bridge system, resulting in strain data for the arch and FRP shell. The test results show that strain behavior is linear elastic at service loads and the FRP shell has a linear strain profile. Curvature from strain data is used to find internal bending forces, and the proportion of load within the arch is found. Additionally, a stress integration method is used to confirm the internal force contributions. The tied arch carries about 80% of the total load for the non-composite case without a bridge deck. When composite with a bridge deck, the arch has a minimal contribution to the HCB stiffness and strength because most of the arch is below the neutral axis and cracks under the maximum live load expected for the bridge. For this composite case the FRP shell and prestressing strands resist about 80% of the applied load while the bridge deck carries the remaining 20% to the end diaphragms and bearings.

3.2 Introduction

This research examines the behavior of the hybrid-composite beam (HCB) system. The HCB consists of three parts: a glass fiber reinforced polymer (FRP) shell, a concrete arch within the shell, and tension reinforcement tying the ends of the arch. Figure 3-1a shows these main parts.

a)

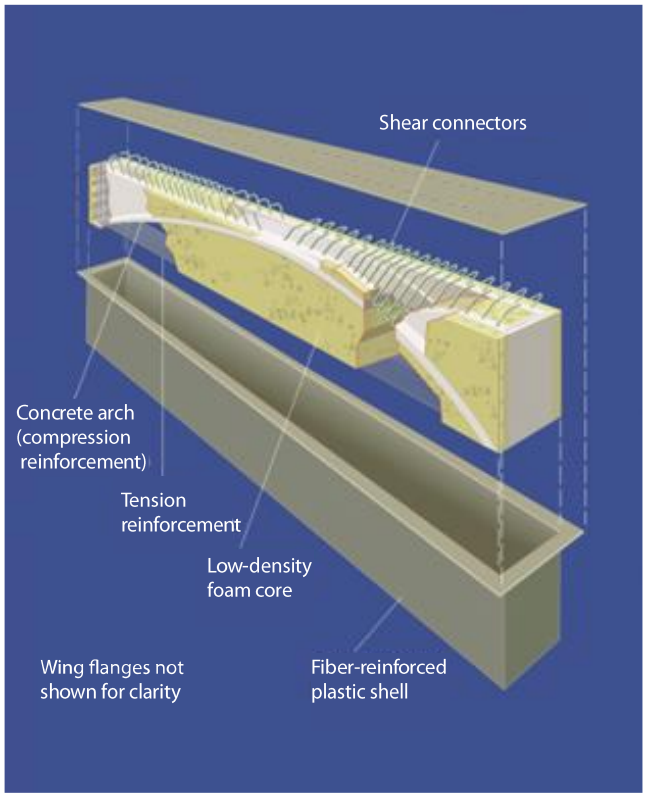

b)

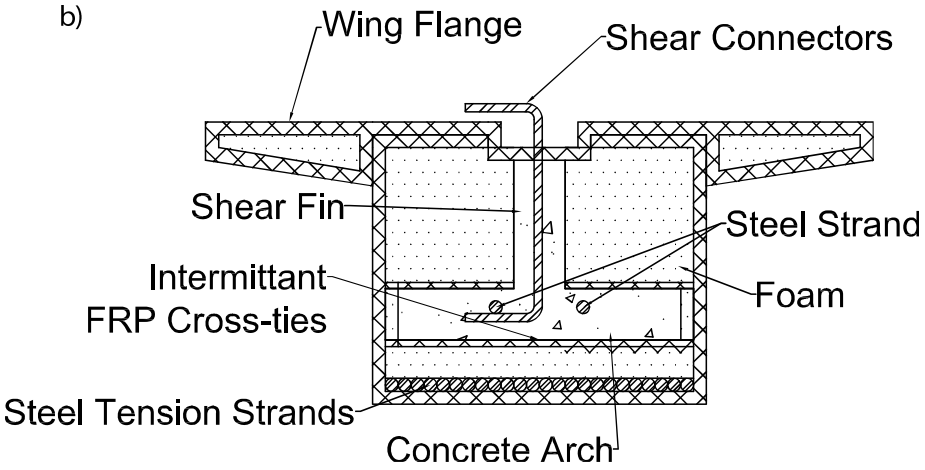

Figure 3-1 View of the HCB Showing a) Main Components (from http://www.hcbridge.com/) and b) Detailed Cross Section

The beam shell includes glass fiber reinforced polymer top and bottom flanges, two vertical webs, and cross ties at discrete points to improve shell stability, and a conduit used to form the concrete arch. The FRP composites used are E-QX-10200 and E-BXXS-24, which have glass strands oriented in a quad weave (layers oriented at angles of 0°, 45°, 90° and -45°). The conduit is formed by P200 ELFOAM (rigid polyisocyanurate foam) (Elliot Company). Additionally, FRP "wing" flanges extend at the top of the beam to aid deck construction, as seen above in Figure 3-1b. These wings are also filled with ELFOAM. The concrete arch is formed by pumping self-consolidating concrete into the conduit, following a parabolic path starting at the bottom at the supports with an apex at the center of the beam. The arch also has a "shear fin" of concrete extending upward to the top of the beam to hold reinforcing steel for force transfer between a concrete deck and the beam. Steel strands are present in the arch for tying the shear connectors. At each support the concrete fills a block the full height of the beam to anchor prestressing strands that provide tension reinforcement. This paper focuses on analysis of the beam as a combination of two systems (the tied arch and the FRP box) as well as how the beams act when in a composite bridge system.

The primary application for the HCB is use as bridge girders for spans of 30 to 80 ft (9.14 to 24.4 m). Originally designed for use in freight train bridges, they are also suitable for use in highway bridges and have been used in a number of replacement projects. With their light weight and modular design they can be installed faster than traditional concrete girders, resulting in less construction time and therefore less congestion during bridge replacement. Currently, bridges in Illinois (seen in Figure 3-2), Missouri, New Jersey, and Maine have used HCBs, with future plans for use in Maryland, West Virginia, Utah and Virginia (HCBridge).

Figure 3-2 Underside of High Road Bridge in Illinois (from http://www.hcbridge.com)

This beam offers a number of advantages for bridge construction. The shells are fabricated in shops, offering similar advantages to precast concrete, but transport is easier due to the lighter weight. The HCB also uses corrosion resistant materials, increasing service life and resulting in anticipated improved life cycle costs. FRP materials used alone are too flexible and expensive to be competitive with traditional steel and concrete. The HCB takes advantage of the strengths of each material, resulting in a cost competitive member with its own unique benefits.

3.3 Previous Research

In 2008 a report was published detailing the fabrication and testing of a prototype HCB. Lessons learned from manufacturing the beams were incorporated into the fabrication process, followed by making eight 30 ft (9.1 m) beams to test as a railroad bridge. Concerns of bridge engineers regarding the durability and fire resistance of FRP were brought up but require further investigation. The field test found that "the stresses, strains, and deflections proved to be predictable and within the code specified limits (Hillman 2008)."

In 2009, a report came out of the University of Maine summarizing tests of a 70 ft (21.3 m) HCB representative of those used in a Maine Department of Transportation project. Overall, the beam was found adequate for all required loads but some suggestions for improvements were made. To improve performance while the concrete arch is curing, recommendations were made to stiffen the box with wings on both sides of the beam (as used in current tests), make the top flange and wings one segment and provide more cross ties within the box. Calculations were found to under-predict the required camber since both the self-weight of the beam and effects of concrete shrinkage had been neglected. Static tests showed linear load-deflection behavior within service loads, and no fatigue degradation of flexural stiffness during cyclical loading. The FRP materials properly resisted weathering caused by UV treatments and exposure to humidity, with limited effect to the outer surface that actually improved material performance. During the final test the beam was loaded to failure, which occurred when the tension reinforcement broke free of its anchoring. The failure was brittle, with the beam holding 209 kips (930 kN) before failing compared to the design load of 135 kips (601 kN) for an HL-93 truck with impact loads (Snape and Lindyberg 2009).

Previous studies on hybrid composite FRP beams with other cross-sections also were reviewed to find analysis methods and failure mechanisms. Honickman's examination of stay-in-place FRP concrete deck forms used section analyses based on force equilibrium and strain compatibility, which worked well (Honickman and Fam 2009). Other studies on composite members used a transformed area method to calculate flexural rigidities *EI*. One example is Nordin's FRP I-beams topped with concrete blocks, which had failure in the concrete deck (Nordin and Täljsten 2004). Hejil's bridge girders made of four FRP rectangles also used this method, and these beams failed suddenly due to buckling of the top flange (Hejil et al. 2005). Finally, recent

studies by Karimi on composite columns made of a steel I-beam encased in concrete constrained by FRP use an analysis that adds the force that each component can take to find the ultimate failure mode (Karimi et al. 2012). Failure occurred due to rupture of the FRP. After seeing these studies, approaches involving flexural rigidities from transformed areas, the addition of component forces, and section analysis from strain profiles were used to examine the HCB. Additionally, in multiple studies the failure mechanism was within the FRP, and so it would not be unusual for these beams to be designed for much higher forces as a result of not having a ductile failure.

3.4 Research Motivation

The goal of this research was to study the structural behavior of an HCB in flexure, specifically the load paths and load distributions in the arch and FRP shell. Previous tests proved its ability to carry service loads, but the present HCB design process has room for improvement. Current design procedures use a transformed area method to change all materials into an equivalent FRP area by multiplying their width by the modular ratio $n=E_{material}/E_{FRP}$. The true distribution of forces to different components is unknown. The actual loads carried by the FRP and arch are determined in this test program, and work is ongoing to develop a generalized design approach that can be used for any beam span and HCB geometry.

3.5 Hypothesis

The hypothesis for this research was that the beam can be broken down into two separate systems for analysis: the tied arch consisting of the concrete arch and tension reinforcement, and the FRP shell. The majority of the flexural capacity was expected to be provided by the tied arch system before the bridge deck is placed. The decomposition of the system can be performed by examining the flexural rigidity, *EI*, of the two components of the beam and seeing how they compare to the stiffness of the entire system. The actual forces each component carries could then

be found, accommodating design checks based on internal demand forces on the concrete arch, the steel arch tie, the FRP shell, and the bridge deck. It was important to fully understand the behavior of the beam both with and without a bridge deck as it is so unlike traditional bridge girders, and these studies are summarized in the following sections.

3.6 Non-Composite Testing

Data comes from testing performed at Virginia Tech during 2012 (Ahsan 2012). Full scale testing was performed on an empty FRP shell (which includes the tension reinforcement), three complete beams (FRP shells with arches placed), and a bridge system with a deck in place on the three beams. Each beam's span, *L*, was 43 ft (13.12 m), and the plan, elevation and cross section views are shown in Figure 3-3.

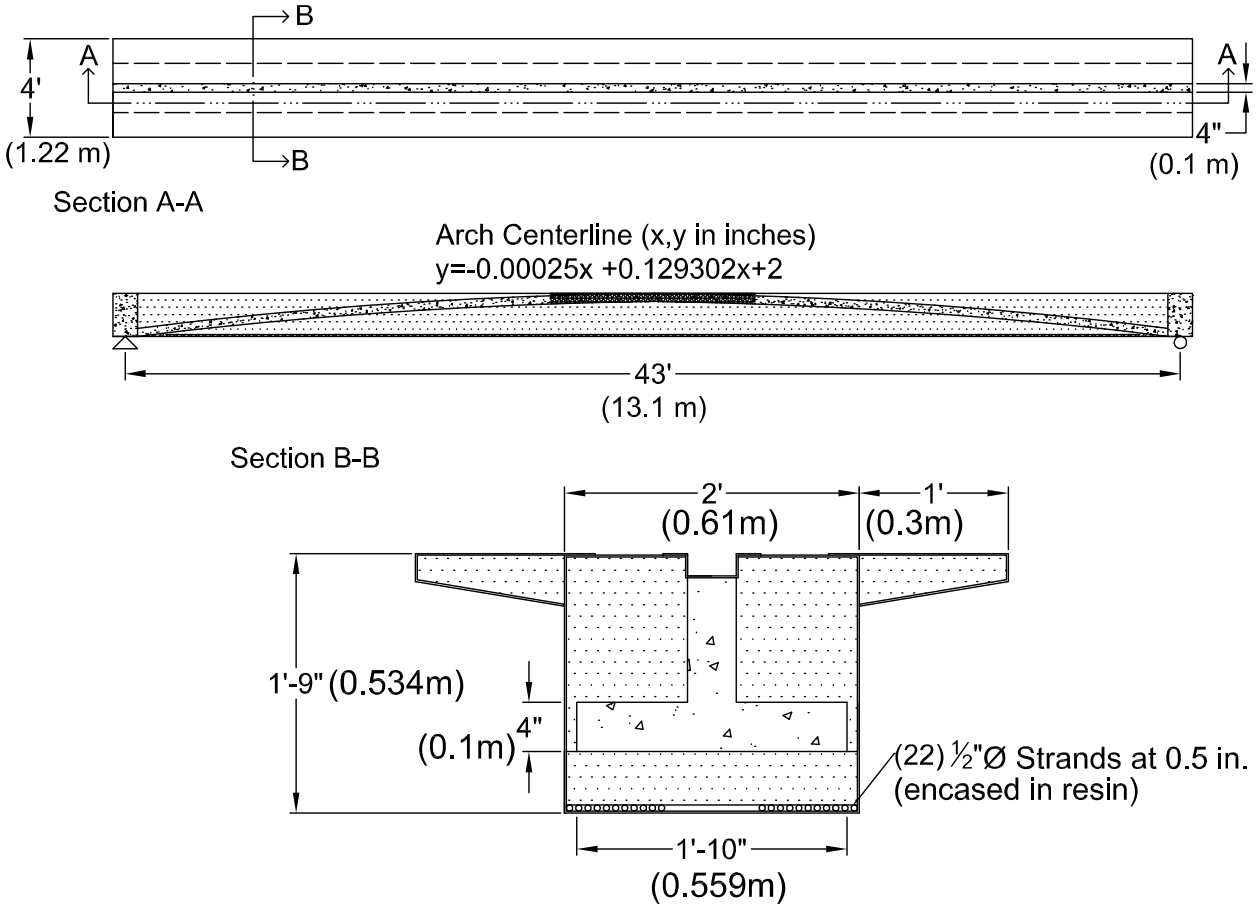

Figure 3-3 Beam Dimensions in a) Plan b) Side Elevation and c) Cross Section Views

Performance was measured by strain gages attached to the FRP shell and tension reinforcement, vibrating wire strain gages within the concrete arch, and wire potentiometers to measure deflection. Additionally, photogrammetry was used during testing of one beam to investigate out-of-plane web deformation and arch displacement relative to the FRP shell (Mascaro 2012). The positions of the strain gages can be seen in Figure 3-4.

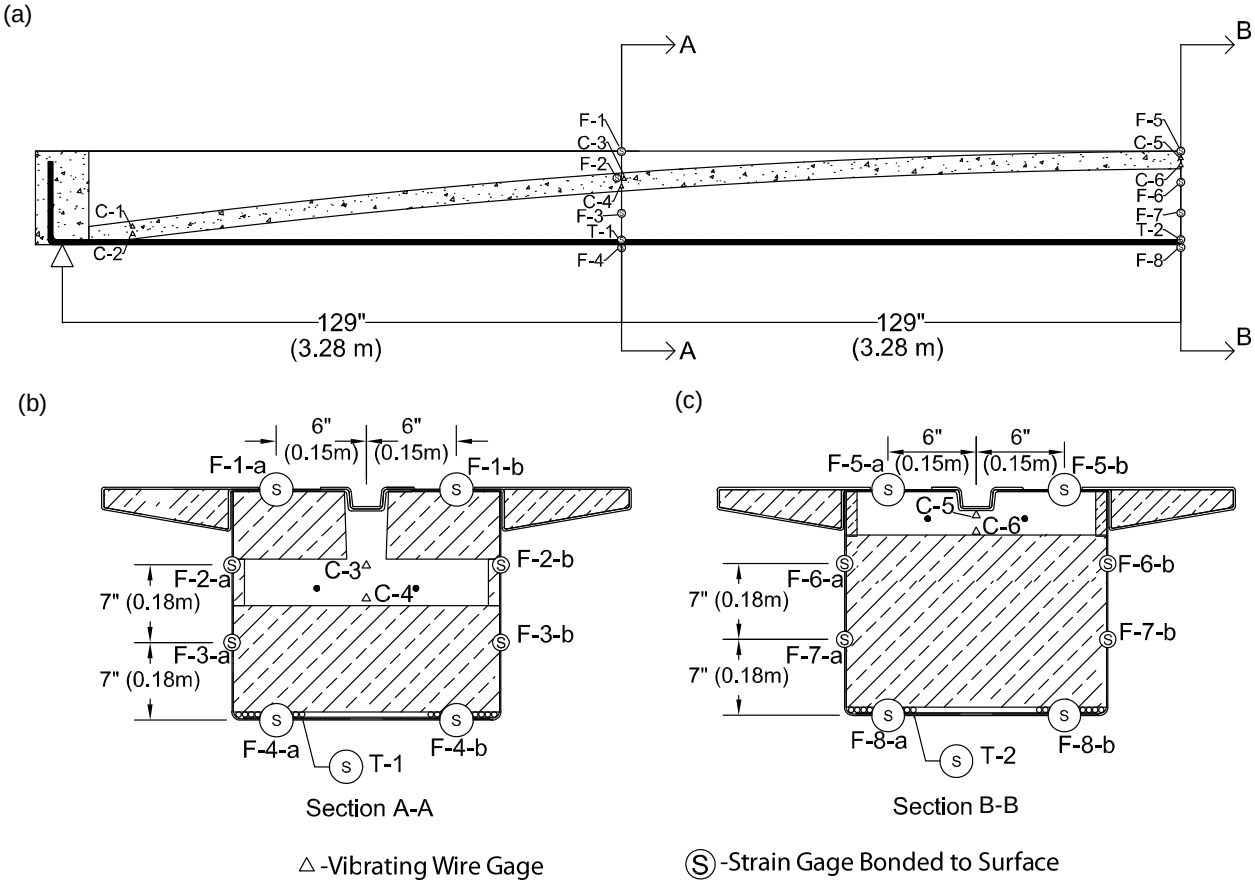

Figure 3-4 Beam Instrumentation (a) Along Length of Beam and on Cross Section (b) at Quarter Point and (c) at Midspan

Concrete cylinders were cast for each batch of concrete and used to determine material properties to ensure that the concrete developed proper strength. Modulus tests were performed according to ASTM C469-02 and compressive strength tests followed ASTM C 39-05 (ASTM 2002, ASTM 2005). The arch concrete's modulus of elasticity at 28 days was measured as 4,500

ksi (31,000 MPa) with an ultimate strength of 6,200 psi (42.7 MPa). At 45 days, when beam loading occurred, the measured modulus was lower, but there may have been problems with the collar (Ahsan, 2012). Due to better matching the specified modulus and the empirical equation based on concrete strength at 45 days, the 28 day value was used. For the steel strand and FRP the values provided by the manufacturers were used: 27,500 ksi (190,000 MPa) for the steel strand and 3,100 ksi (21,400 MPa) for the glass FRP. Since strain gages attached to the steel strand were attached to individual spiraling wires, a conversion factor was needed to change the angled wire strain to the longitudinal strain of the strand as a whole. Tests on a sample piece of strand using a universal testing machine resulted in a conversion factor of 1.178 that strain readings were multiplied by to transform them into longitudinal strain *(*Ahsan 2012*).*

Two loading configurations were used during individual beam testing: a single point load of 15 kips (66.7 kN) at midspan and two identical point loads applied at quarter points totaling 25 kips (111.2 kN) (i.e., 12.5 kips (55.6 kN) on each quarter point). The load was applied in increments of 5 kips (22.2kN). Each test was performed twice on each of the three beams.

3.6.1 Strain Profiles

After testing, strain readings from the maximum applied loads were plotted for each test repetition, as seen in Figure 3-5. The average value for each height is connected with a line to show the strain profile. A predicted strain profile using a transformed section analysis is also shown as a dashed cyan line. Individual data points are shown, and some locations, particularly at the top of the beam, have large spreads. Separating the data showed that the large spreads are due to slight differences among the beams, as each beam has a smaller self-contained spread.

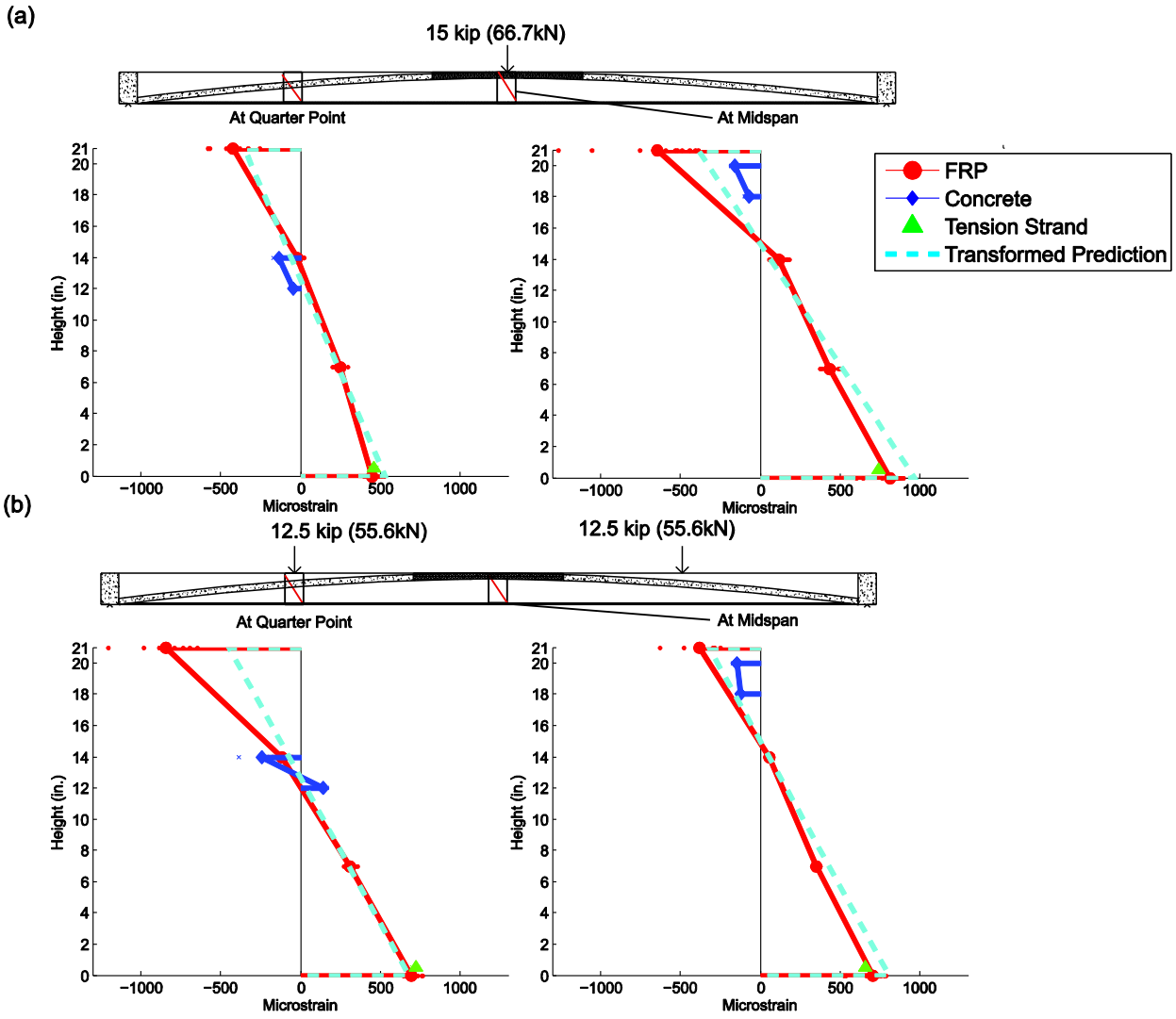

Figure 3-5 Strain Profile at Quarter Point and Midspan during (a) Midspan Loading and (b) Quarter Point Loading

The FRP had a relatively linear strain distribution with some variation near the top of the beam, as discussed below. The strand strain values were close to FRP values, showing strain compatibility between the tension reinforcement and shell. The neutral axes (measured from the bottom of the beam) were at about 12.6 in. (32 cm) at the quarter point and 15 in. (38 cm) at midspan, compared to the transformed section predictions of 12.7 in. (32.3 cm) and 15 in. (38cm). Unlike previous designs, calculations for neutral axis location and flexural rigidity include the wing flanges and shear fin.

The concrete arch experienced both axial compression and bending, though the amounts depended on how the beam was loaded. When loaded at midspan, the arch had compression and bending both at the quarter point and midspan. However, the quarter point loading had only bending at the quarter point and mostly axial force at midspan. The extreme arch bending was due to localized effects that can occur when applying a concentrated load on a shallow arch, causing beamlike behavior. The midspan loading lacked these local effects due to the presence of construction bracing in the form of an additional layer of FRP that connects the sides of the arch to the FRP webs, shown as shaded sections in the elevations in Figure 3-5. These connections prevent relative deflection of the arch, increasing its stiffness to allow it to carry a greater amount of load without the bending seen at quarter points.

The transformed section strain predictions were consistent with the actual strains observed during testing for the FRP. The biggest exception was the strain profile of the quarter point during quarter point loading, where the top FRP strain was more than double the prediction. This nonlinearity occurred because of local bending in the arch which caused the FRP shell to carry more of the load. The arch concrete strains differed enough to show that a transformed section strain compatibility analysis cannot be used to predict concrete arch strains when the HCB is not composite with a bridge deck.

3.6.2 Calculated Arch Internal Forces

The axial forces within the concrete arch and steel strand tie were calculated using Hooke's Law with strain data to find stress values, and then multiplying by the cross-sectional area of the material. For the concrete arch the average of the two concrete strain values was taken as the strain at midheight and multiplied only by the arch area (without the shear fin as no data within the fin was available). The internal bending in the arch, calculated through moment-curvature methods

(described below) was also included. A summary of the values of forces can be seen in Figure 3-6.

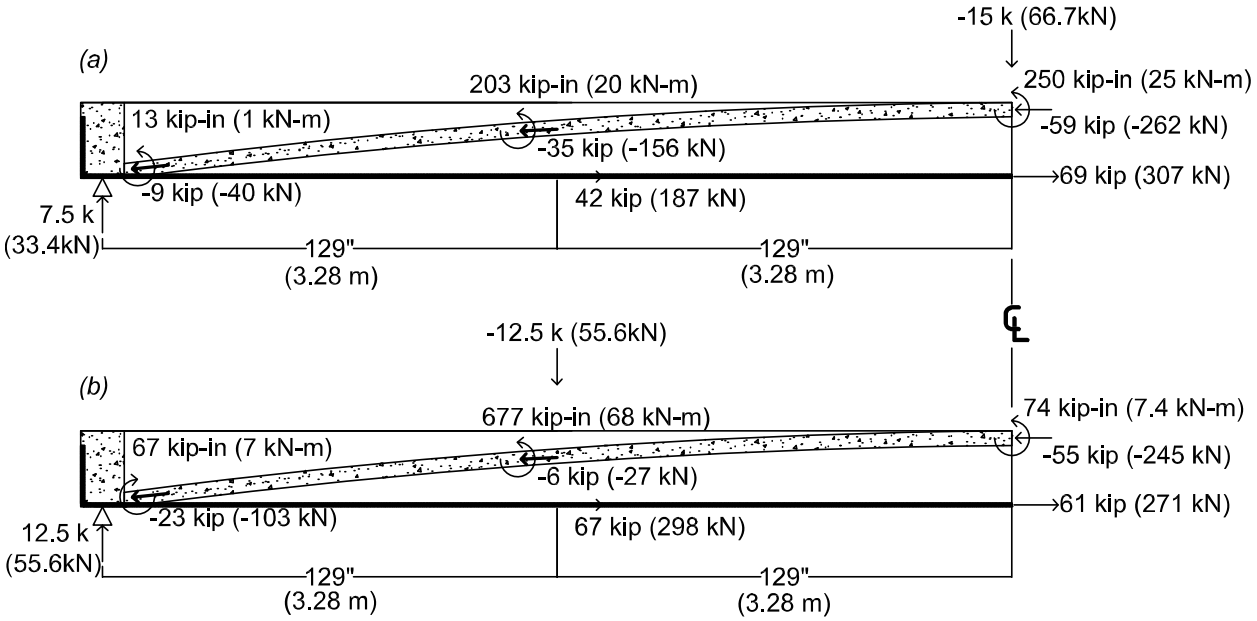

Figure 3-6 Diagram Showing Average Internal Forces in Arch and Strands at Maximum Applied Loads for (a) Midpoint Loading and (b) Quarter Point Loading

These calculated forces reinforce the observations from the strain profiles concerning local bending effects. While the quarter point test caused bending in the arch due to local effects, the midspan test is able to resist these local effects due to the extra FRP connection present that supports and stiffens the arch. The redistribution of force from the arch into the shear fin can be seen as the reported arch axial forces and moments decreased near the support when the force has had space to spread out and the depth of the shear fin has increased.

While the tension reinforcement must have the same axial load over its length in a tied arch model, within the HCB the strand clearly shed force to the FRP shell during the midpoint test. This reinforces the strain compatibility suggested earlier in Figure 3-5, as the only component of the cross-section to which force can be shed was the FRP shell.

3.6.3 Curvature Methods

The strain profiles in Figure 3-5 were used with the moment curvature equation, $1/\rho=M/EI$, in two different ways. First, to confirm the accuracy of the transformed section values, the flexural rigidity from the transformed sections of the empty shell and total beam were compared to that measured during testing. Plugging in the applied moment M and curvature $1/\rho=\varepsilon/y$ let EI be calculated. For example, during the midspan test, M=1,935 kip-in (219 kN-m) and ε/y=-69με/in. (-27/cm) (calculated by fitting a straight line from top to bottom, i.e., (-643-812)/21 in. ((-643-812)/53.4 cm) resulting in a flexural rigidity of $28x10^6$ kip-in.^{2} (80,360 kN-m^2), which was close to the value determined from deflection measurements and simple-span deflection equations of $27x10^6$ kip-in.^{2} (77,490 kN-m^2). The flexural rigidity calculated in the same way with data from the quarter point test was $31x10^6$ kip-in^2 (88,970 kN-m^2). Additionally, test data from shell testing (the FRP and strand without the concrete arch) was examined and both the strain and deflection data agreed that the flexural rigidity was $12x10^6$ kip-in.^{2} (34,440 kN-m^2). These test values were then compared to the transformed area method, which predicted the shell with no arch to have EI=$13x10^6$ kip-in.^{2} (37,310 kN-m^2) while the completed beam with arch would have $24x10^6$ kip-in.^{2} (68,880 kN-m^2) at the quarter point and $31x10^6$ kip-in.^{2} (88,970 kN-m^2) at midspan due to the changing cross section.

Comparing the different values for the shell alone showed that the transformed area method is accurate for predicting the flexural rigidity before the concrete arch is added. The values for the full beam were more challenging to interpret. All values were relatively close to each other, but the variable cross section makes calculating the rigidity more complicated. The average of the calculated flexural rigidity at midspan and the quarter point of the full beam was close to the measured EI during testing.

Next, the resisting moment *M* for the beam components was calculated by using the calculated *EI* values and known curvature for all beam components. The calculated *EI* of the FRP shell (without the tension reinforcement) was 6.2×10^6 kip-in.^{2} (17,790 kN-m^2), which is about 20% of the total beam rigidity. The concrete arch rigidity at midspan was calculated to be 5.9×10^6 kip-in.^{2} (16,930 kN-m^2) (not including the strand as it does not have bending capacity) and curvature ε/y was found using the vibrating wire gage data. The moment carried by each component is shown in Table 3-1. In this table, *M* is the total applied moment, M_s is the moment carried by the shell, M_{a1} is the moment carried by the force couple in the tied arch, and M_{a2} is the moment provided by arch bending.

Table 3-1 Resisting Moment of Components in HCB at Midspan

Component	**Moment *M*, kip-in (kN-m)**	**Proportion to M_{tot}**
Midspan Load (*M*=1935 kip-in. (218 kN-m) is applied)		
M_s (Shell)	430 (48.6)	0.22
M_{a1} (Arch Couple)	1303 (147.2)	0.66
M_{a2} (Arch Bending)	251 (28.4)	0.12
$M_{tot}=M_s+M_{a1}+M_{a2}$	1984 (224.2)	1.00
Quarter Span Loads (*M*=1612 kip-in. (182 kN-m) is applied)		
M_s (Shell)	320 (36.2)	0.21
M_{a1} (Arch Couple)	1153 (130.3)	0.74
M_{a2} (Arch Bending)	74 (8.4)	0.05
$M_{tot}=M_s+M_{a1}+M_{a2}$	1548 (174.9)	1.00

As can be seen, in both loading scenarios the shell took about 20% of the load, while the arch took 80%, mainly provided by the concrete arch-steel tie moment couple.

3.6.4 Strain Integration

Another method to calculate load proportions was to multiply the strains in Figure 3-5 by Young's Modulus (*E*=4,480 ksi (30,890 MPa) for the concrete (from cylinder tests), *E*=3,100 ksi (21,370 MPa) for the FRP, and *E*=27,500 ksi (189,600 MPa) for the steel strand) to create stress profiles. The stress diagram was broken up into simple shapes, and the area and centroid of each

was found. The stress was then multiplied by the thickness of material to find the force acting at the centroid of the stress block. In equation form, this is $F=\varepsilon Eht$ where ε is the average strain for the shape, E is Young's Modulus for the material, h is the height of the stress shape, and t is the thickness of the material. For example, in the midspan test the portion of FRP web from 0 to 7 in. (17.8 cm) had a strain profile that can be separated into a rectangle of height 436με and a triangle with height 376με. The rectangle provided a force of

$$376\mu\varepsilon \cdot 4{,}480\text{ksi} \cdot 7\text{in.} \cdot 0.11\text{ in.} = 1.29\text{kip}$$

$$(376\mu\varepsilon \cdot 30{,}890\text{MPa} \cdot 17.8\text{cm} \cdot 0.28\text{cm} = 5.74\text{kN})$$

at a height 3.5 in. (8.9 cm) from the bottom web. The triangle provided a force of

$$0.5 \cdot 376\mu\varepsilon \cdot 4{,}480\text{ksi} \cdot 7\text{in.} \cdot 0.11\text{in.} = 0.65\text{kip}$$

$$(0.5 \cdot 376\mu\varepsilon \cdot 30{,}890\text{MPa} \cdot 17.8\text{cm} \cdot 0.28\text{cm} = 2.9\text{ kN})$$

at a height of 2.33 in. (5.92 cm) from the bottom web. Equilibrium was then checked to ensure the forces were close to balancing. While the quarter point test is close, the midspan test had a force imbalance of about 15 kips (66.7 kN) between the concrete and steel. While there may be some error in the tested modulus of elasticity of the concrete, it is also suspected that the vibrating wire gages could not correctly converge when the load at the gage location due to vibrations from the actuator. For the midspan test the concrete strain values were increased by 30 με to achieve equilibrium. Along with the axial force acting as part of the moment couple, the arch provided some moment from bending as well, which was included in its total resisting moment. These forces F were then multiplied by the distance to the neutral axis, d, to find the moment they provide, shown in Table 3-2.

Table 3-2 Moment Contributions Calculated by Integrating Stress Diagrams at Midspan

	Midspan Test				Quarter Points Test			
Component	Force *F*, kips (kN)	Moment Arm *d*, in. (cm)	Moment, kip-in. (kN-m)	Proportion	Force *F*, kips (kN)	Moment Arm *d*, in. (cm)	Moment, kip-in. (kN-m)	Proportion
FRP Shell			**407 (46)**	**0.21**			**313 (35.4)**	**0.21**
Tension	19.5 (87)	13.9 (35.3)	271 (30.6)		16.6 (74)	13.9 (35.3)	230 (26)	
Compression	-24.9 (-111)	-5.5 (-14)	136 (15.4)		-14.7 (-65)	-5.6 (-14.2)	83 (9.4)	
Tied Arch			**1498 (169.2)**	**0.79**			**1174 (126.9)**	**0.79**
Strand	68.6 (305)	14.6 (37.1)	1001 (113.1)	*0.53*	60.7 (270)	14.4 (36.6)	875 (98.9)	*0.59*
Concrete (Axial Force)	-59.4 (-264)	-4.3 (-10.9)	246 (27.8)	*0.13*	-55.3 (-246)	-4.2 (-10.7)	225 (25.4)	*0.15*
Concrete (Bending)	N/A	N/A	251 (28.3)	*0.13*	N/A	N/A	74 (2.6)	*0.05*
Total			**1904 (215.2)**				**1487 (162.3)**	

The total calculated moment from stress integration for both tests was less than the applied moment by about 8% (1,486 kip-in./1,612 kip-in. (162.3kN-m/182kN-m) for the quarter point test and 1,904 kip-in./1,935 kip-in. (215.2kN-m/218kN-m) for the midspan test). The arch system was again responsible for resisting 80% of the applied moment, similar to the proportion seen earlier using curvature for the FRP.

3.7 Composite Testing (Testing of Beam with Composite Deck)

After completing testing of the individual beams a concrete bridge deck was placed to test the bridge system. The beams had end diaphragms and a 45 degree skew angle to mimic a current VDOT project. Strain gages were attached to rebar within the bridge deck to be able to make a complete strain profile. The tested modulus of elasticity *E* of the deck concrete at 28 days was

4,700 ksi (32,410 MPa) with strength 4,000 psi (27.6 MPa). The arch concrete was also retested (now at age 206 days), and no increase in properties was seen. Views of the composite bridge system can be seen in Figure 3-7.

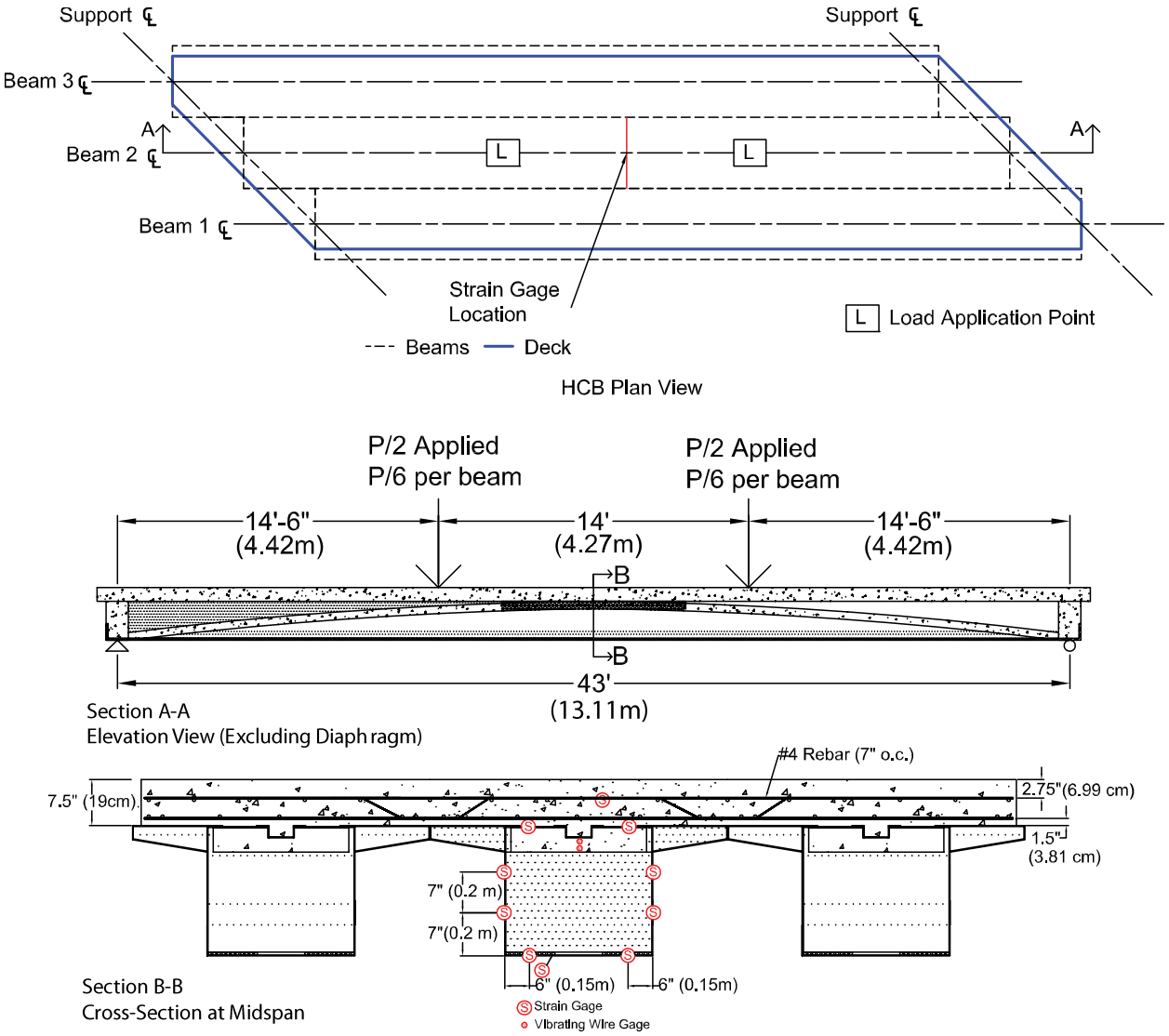

Figure 3-7 Composite Bridge System in a) Plan b) Elevation and c) Section Views

The examined tests used the load configuration shown above in Figure 3-7(b), with a load applied to a spreader beam supported at approximately the third points of the beam. Since the system was indeterminate the exact moments applied to the beams are not known. However, the deflection data for all three beams was about equal, and so it was assumed that each beam took

equal amounts of load. Beam 2 was examined as the loads were centered over it, and the applied loads are estimated as the total load *P* divided by 6. The effective width of concrete was taken as 24 in. (the width of the beam without wings) in order to create internal force equilibrium for the 150 kip test (as discussed later).

3.7.1 Strain Profiles

After performing the tests, strain profiles were created, seen in Figure 3-8. The arch was now in tension, and the vibrating wire gage readings became erratic. It is hypothesized that the concrete in the arch cracked, and so its strain was not plotted.

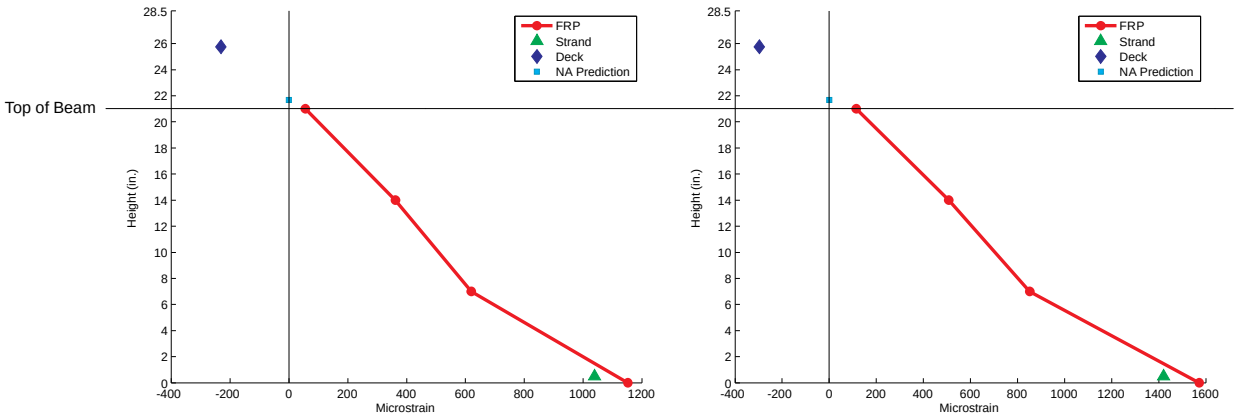

Figure 3-8 Strain Profiles of Beam 2 During Large Magnitude Load Tests

In both tests the FRP had a linear strain profile with one data point slightly diverging. Measured compressive strain in the concrete deck is consistent with the FRP strain trends, and strain compatibility between the FRP and steel strand can be seen as well. The cyan square shows the predicted neutral axis location.

As expected, the addition of the deck caused the neutral axis to shift up when compared to the individual beam tests in Figure 5. This caused the entire HCB to be in tension, including the arch. The transformed section predicted the neutral axis to be at 21.7 in. while the average neutral axis from tests was at 21.8 in.

3.7.2 Curvature Method

As in the individual beam testing, the curvature equation $1/\rho=M/EI$ was used to verify the stiffness of the beam and then predict the moment capacity. The transformed section approach resulted in a constant *EI* of 63.2×10^6 kip-in^2 over the length of the beam as the concrete arch was assumed cracked and ignored. From curvature, the calculated *EI*'s from the two tests were 74.9×10^6 kip-in^2 (215,000 kN-m^2) for the 150 kip test and 68.9×10^6 kip-in^2 (197,700 kN-m^2) for the 200 kip test, higher than the prediction.

The resisting moment *M* was then calculated using the curvature known from strain, $1/\rho$, and the theoretical flexural rigidity $EI=63.2 \times 10^6$ kip-in^2 (181,400 kN-m^2). For the 150 kip (667kN) test the applied moment was 4,524 kip-in (511 kN-m) and the resisting moment was 3,817 kip-in (431 kN-m), a 15% difference. For the 200 kip (890kN) test the applied moment was 5,974 kip-in (675 kN-m) and the calculated resisting moment was 5,479 kip-in (619 kN-m), an 8% difference. These results demonstrate that the transformed area flexural rigidity is fairly accurate. The missing moment may be carried by the concrete deck portions that are on the wing flanges.

3.7.3 Strain Integration

Using the same process as in the individual beam testing, the strain profiles were transformed to stress and integrated in order to calculate the moment. Again, the arch concrete was ignored due to cracking. In order to balance the internal forces the effective width of deck concrete was chosen to establish internal equilibrium. Ultimately, an effective width of 24 in. (61 cm) was used to be conservative for calculating moment capacity. The total moment resistance was calculated by summing the moments taken about the concrete deck force, as seen in Table 3**.** Similar to the arch in the non-composite case, the bending moments of the arch and FRP shell were calculated using curvature and added to the moment couples.

Table 3-3 Moment Contributions from Stress Integration of Composite Section at Midspan

	150 kip test				200 kip test			
	Force, kips (kN)	Moment Arm *d*, in.(cm)	Moment, kip-in. (kN-m)	Proportion	Force, kips (kN)	Moment Arm *d*, in.(cm)	Moment, kip-in. (kN-m)	Proportion
Beam			**3802 (429.6)**	**0.86**			**5236 (591.6)**	**0.85**
FRP	32.4 (144)	22.6 (57.4)	733 (82.8)	0.17	45.9 (204)	22.3 (56.6)	1024 (115.7)	0.17
Bending	N/A	N/A	580 (65.5)	0.13	N/A	N/A	771 (87.1)	0.12
Steel Strand	96.2 (428)	25.9 (65.8)	2489 (281.2)	0.56	131.5 (585)	26.2 (66.5)	3441 (388.8)	0.56
Deck			**638 (72.1)**	**0.14**			**916 (103.5)**	**0.15**
Compression	-146.7 (-653)	0	0	0.00	-179.7 (-799)	0	0	0
Bending	N/A	N/A	638 (72.1)	0.14	N/A	N/A	916 (103.5)	0.15
Total			**4440 (501.7)**				**6151 (695)**	

The beam (consisting of FRP and steel strand) took about 85% of the load and the deck carried 15% of the load in bending. The calculated resisting moment was within 3% of the applied moment (assuming simply supported end conditions) for both load cases. Assuming that the arch is cracked, the FRP and tension reinforcement are still responsible for resisting the majority of the applied flexural forces.

3.8 Design Recommendations and Conclusions

For the non-composite beams tested in this study, the arch system took about 80% of the total load while the shell system took about 20%. This was shown by comparing the contributions of all beam components calculated from curvature and from stress profiles. The proportion of the flexural rigidity *EI* of the tied arch to the beam as a whole (including the shell) was 80% as well. This ratio is the key for optimizing HCBs with different cross-sections. It is not feasible to perform

testing of this nature for any project using a new beam size, but this relationship means that the required forces can be easily predicted.

The current transformed area design method was confirmed to be accurate for the FRP and tension reinforcement, but the arch concrete does not have strain compatibility with the rest of the system. While neutral axis calculations are accurate, the FRP wings and shear fin should be taken into account to improve predictions. It is also important to consider these elements when finding the flexural rigidity of the beam. Strain within the FRP shell was found to be linear in the non-composite case, and all strains were below the elastic limit at service levels. High point loads applied away from the midspan also must be carefully analyzed due to the possibility of arch bending causing larger strains in the top flange of FRP.

Tests on the composite section also show that the transformed area method is acceptable for predicting system behavior. After breaking down the composite system into the beam and deck it was seen that even without the arch, the HCB is responsible for the majority of the moment capacity. Making the assumption that the arch is cracked leads to an easier design process since the cross section is then constant. Knowing at what load the arch cracks for the composite beam can be determined with a transformed section analysis including the arch. For the beam tested in this study, the arch was only important for ensuring the deck placement can be completed without excessive deflections.

Further testing on beams with different geometries would be very useful to further confirm the behavior found in this paper. More detailed strain measurements are needed to fully map the distribution and flow of forces in the shear fin, especially in the case of discrete point loads applied to the bridge deck. Having vibrating wire gages within the shear fin could allow arch behavior to be better understood, and analysis of internal forces away from midspan. Ongoing research will

determine a design method for shear forces and create a finite element model to examine overall behavior.

3.9 References

ASTM. (2002). *Standard Test Method for Static Modulus of Elasticity and Poisson's Ratio of Concrete in Compression.* (ASTM International, West Conshohocken, PA.)

ASTM. (2005). *Standard Test Method for Compressive Strength of Cylindrical Concrete Specimens.* (ASTM International, West Conshohocken, PA.)

Ahsan, S. (2012) "Evaluation of Hybrid-Composite Beam for Use in Tide Mill Bridge." Virginia Tech, Blacksburg, VA, 2012.

Elliot Company of Indianapolis. (2012) "ELFOAM Technical Data." *Elliot Company of Indianapolis*, <http://www.elliottfoam.com/tech.html> (7/21/12)

HC Bridge Company. "Build Better with HC Bridge Company." *HC Bridge Company*, <http://www.hcbridge.com/4801.html> (7/24/12)

Hillman, J.R. (2008). "Product Application of a Hybrid-Composite Beam System." *IDEA Program Final Report.* <http://onlinepubs.trb.org/onlinepubs/archive/studies/idea/finalreports/highspeedrail/hsr-43final_report.pdf>.

Hejll, A, Täljsten, B, and Motavalli, M. (2005). "Large scale hybrid FRP composite girders for use in bridge structures- theory, test, and field application." *Composites Part B.* 36, 573-585.

Honickman, H and Fam, A. (2009) "Investigating a Structural Form System for Concrete Girders Using Commercially Available GFRP Sheet-Pile Sections." *Journal of Composites for Construction, ASCE*. 13(5), 455-465.

Karbhari, V.M. (2002). "Durability of FRP composites for civil infrastructure- myth, mystery or reality." *Proc. Advanced polymer composites for structural applications in construction*. 33-44.

Karimi, K, Tait, M.J. and El-Dakhakhni, W.W. (2012). "Analytical modeling and axial load design of a novel FRP-encased steel-concrete composite column for various slenderness ratios." *Engineering Structures.* 46, 526-534.

Mascaro, M. (2012) "Out-of-Plane Web Deformation and Relative Arch Movement of Hybrid-Composite Beams Based on Photogrammetry." Virginia Tech, Blacksburg, VA, 2012.

Nordin, H. and Täljsten, B. (2004) "Testing of hybrid FRP composite beams in bending." *Composites Part B.* 35, 27-33.

Snape, T and Lindyberg, R. (2009) "Test Results: HC Beam for the Knickerbocker Bridge." AEWC Report 10-16 Project 671. MDOT 2009. < http://www.maine.gov/mdot/tr/documents/pdf/AEWC%20Project%20671%20Report%2010-16%20Testing%20of%20HCB%20for%20Knickerbocker%20Bridge.pdf> (7/24/13)

Wu, T.J. and Hahn, H. T. (1997). "Mechanical Properties of E-Glass/Vinyl Ester Composite Fabricated by VARTM." *Proc., International SAMPE Symposium and Exhibition*, SAMPE, Covina, CA, 1-12.

4 Conclusions

This thesis detailed work performed to determine the load distribution within a hybrid composite beam. The distribution of load within the non-composite beam corresponded to the proportion of flexural rigidity of the two main components, the tied arch and FRP shell, compared to the beam as a whole. Previous design assumptions concerning strain compatibility and a linear strain profile were shown to be valid, though the concrete arch did not show strain compatibility with the other components. During composite loading the arch in the specimens was acting in tension and cracked, but the beams still were capable of providing the necessary strength for design loads.

Future work at Virginia Tech will further examine design for shear and ultimate limit states of the HCB, as well as model a finite element analysis of the beam. Other recommended future work is tests on beams of differing cross-section to verify the conclusions made in this paper. Placing additional gages in the shear fin, as shown in Figure 4-1, can lead to better understanding of the force path within the arch. An additional gage in the deck can also help determine the stain properties within the deck- placing them on the lower rebar will create a better profile.

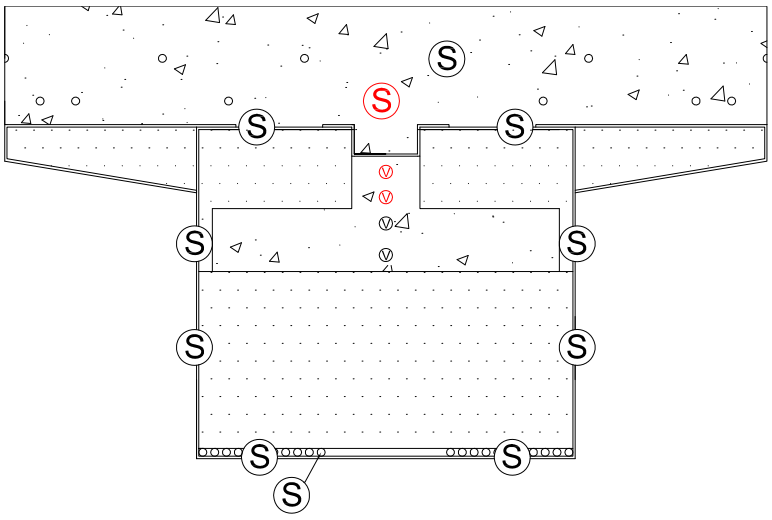

Figure 4-1 Cross-Section View with Additional Gages for Strain Profile in Shear Fin

Additionally, having strain data within the arch during the deck pour would be helpful for keeping track of the overall strain in the concrete to verify whether it has exceeded its rupture strain during testing.

The following appendices offer a further look at work done for this thesis. Appendix A details the testing, data, and analysis further, providing the exact data points and spreadsheets used to find transformed section properties and internal forces. Appendix B provides guidance on limit states for design and includes a Mathcad sheet that can be used for design of an HCB.

References

AASHTO. (2008). *Guide Specifications for Design of FRP Pedestrian Bridges*, 1st ed. (American Association of State Highway and Transportation Officials, Washington, DC.)

ASCE. (1984). *Structural Plastics Design Manual*. ASCE Manual No. 63. (American Society of Civil Engineers, Reston, VA.)

ASTM. (2002). *Standard Test Method for Static Modulus of Elasticity and Poisson's Ratio of Concrete in Compression.* (ASTM International, West Conshohocken, PA.)

ASTM. (2005). *Standard Test Method for Compressive Strength of Cylindrical Concrete Specimens.* (ASTM International, West Conshohocken, PA.)

Ahsan, S. (2012) "Evaluation of Hybrid-Composite Beam for Use in Tide Mill Bridge." Virginia Tech, Blacksburg, VA, 2012.

Culmo, M.P. and Seraderian, R.L. (2010). "Development of the northeast extreme tee (NEXT) beam for accelerated bridge construction." *PCI Journal*. Summer 2010. 86-101.

Elliot Company of Indianapolis. (2012) "ELFOAM Technical Data." *Elliot Company of Indianapolis,* <http://www.elliottfoam.com/tech.html> (7/21/12)

Federal Highway Administration (FHWA). (2009). "Connection details for prefabricated bridge elements and systems." *FHWA-PL-05-003*, Office of Engineering, Bridge Division, Washington, DC.

Findley, W.N. (1987) "26-year creep and recovery of poly (vinyl chloride) and polyethylene. *Polymer Engineering and Science*. 27(8), 582-585.

Fleck, S. and Kuzy, G. (2012). "Bridge-In-a-Backpack: Saving the Nation's Bridges One Backpack at a Time." < 136.142.82.187/eng12/Author/data/2266.doc> (4/7/13)

Hällmark, R., White, H., Collin, P. (2012). "Prefabricated Bridge Construction across Europe and America." *ASCE Practice Periodical on Structural Design and Construction.* 17(3), 82-92.

Hanus, J.P., Bank, L.C., Ray, J.C., Velazques, G.I. (2006). "Optimized Design and Testing of a Prototype Military Bridge System for Rapid In-Theater Construction." < http://www.dtic.mil/cgi-bin/GetTRDoc?AD=ADA481580> (4/7/13).

HC Bridge Company. "Build Better with HC Bridge Company." *HC Bridge Company*, <http://www.hcbridge.com/4801.html> (7/24/12)

Hillman, J.R. (2008). "Product Application of a Hybrid-Composite Beam System." *IDEA Program Final Report*. <http://onlinepubs.trb.org/onlinepubs/archive/studies/idea/finalreports/highspeedrail/hsr-43final_report.pdf>.

Hejll, A, Täljsten, B, and Motavalli, M. (2005). "Large scale hybrid FRP composite girders for use in bridge structures- theory, test, and field application." *Composites Part B*. 36, 573-585.

Hollaway, L.C. (2010). "A review of the present and future utilisation of FRP composites in the civil infrastructure with reference to their important in-service properties." *Construction and Building Materials*. 24, 2419-2445.

Honickman, H and Fam, A. (2009) "Investigating a Structural Form System for Concrete Girders Using Commercially Available GFRP Sheet-Pile Sections." *Journal of Composites for Construction, ASCE*. 13(5), 455-465.

Karbhari, V.M. (2002). "Durability of FRP composites for civil infrastructure- myth, mystery or reality." *Proc. Advanced polymer composites for structural applications in construction*. 33-44.

Karimi, K, Tait, M.J. and El-Dakhakhni, W.W. (2012). "Analytical modeling and axial load design of a novel FRP-encased steel-concrete composite column for various slenderness ratios." *Engineering Structures.* 46, 526-534.

Mascaro, M. (2012) "Out-of-Plane Web Deformation and Relative Arch Movement of Hybrid-Composite Beams Based on Photogrammetry." Virginia Tech, Blacksburg, VA, 2012.

Microsoft. (2013) *Microsoft Excel 2013*, (computer software).

Nordin, H. and Täljsten, B. (2004) "Testing of hybrid FRP composite beams in bending." *Composites Part B.* 35, 27-33.

Sá, M.F., Gomes, A.M., Correia, J.R., Silvestre, N. (2011). "Creep behavior of pultruded GFRP elements- Part 1: Literature review and experimental study." *Composite Structures*. 93, 2450-2459.

Scott, D., Lai, J., Zureick, A. (1995). "Creep Behavior of Fiber-Reinforced Polymeric Composites: A Review of Current Literature." *Journal of Reinforced Plastics and Composites*, 14(6), 588.

Snape, T. and Lindyberg, R. (2009) "Test Results: HC Beam for the Knickerbocker Bridge." AEWC Report 10-16 Project 671. MDOT 2009. < http://www.maine.gov/mdot/tr/documents/pdf/AEWC%20Project%20671%20Report%2010-16%20Testing%20of%20HCB%20for%20Knickerbocker%20Bridge.pdf> (7/24/13)

United States Dept. of the Army. (2006). "Technical Manual 5-5420-280-23&P for Rapidly Emplaced Bridge." < http://test.steelsoldiers.com/upload/misc/TM5-5420-280-23&P.pdf> (4/7/13)

Van Nosdall, S, Moen, C, Cousins, T, and Roberts-Wollmann, C. (2013). "Experiments on a Hybrid-Composite Beam for Bridge Applications." *Transportation Research Record: Journal of the Transportation Research Board*, Transportation Research Board, Washington, D.C., (forthcoming).

Wu, T.J. and Hahn, H. T. (1997). "Mechanical Properties of E-Glass/Vinyl Ester Composite Fabricated by VARTM." *Proc., International SAMPE Symposium and Exhibition*, SAMPE, Covina, CA, 1-12.

APPENDIX A Review of Data and Calculations

A1 Testing Program

Three 44 foot long beam shells were fabricated at Harbor Technologies plant in Brunswick, ME and then shipped to Virginia Tech. Design was completed by the HCBridge Company. Once in the lab the beams were set up with a 43 foot simple span (pin on one end, roller on other) and the lids were attached using epoxy and screws.

Preparation for the first phase of testing began by placing the shear connectors in the beam, which were #4 bars with 90 degree bends. A concrete pump used to fill the conduit with self-consolidating concrete by filling holes at either end of the beam until the concrete reached the top of the lid, then moving on to the next hole. The arches cured over 28 days. Testing was performed to determine the behavior of the individual HCBs. A load-frame was assembled at the midspan of the beam and a hydraulically powered 100 kip actuator was placed above the centerline of the beam. The frame and actuator were moved into similar positions for tests on the other two beams. Each beam had a total of 4 tests performed- twice with a load of 15 kips at midspan and twice with two 12.5 kip point loads at the quarter points. The quarter point loads were accomplished by setting up a spreader beam resting on two short W sections placed over the quarter points. Each test was performed in increments of 5 kips.

Finally, preparation began for the composite testing on the three girder bridge system with skew angle. The end diaphragms and deck reinforcement imitated the actual designs planned for use in the Tide Mill Bridge, and the concrete used for each was the standard A4 mix used by VDOT. The diaphragms were placed first, followed by construction of the formwork for the deck. Deck placement required two trucks, and each batch had samples taken for material testing. The deck was moist-cured for 21 days. Service level testing then commenced on the bridge system.

This research focuses on the final tests performed on the system, where it was under design loads. For these tests, the actuator was focused over the midpoint of the center beam, and a spreader beam distributed the load into two point loads over approximately the third points of the beam. Two tests were performed, one to a total of 150 kips and the other to 200 kips. Due to the large number of gages present on the system full data was only available for the center beam.

A2 Instrumentation

A2.1 Tension Reinforcement

During the fabrication process of the FRP shells one tension strand in each beam was instrumented at the midspan and one quarter point using 1/8 in. long electrical resistance strain gages. These gages were selected due to their low cost and profile. It was important that the gages not be bulky as that could have interfered with the FRP infusion process. The gages were attached in the longitudinal direction on one of the seven wires that made up each strand. Since the wires spiraled around each other the measured strains were of a direction parallel to one wire, and had to be converted to the direction of the overall strand. Testing for this conversion factor was performed at Virginia Tech, as detailed by Ahsan.

A2.2 FRP Shell

Adhesively bonded ¼ in. long electrical resistance strain gages were attached to the exterior faces of the FRP shell of all three beams at one quarter point and the midspan. Gages were placed at depths of 0 in., 7 in., 14 in. and 21 in. to provide data for a full strain profile. A cross section view showing gage locations can be seen in Figure A-1.

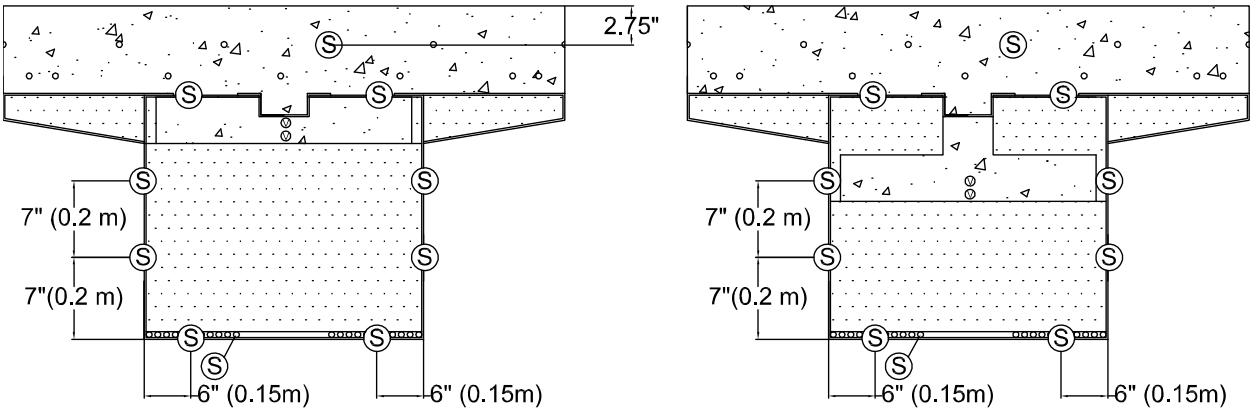

Figure A-1 Diagram of Instrumentation Positions

A2.3 Deck Reinforcement

1/8 in. adhesively bonded gages were placed on a piece of longitudinal steel reinforcement above each beam. These gages, again placed at midspan and a quarter point, allowed for a composite strain profile to be created.

A2.4 Vibrating Wire Gages

To measure strains within the concrete arch vibrating wire gages were placed before the arch was poured. Two gages were used to be able to show bending, with gages placed approximately an inch from the top and bottom of the arch. The bottom gages were attached to the loose tension strands that run through the arch for tying the shear connectors. The top gages at quarter points were held by cages of tie wire that connected into the top foam. At midspan the gage was tied to a chair and held in place to ensure proper alignment.

A2.5 Potentiometers

Deflections of all beams were measured at both quarter points and midspan using wire potentiometers. The wires were connected to the beam using Nylon string as the wires otherwise could not reach the bottom of the beam. Accuracy of potentiometers was to the nearest 0.005 in.

A3 Data Analysis

All conclusions were based on strain data coming from the testing of full scale specimens in Virginia Tech's structural engineering lab. Electronic strain gages (on the FRP and steel) had measurements recorded at a rate of ten readings per second. The vibrating wire gages were recorded at a rate of 50 readings per second during non-composite testing and reduced to match the rate of the electronic gages.

Each spreadsheet had an overwhelming amount of data, so MATLAB was used to pick out data points to be analyzed. A function was written to check the applied load for the load cell to find when the applied load had reached one of the 5 kip increments, then retrieved a row from that period. The function then wrote the strain values into another Excel spreadsheet that had been set-up to be easier to read. Values from the beginning of the test (with no applied load from the actuator) were also read and placed in the new sheet in order to normalize the data. The data then could be examined for each test, showing the progression of each gage's readings at each load increment, as seen below in Tables A-2 through A-5. The test naming convention established by Ahsan was reused in these tables, with the form B(Beam #)-(Loading Configuration)(Test #). For "Loading Configuration" a "P" indicates a test with the point load at midspan, while a "Q" indicates the point loads at quarter points. For example, test "B1-P2" indicates the second midspan loading test performed on beam 1. The positions of gages can be seen in Figure A-2.

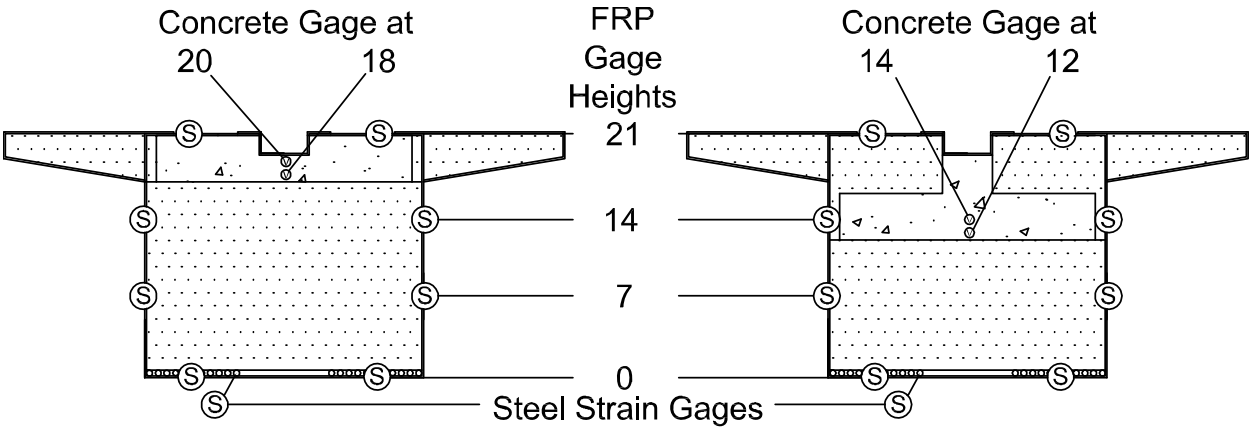

Figure A-2 Instrumentation with Heights Labeled For Tables A-2 to A-5

Readings were checked for accuracy, and any gages though to be in error were noted and discarded. The criteria for doing this was checking that the gage readings reflected the logical trend- simply put, that the gage readings were showing compression above the neutral axis and tension below, the magnitude of strain values did not decrease as the load increased. Similar processes were used to examine the strain values recorded by the tension strand gages and vibrating wire gages. For the strand gages there was an additional step of multiplying by a conversion factor to account for the fact that gages were attached to a spiraling wire, but the desired strain was longitudinal.

Table A-1 Midspan Strain Readings During Midspan Test

Midspan Point Strains During Test B1-P1 (με)				
Gage Height (in.)	5 kips	10 kips	15 kips	Use Data?
FRP Gages				
21	1655.5	1441.7	1229.0	NO
	-138.7	-291.0	-441.9	Yes
14	31.8	58.4	86.9	Yes
	54.6	110.6	168.0	Yes
7	136.3	276.4	413.2	Yes
	156.3	322.2	485.7	Yes
0	283.2	580.0	869.7	Yes
	276.1	568.0	854.3	Yes
Steel Strand Gage				
0.5	238.5	492.3	744.6	Yes
Concrete Vibrating Wire Gage				
12	-29.9	-62.9	-96.1	Yes
14	-41.1	-86.5	-131.6	Yes

Midspan Point Strains During Test B1-P2 (με)				
Gage Height (in.)	5 kips	10 kips	15 kips	Use Data?
FRP Gages				
21	-163.5	-344.0	-538.6	Yes
	-137.2	-262.5	-402.5	Yes
14	28.5	56.0	85.9	Yes
	59.4	118.8	182.0	Yes
7	135.8	273.6	418.5	Yes
	162.9	328.3	501.2	Yes
0	285.6	580.0	886.4	Yes
	279.6	569.3	872.5	Yes
Steel Strand Gage				
0.5	242.5	496.3	765.6	Yes
Concrete Vibrating Wire Gage				
12	-27.6	-60.2	-92.6	Yes
14	-38.9	-83.1	-127.5	Yes

Midspan Point Strains During Test B2-P1 (με)				
Gage Height (in.)	5 kips	10 kips	15 kips	Use Data?
FRP Gages				
21	-168.4	-345.2	-520.1	Yes
	-178.7	-420.6	-1051.5	Yes
14	18.5	40.9	59.9	Yes
	50.1	106.3	141.6	Yes
7	121.1	249.9	387.3	Yes
	144.3	291.9	436.3	Yes
0	282.3	579.5	895.4	Yes
	256.2	552.9	860.2	Yes
Steel Strand Gage				
0.5	240.4	486.5	742.3	Yes
Concrete Vibrating Wire Gage				
12	-24.0	-46.4	-72.2	Yes
14	-58.2	-119.4	-184.9	Yes

Midspan Point Strains During Test B2-P2 (με)				
Gage Height (in.)	5 kips	10 kips	15 kips	Use Data?
FRP Gages				
21	-323.5	-541.2	-753.1	Yes
	-192.4	-561.3	-1261.3	Yes
14	20.0	37.6	56.6	Yes
	46.2	87.7	127.3	Yes
7	125.9	249.5	376.9	Yes
	138.1	274.8	414.4	Yes
0	285.2	570.5	861.8	Yes
	266.7	535.4	809.5	Yes
Steel Strand Gage				
0.5	233.7	466.9	709.7	Yes
Concrete Vibrating Wire Gage				
12	-22.6	-45.7	-68.1	Yes
14	-59.0	-121.2	-182.9	Yes

Midspan Point Strains During Test B3-P1 (με)				
Gage Height (in.)	5 kips	10 kips	15 kips	Use Data?
FRP Gages				
21	-195.6	-363.1	-532.5	Yes
	-246.9	-418.4	-588.8	Yes
14	43.6	75.8	110.4	Yes
	67.9	118.2	165.2	Yes
7	166.0	300.8	433.7	Yes
	197.0	351.0	502.7	Yes
0	232.5	429.9	643.6	Yes
	296.1	549.8	821.1	Yes
Steel Strand Gage				
0.5	N/A	N/A	N/A	NO
Concrete Vibrating Wire Gage				
12	-20.4	-35.7	-50.5	Yes
14	-61.3	-111.3	-160.6	Yes

Midspan Point Strains During Test B3-P2 (με)				
Gage Height (in.)	5 kips	10 kips	15 kips	Use Data?
FRP Gages				
21	-159.5	-327.0	-386.3	Yes
	-154.6	-320.6	-488.5	Yes
14	34.6	67.3	101.9	Yes
	48.4	100.6	150.0	Yes
7	134.3	270.0	404.3	Yes
	151.1	309.3	463.8	Yes
0	183.1	385.8	599.5	Yes
	232.3	491.8	765.1	Yes
Steel Strand Gage				
0.5	N/A	N/A	N/A	NO
Concrete Vibrating Wire Gage				
12	-15.5	-32.6	-50.1	Yes
14	-47.2	-99.3	-152.2	Yes

Table A-2 Quarter Point Strain Readings During Midspan Test

Midspan Point Strains During Test B1-P1 (με)				
Gage Height (in.)	5 kips	10 kips	15 kips	Use Data?
FRP Gages				
21	-82.4	-169.1	-256.7	NO
	-126.6	-275.3	-424.0	Yes
14	-14.7	-22.2	-27.4	Yes
	-4.3	-12.8	-19.4	Yes
7	67.4	139.0	210.2	Yes
	80.8	169.6	259.9	Yes
0	111.3	228.4	342.6	Yes
	138.8	286.7	431.8	Yes
Steel Strand Gage				
0.5	146.0	296.6	445.0	Yes
Concrete Vibrating Wire Gage				
12	-3.7	-9.2	-16.3	Yes
14	-40.7	-85.2	-128.2	Yes

Midspan Point Strains During Test B1-P2 (με)				
Gage Height (in.)	5 kips	10 kips	15 kips	Use Data?
FRP Gages				
21	-127.9	-235.9	-328.8	Yes
	-169.3	-325.7	-467.0	Yes
14	-18.0	-28.9	-30.3	Yes
	-6.2	-4.3	6.6	Yes
7	63.0	126.5	202.5	Yes
	66.1	136.4	218.2	Yes
0	110.4	222.2	344.0	Yes
	136.5	277.2	429.9	Yes
Steel Strand Gage				
0.5	141.4	283.4	436.3	Yes
Concrete Vibrating Wire Gage				
12	-221.9	-491.6	-672.9	NO
14	-339.7	-674.0	-870.7	NO

Midspan Point Strains During Test B2-P1 (με)				
Gage Height (in.)	5 kips	10 kips	15 kips	Use Data?
FRP Gages				
21	-29.9	-44.1	-45.0	Yes
	-184.0	-378.5	-580.9	Yes
14	4.8	8.1	21.4	Yes
	22.3	17.6	15.7	Yes
7	82.3	167.1	261.8	Yes
	87.5	172.1	262.5	Yes
0	130.8	265.5	414.1	Yes
	125.4	257.9	405.1	Yes
Steel Strand Gage				
0.5	151.4	306.8	470.7	Yes
Concrete Vibrating Wire Gage				
12	-12.7	-25.4	-38.4	Yes
14	-37.9	-76.6	-119.5	Yes

Midspan Point Strains During Test B2-P2 (με)				
Gage Height (in.)	5 kips	10 kips	15 kips	Use Data?
FRP Gages				
21	-27.0	-37.0	-43.6	Yes
	-187.3	-377.5	-564.7	Yes
14	7.6	15.2	23.3	Yes
	0.9	-0.9	-3.3	Yes
7	86.6	170.9	259.5	Yes
	82.7	168.3	254.8	Yes
0	132.7	267.0	406.4	Yes
	127.7	258.3	398.5	Yes
Steel Strand Gage				
0.5	151.4146	303.431	458.8662	Yes
Concrete Vibrating Wire Gage				
12	-12.0	-24.5	-37.8	Yes
14	-37.8	-77.9	-117.1	Yes

Midspan Point Strains During Test B3-P1 (με)				
Gage Height (in.)	5 kips	10 kips	15 kips	Use Data?
FRP Gages				
21	-70.7	-96.8	-100.1	Yes
	-150.5	-270.6	-396.8	Yes
14	-19.4	-36.9	-52.1	Yes
	-11.9	-28.5	-46.2	Yes
7	112.8	202.0	293.5	Yes
	96.4	172.4	248.9	Yes
0	192.9	347.4	509.1	Yes
	200.2	360.3	527.0	Yes
Steel Strand Gage				
0.5	N/A	N/A	N/A	NO
Concrete Vibrating Wire Gage				
12	-18.4	-33.4	-47.0	Yes
14	-125.3	-144.0	-168.8	Yes

Midspan Point Strains During Test B3-P2 (με)				
Gage Height (in.)	5 kips	10 kips	15 kips	Use Data?
FRP Gages				
21	-47.5	-80.2	-100.1	Yes
	-116.3	-244.0	-378.8	Yes
14	-11.8	-28.9	-46.4	Yes
	-15.7	-33.8	-50.0	Yes
7	88.2	178.3	268.0	Yes
	73.1	152.5	231.8	Yes
0	153.5	313.7	473.0	Yes
	160.0	326.2	491.0	Yes
Steel Strand Gage				
0.5	155.5	316.0	474.4	Yes
Concrete Vibrating Wire Gage				
12	-13.9	-28.6	-44.7	Yes
14	111.6	180.7	119.3	NO

Figure A-4 Midspan Strain Readings During Quarter Point Test

Midspan Point Strains During Test B1-Q1 (με)						
Gage Height (in.)	5 kips	10 kips	15 kips	20 kips	25 kips	Use Data?
FRP Gages						
21	-65.5	-137.2	-210.8	-284.4	-360.8	Yes
	-47.3	-97.5	-148.6	-198.7	-251.2	Yes
14	10.4	20.4	29.4	42.7	60.7	Yes
	12.8	26.1	39.4	51.7	64.1	Yes
7	67.0	137.3	206.1	272.2	342.0	Yes
	70.6	144.5	218.4	291.9	366.3	Yes
0	146.9	301.0	454.1	603.1	759.2	Yes
	142.9	292.6	444.1	589.1	741.7	Yes
Steel Strand Gage						
0.5	125.5	255.5	387.9	516.8	653.8	Yes
Concrete Vibrating Wire Gage						
12	-23.8	-48.4	-73.3	-98.9	-124.2	Yes
14	-26.0	-52.5	-79.8	-107.5	-134.7	Yes

Midspan Point Strains During Test B1-Q2 (με)						
Gage Height (in.)	5 kips	10 kips	15 kips	20 kips	25 kips	Use Data?
FRP Gages						
21	-64.0	-135.5	-207.6	-279.6	-358.2	Yes
	-47.3	-97.4	-200.0	-246.3	-298.3	Yes
14	5.7	11.9	32.3	38.9	46.0	Yes
	14.2	27.5	46.1	58.4	71.7	Yes
7	67.0	136.3	206.1	275.5	348.7	Yes
	70.6	146.9	223.2	296.7	375.4	Yes
0	146.4	301.0	459.4	612.6	773.5	Yes
	141.5	292.4	446.8	595.5	753.7	Yes
Steel Strand Gage						
0.5	123.2	256.1	394.1	528.2	669.1	Yes
Concrete Vibrating Wire Gage						
12	-22.5	-47.1	-72.5	-97.7	-124.5	Yes
14	-24.5	-51.2	-79.1	-106.4	-135.7	Yes

Midspan Point Strains During Test B2-Q1 (με)						
Gage Height (in.)	5 kips	10 kips	15 kips	20 kips	25 kips	Use Data?
FRP Gages						
21	-88.1	-170.1	-243.0	-314.0	-387.4	Yes
	-90.2	-208.9	-349.9	-503.2	-624.1	Yes
14	4.8	10.5	17.6	23.3	29.5	Yes
	14.8	30.0	40.0	54.8	68.7	Yes
7	66.1	132.1	198.2	263.8	330.9	Yes
	70.5	139.5	205.7	276.2	346.8	Yes
0	156.6	312.8	468.1	625.8	785.5	Yes
	146.7	293.4	436.3	583.6	733.8	Yes
Steel Strand Gage						
0.5	130.6	260.7	387.9	520.9	655.5	Yes
Concrete Vibrating Wire Gage						
12	N/A	N/A	N/A	N/A	N/A	NO
14	N/A	N/A	N/A	N/A	N/A	NO

Midspan Point Strains During Test B2-Q2 (με)						
Gage Height (in.)	5 kips	10 kips	15 kips	20 kips	25 kips	Use Data?
FRP Gages						
21	-86.7	-163.9	-242.0	-323.4	-388.8	Yes
	-69.3	-168.1	-278.3	-388.9	-476.2	Yes
14	6.2	12.8	18.5	26.1	32.3	Yes
	14.8	27.2	39.1	50.5	62.9	Yes
7	63.2	131.2	194.9	261.9	328.0	Yes
	68.1	137.1	204.3	272.4	339.6	Yes
0	151.4	307.2	459.6	618.3	772.7	Yes
	141.9	288.2	431.2	577.5	722.5	Yes
Steel Strand Gage						
0.5	125.5	257.3	382.9	514.7	644.8	Yes
Concrete Vibrating Wire Gage						
12	-25.5	-52.9	-79.6	-106.6	-133.8	Yes
14	-33.0	-68.1	-102.0	-136.6	-171.4	Yes

Midspan Point Strains During Test B3-Q1 (με)						
Gage Height (in.)	5 kips	10 kips	15 kips	20 kips	25 kips	Use Data?
FRP Gages						
21	-73.9	-154.0	-237.0	-321.3	-404.2	Yes
	-55.6	-113.6	-170.2	-228.7	-286.7	Yes
14	11.8	20.8	32.2	42.6	55.9	Yes
	12.3	26.1	37.0	47.5	58.9	Yes
7	69.3	134.7	201.6	270.0	342.1	Yes
	73.4	145.9	217.9	289.9	364.8	Yes
0	101.1	201.7	307.1	417.3	536.5	Yes
	126.8	254.6	388.6	528.8	679.5	Yes
Steel Strand Gage						
0.5	N/A	N/A	N/A	N/A	N/A	NO
Concrete Vibrating Wire Gage						
12	-21.7	-44.0	-67.4	-90.5	-113.6	Yes
14	-13.6	-53.2	-2407.0	-2407.0	-146.7	NO

Midspan Point Strains During Test B3-Q2 (με)						
Gage Height (in.)	5 kips	10 kips	15 kips	20 kips	25 kips	Use Data?
FRP Gages						
21	-70.2	-152.7	-235.1	-313.8	-389.1	Yes
	-55.7	-112.3	-170.7	-227.8	-285.8	Yes
14	11.4	22.3	33.6	45.0	51.2	Yes
	11.9	23.7	35.1	47.5	65.0	Yes
7	67.4	134.3	203.1	272.5	335.1	Yes
	71.5	146.9	218.9	291.4	368.2	Yes
0	96.8	199.9	303.4	413.1	521.5	Yes
	118.8	247.6	379.7	519.0	658.7	Yes
Steel Strand Gage						
0.5	N/A	N/A	N/A	N/A	N/A	NO
Concrete Vibrating Wire Gage						
12	-20.7	-43.3	-66.4	-89.7	-113.1	Yes
14	-2418.2	-2418.2	-2418.2	-2418.2	-2418.2	NO

Figure A-5 Quarter Point Strain Readings During Quarter Point Test

Quarter Point Strains During Test B1-Q1 (με)						
Gage Height (in.)	5 kips	10 kips	15 kips	20 kips	25 kips	Use Data?
FRP Gages						
21	-151.0	-312.9	-470.0	-604.4	-731.1	Yes
	-159.7	-313.1	-452.4	-576.1	-694.0	Yes
14	-30.3	-70.0	-102.7	-139.6	-169.4	Yes
	-17.5	-30.8	-41.2	-47.4	-53.1	Yes
7	55.0	111.9	167.8	221.8	280.2	Yes
	55.6	113.5	174.3	235.6	301.7	Yes
0	100.0	203.4	308.6	409.6	517.3	Yes
	124.7	255.1	387.0	515.6	650.9	Yes
Steel Strand Gage						
0.5	N/A	N/A	N/A	N/A	N/A	NO
Concrete Vibrating Wire Gage						
12	75.7	181.5	285.0	390.3	471.1	Yes
14	-88.2	-190.3	-279.2	-353.5	-413.9	NO

Quarter Point Strains During Test B1-Q2 (με)						
Gage Height (in.)	5 kips	10 kips	15 kips	20 kips	25 kips	Use Data?
FRP Gages						
21	-151.5	-298.8	-431.3	-542.0	-644.7	Yes
	-191.8	-378.4	-561.1	-725.3	-882.4	Yes
14	-32.6	-71.0	755.3	733.0	710.8	NO
	-18.5	-34.6	-47.9	-57.8	-67.3	Yes
7	51.1	105.0	172.4	226.8	283.6	Yes
	53.2	111.7	146.9	209.2	274.8	Yes
0	98.6	203.4	-1942.2	-1939.8	-1879.4	NO
	122.3	253.7	390.7	520.7	661.2	Yes
Steel Strand Gage						
0.5	N/A	N/A	N/A	N/A	N/A	NO
Concrete Vibrating Wire Gage						
12	11.7	69.7	69.7	69.7	69.7	NO
14	-191.0	-336.5	-457.6	-555.7	-644.5	Yes

Quarter Point Strains During Test B2-Q1 (με)						
Gage Height (in.)	5 kips	10 kips	15 kips	20 kips	25 kips	Use Data?
FRP Gages						
21	-196.1	-283.7	-309.3	-312.1	-317.8	NO
	-158.4	-364.8	-538.8	-693.2	-827.2	Yes
14	-9.5	-13.3	-26.2	-41.4	-58.5	Yes
	-12.8	-38.0	-70.7	-10.4	33.2	NO
7	62.4	143.8	211.4	279.6	346.3	Yes
	65.1	146.9	216.4	286.3	354.8	Yes
0	123.3	264.7	395.1	530.9	675.7	Yes
	117.3	255.6	385.4	524.7	674.0	Yes
Steel Strand Gage						
0.5	139.6	289.5	431.4	577.4	730.1	Yes
Concrete Vibrating Wire Gage						
12	N/A	N/A	N/A	N/A	N/A	NO
14	N/A	N/A	N/A	N/A	N/A	NO

Quarter Point Strains During Test B2-Q2 (με)						
Gage Height (in.)	5 kips	10 kips	15 kips	20 kips	25 kips	Use Data?
FRP Gages						
21	-107.5	-190.8	-218.3	-241.5	-253.8	NO
	-188.9	-370.0	-522.2	-661.4	-789.2	Yes
14	-16.2	-33.3	-49.0	-62.3	-77.1	Yes
	-9.5	-13.8	-11.9	-10.0	-4.7	NO
7	57.6	117.6	176.7	242.4	306.3	Yes
	63.7	129.3	194.5	261.6	330.5	Yes
0	123.3	251.4	379.5	512.9	646.3	Yes
	117.4	243.3	372.6	510.0	647.4	Yes
Steel Strand Gage						
0.5	135.2	277.1	415.1	557.7	699.8	Yes
Concrete Vibrating Wire Gage						
12	2.8	12.4	35.4	87.3	165.4	Yes
14	-103.5	-218.2	-302.0	-356.6	-398.1	Yes

Quarter Point Strains During Test B3-Q1 (με)						
Gage Height (in.)	5 kips	10 kips	15 kips	20 kips	25 kips	Use Data?
FRP Gages						
21	-196.3	-265.1	-200.6	-195.4	-187.3	NO
	-212.5	-414.1	-616.0	-803.2	-978.9	Yes
14	-34.6	-72.4	-98.9	-122.1	-141.5	Yes
	-35.7	-73.7	-112.3	-155.1	-200.2	Yes
7	63.5	124.3	188.3	252.3	321.2	Yes
	55.1	111.2	168.7	227.1	288.9	Yes
0	145.5	286.8	431.9	578.1	732.3	Yes
	151.1	298.4	450.0	603.6	763.4	Yes
Steel Strand Gage						
0.5	143.7	285.2	430.7	577.4	730.8	Yes
Concrete Vibrating Wire Gage						
12	19.7	43.8	68.5	93.6	125.0	Yes
14	-25.9	-58.7	-2187.8	-136.6	-164.9	Yes

Quarter Point Strains During Test B3-Q2 (με)						
Gage Height (in.)	5 kips	10 kips	15 kips	20 kips	25 kips	Use Data?
FRP Gages						
21	-229.2	-323.1	-242.9	-233.5	-77.8	NO
	-202.2	-413.8	-622.4	-831.5	-1193.4	Yes
14	-35.0	-74.8	-103.2	-129.7	-171.3	Yes
	-36.2	-75.7	-115.1	-153.2	-177.9	Yes
7	61.6	127.1	191.1	255.1	310.6	Yes
	52.7	107.9	164.4	223.8	289.9	Yes
0	140.3	287.4	434.4	579.6	721.6	Yes
	145.4	298.9	452.0	605.1	760.2	Yes
Steel Strand Gage						
0.5	139.8	287.5	432.4	580.1	727.4	Yes
Concrete Vibrating Wire Gage						
12	19.8	46.2	72.4	97.9	125.4	Yes
14	-38.1	-59.2	-102.2	-2213.2	-171.7	Yes

Once values were verified, they were transferred to a diagram that would show all readings for an individual test configuration for the maximum load. The diagrams for both test configurations can be seen in Figures A-3 and A-4.

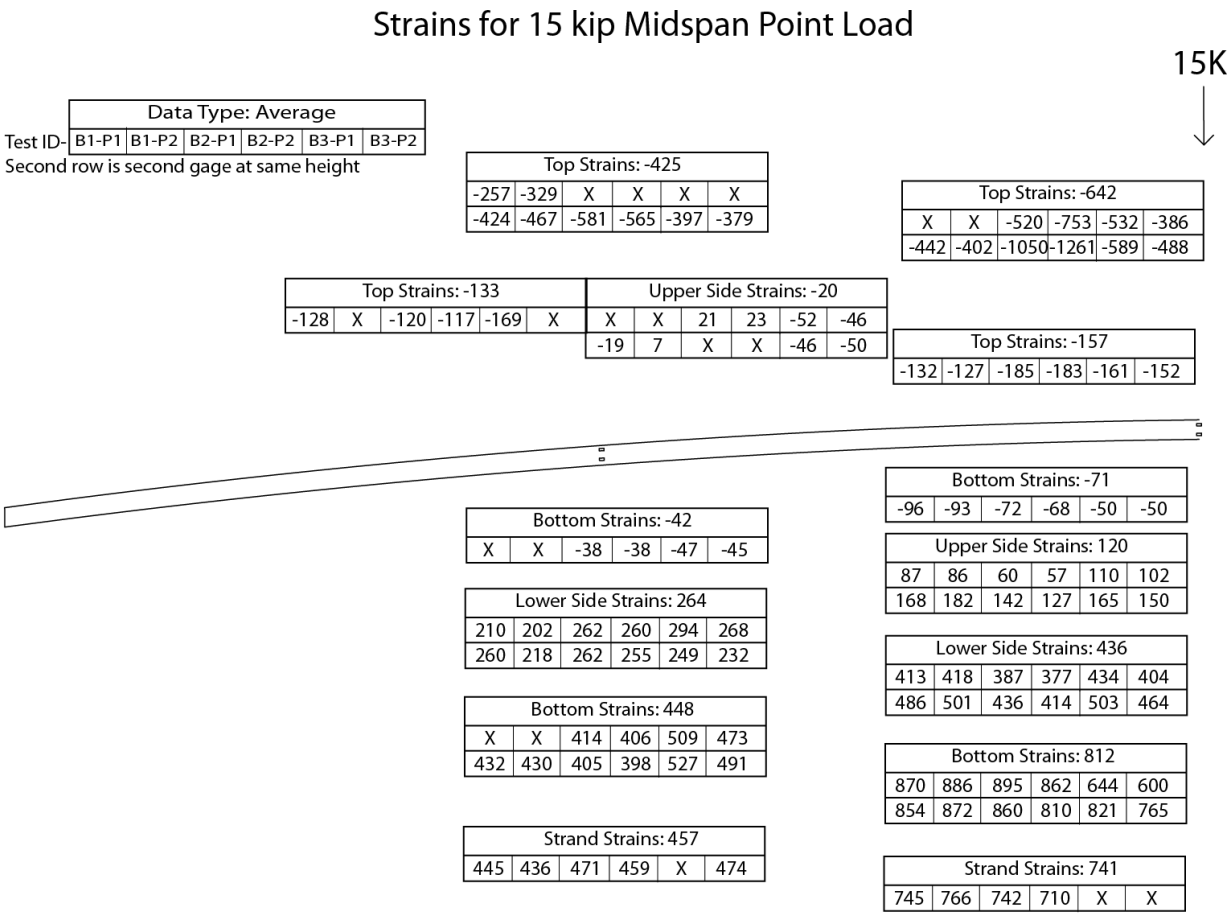

Figure A-3 Strains at Maximum Load During Midspan Test

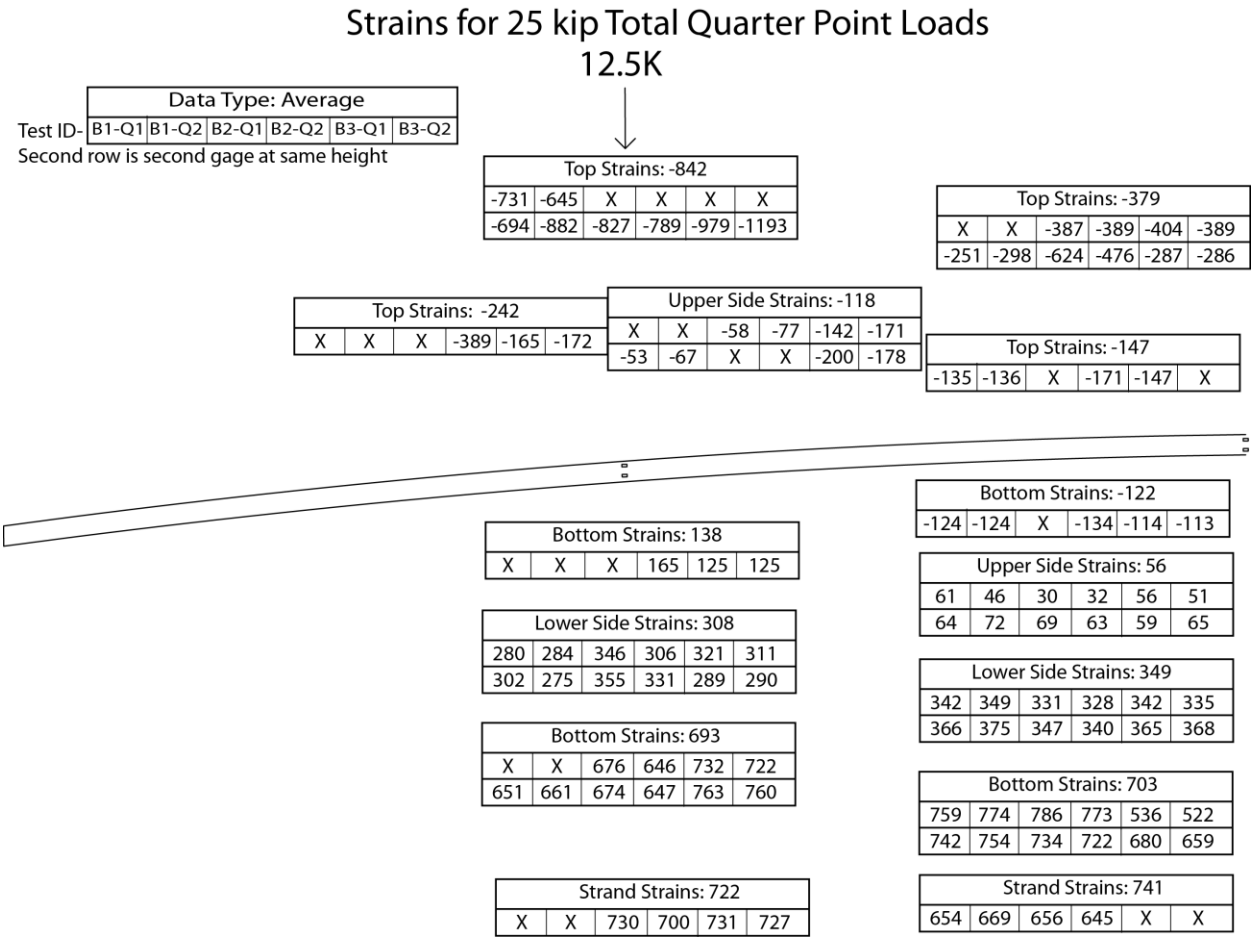

Figure A-4 Strains at Maximum Load During Quarter Point Test

These diagrams show all the individual points as well as the averages. These data points were then plotted to make a strain profile using MATLAB, included in the final report.

It can be observed from the individual data points in the strain profiles in Figure 3-5 that the spread of data is much greater during some tests than others. To better see where the data came from, the following additional plots in Figures A-5 and A-6 were created, displaying the FRP strains differentiated by color according to which beams' tests they came from. In the figure, red circles correspond to the two tests performed on Beam 1, green squares are from the two tests performed on Beam 2, and blue triangles are from the two tests performed on Beam 3.

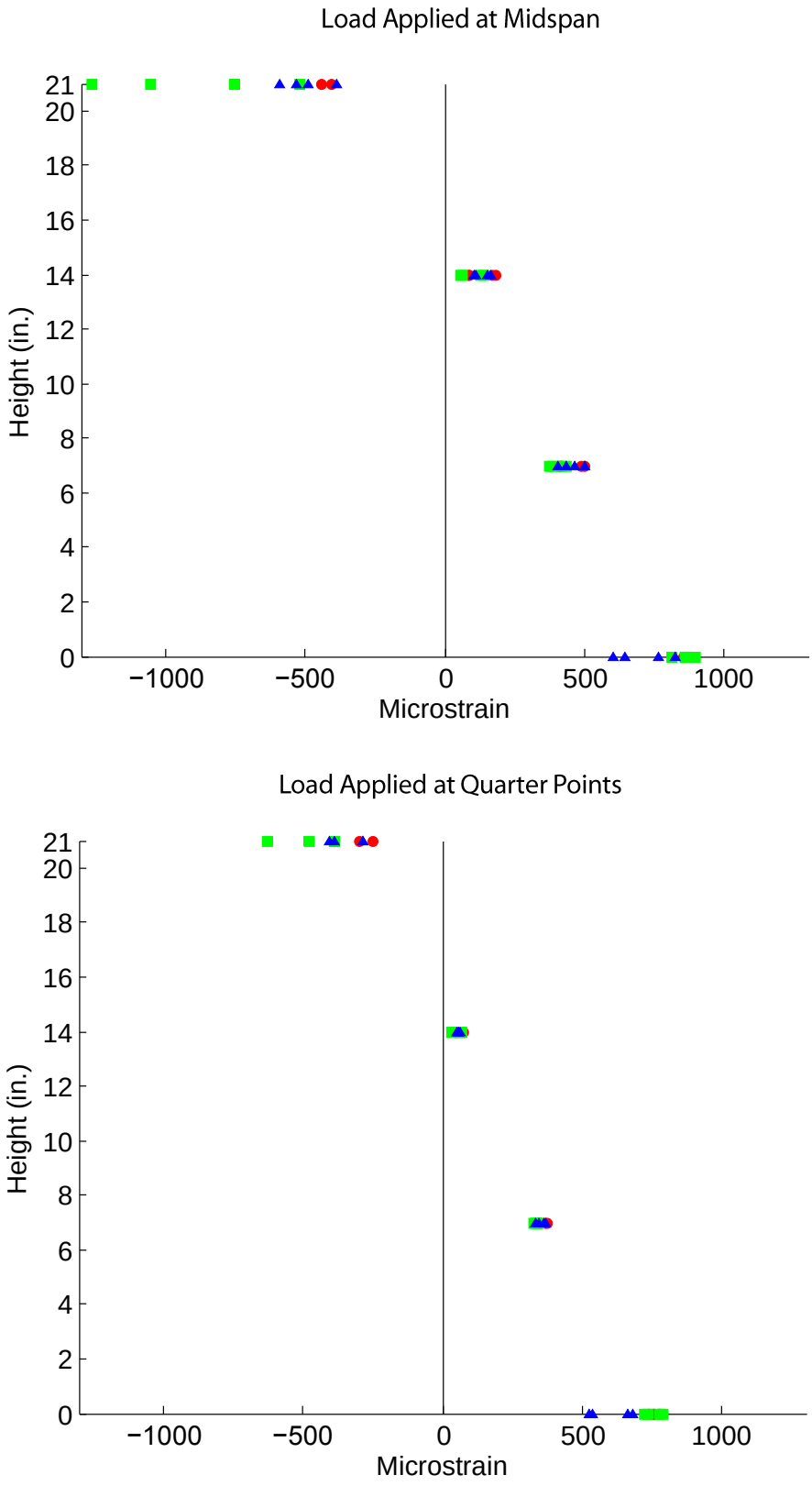

Figure A-5 Data Spread at Midspan Differentiated by Beam

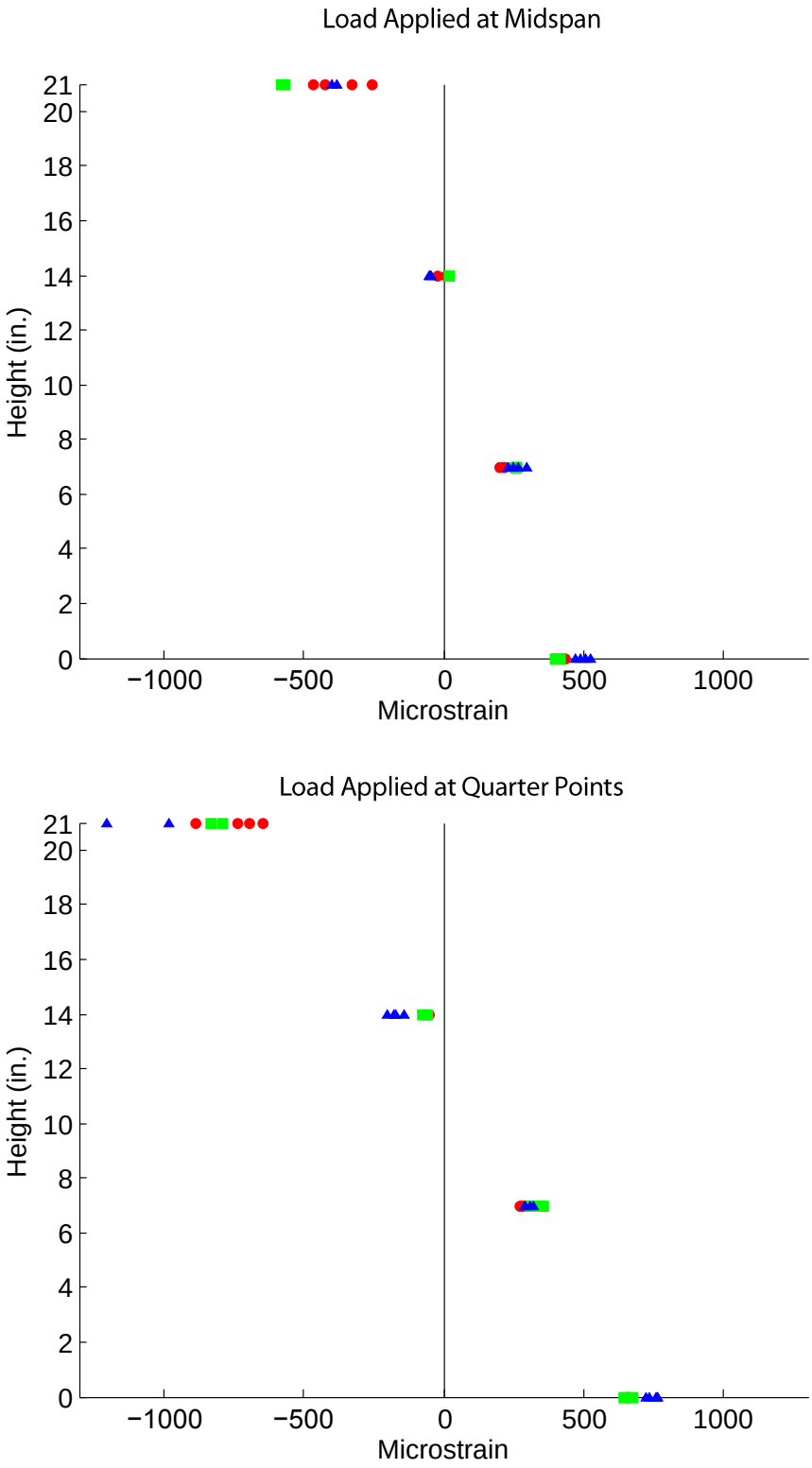

Figure A-6 Data Spread at Quarter Point Differentiated by Beam

The spread of data is highest at the top and bottom of the beams, but it can be seen that the beams tend to be consistent among their individual tests. For example, the strains in Beam 2 (green squares) at midspan are higher than the other two beams, seen in Figure A-4. Overall, this shows that the data is relatively consistent between the tests and individual gages, with differences mainly resulting from any construction differences between the three beams as well as minor inaccuracy in the applied load.

During composite tests there was an even greater number of gages available (since data for all three beams was being recorded), but less test repetitions were available. In light of this, the process of data analysis differed as well. The data spreadsheets were manually examined to find a point in the middle of the maximum load step, and then that row was copied to a spreadsheet set up to show the values in the strain gages relative locations. This data was then used to make strain profiles in MATLAB.

Two major assumptions were made when examining the composite tests. The first involves the applied loads to the beams. In order to replicate the field conditions for the actual bridge the main experiment was based on, the beams were connected using end diaphragms at a 45 degree skew angle, creating an indeterminate system. In order to determine the applied load to a single beam the deflections were examined, knowing that due to stiffness relationships if the deflections were similar then the applied loads were also about the same. As noted in the main body, observed deflections were approximately equal (within 0.1 in.) for all beams, and so it was assumed that each of the three beams took about a third of the total load. Actual deflections for the 150 kip test can be seen in Table A-5.

TABLE A-5 Deflections During Composite Test

	Deflections (in.)		
	Quarter Point 1	Midspan	Quarter Point 2
150 kip Test			
Beam 1	-0.331	-0.439	-0.270
Beam 2	-0.299	-0.451	-0.296
Beam 3	-0.252	-0.414	-0.314
Range:	0.079	0.037	0.044

The second major assumption was that the concrete arch within the beam had cracked. This assumption was based on looking at the stiffness of the beam as well as the strain data from testing. After numerous cracking noises were heard during the test to 200 kips, the 150 kip test was performed to see if any change in the beams could be noticed. After it was completed, the stiffness (load vs. deflection) of a beam during the test was plotted, as seen in Figure A-7.

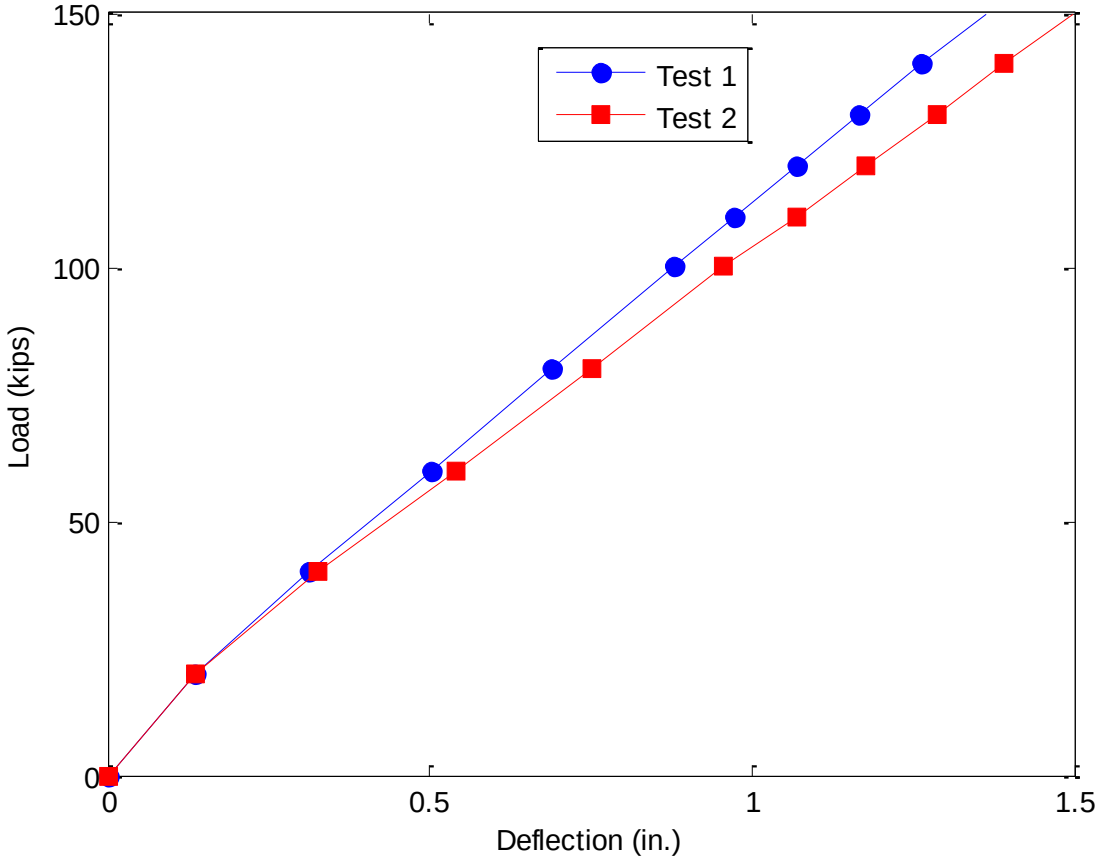

FIGURE A-7 Comparison of Beam Stiffness During Composite Tests

At high loads the line for the second test is showing higher deflections for the same amount of load, indicating a loss in stiffness. Then, the vibrating wire gage readings were used to examine the strain profile within the concrete arch at each increment of 50kips, seen below in Figure A-8.

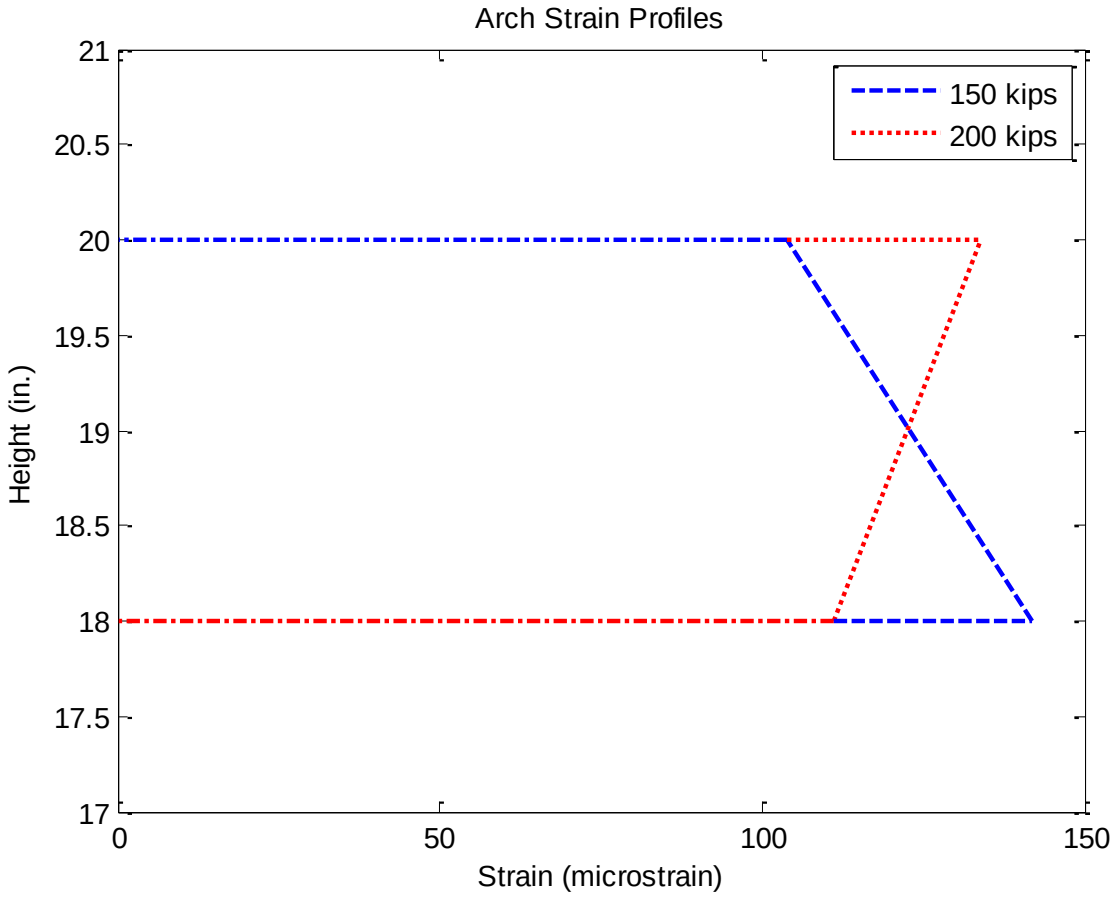

FIGURE A-8 Concrete Arch Strains Showing Change in Curvature

During the initial part of the test the arch has greater tension at the top than the bottom, but before reaching the final load the distribution reverses, and the bottom has a greater tensile strain than the top. This is puzzling in a few ways- notably, that the neutral axis is above the arch, and so the bottom would be expected to be in higher tension than the top. The flip in the distribution indicates some extreme change in the arch that continues for the remainder of the test, and so it is possible that it cracked. As noted in the main body, there were some issues with the vibrating wire gages converging due to the constantly changing load from the actuator, and so it is possible that the data is faulty. Between all of the data, coupled with the fact that concrete is traditionally

assumed to have no tensile strength, the conservative assumption was made to neglect the arch in force calculations.

A4 Excel Calculations

As most calculations performed in this research were exercises in keeping data in order rather than computationally demanding, Microsoft Excel proved to be the most efficient software tool (Microsoft 2013). The sheets used to make calculations are described below and attached.

A4.1 Transformed Section Analyses

Excel Spreadsheets were used in calculating transformed section properties. Properties for each component of the beam were input, including modulus of elasticity, centroid height, and information to calculate areas. The materials were all transformed into equivalent areas of FRP by multiplying by the ratio of the material's *E* to that of the FRP. Then, the central axis theorem was used to calculate the moment of inertia of the transformed section. When calculating any individual component's moment of inertia the moment of inertia contributions were all changed to 0, but areas were still included for centroid calculations (since the piece is still bending about the same neutral axis). An example sheet for calculating the transformed flexural rigidity *EI* is seen in Tables A-6 and A-7.

Table A-6 Inputs for Transformed Section Calculation Sheet

Section Properties and Transformed Area					
FRP Box					
E=	3100	ksi			
ttop=	0.32	in			
tbottom=	0.25	in			
t1web=	0.11	in	EACH		
twing=	0.106	in			
width=	24	in			
height=	21	in			
wheight=	2				
wwidth=	12				
Concrete					
Arch			Parabolic Profile Coefficients		
E=	4500	ksi	y(x) = c x^2 + d x + e		
n=	1.45				
x=	258	in.	c=	-0.00025	
A=	88	in.^2	d=	0.129302	
Aeff=	128	in.^2	e=	2	
ybar=	18.68	in.			
width=	22	in.			
height	4	in.			
Shear Fin					
w=	4	in.			
h=	0.32	in.			
A=	1.28	in.^2			
Aeff=	1.86	in.^2			
ybar=	20.84	in.			
Deck					
E=	4670	ksi			
n=	1.51				
h=	7.5	in			
w=	0	in.			
A=	0	in.^2			
Aeff=	0	in.^2			
Strand					
E=	27500	ksi			
n=	8.87				
A=	3.366	in.^2			
Aeff=	29.86	in.^2			
ybar=	0.5	in.			

Table A-7 Transformed Area Sheet Calculations and Output

	A [in^2]	y [in]	Ay [in^3]	d [in]	Io [in^4]	Ad^2 [in^4]	Ix [in^4]
Top	7.68	20.84	160.1	5.78	0.07	256	256
Bottom	6	0.13	0.8	-14.94	0.03	1339	1339
Webs	4.62	10.5	48.5	-4.56	169.79	96	266
Wing	6.38	19.53	124.6	4.46	14.66	127	142
Arch	127.74	18.68	2386.2	3.62	170.32	1671	1841
Shear Fin	1.86	20.84	38.7	5.78	0.02	62	62
Strand	29.86	0.5	14.9	-14.56	0	6333	6333
Deck	0	24.75	0	-9.69	0	0	0
sum(A)=	184	sum(Ay)=	2774			Sum(Ix)=	10239
ybar=	15.06						
						EI/10^6=	31.74
FRP Shell	EI/10^6=	6.21					
Tied Arch	EI/10^6=	25.53					
Deck	EI/10^6=	0					

A4.2 Internal Force Analyses

All calculation of internal forces was performed using Microsoft Excel as well. The strain profiles that were plotted in MATLAB (using the average value at each height) was input into Excel sheets, along with the height of each gage. The slope of the strain profile, $1/\rho$, was calculated by dividing the change in strain by the height over which the change took place. For non-composite sections the entire height of the beam was used ($1/\rho = (\varepsilon_{21}-\varepsilon_{0})/(21\text{ in.}- 0\text{ in.})$). For composite sections where the data was less linear, particularly in the lower portion of the beam, the curvature at the neutral axis was used ($1/\rho = (\varepsilon_{deck}-\varepsilon_{21})/(25.75\text{ in.}- 21\text{ in.})$). The slope of the line at the neutral axis was calculated for both cases, and basic geometry was used to calculate the position of the neutral axis. A similar process was used for the arch within the non-composite beam, finding the slope of the strain and then extrapolating the strain at the top and bottom faces. The curvature equation $1/\rho=M/EI$ was programmed into the Excel sheet to solve for both *EI* and

M as detailed in the main body. Transformed *EI* values came from the transformed section sheet described above, and the applied moment for each test was manually entered.

The most confusing calculations performed were the stress profile integrations due to the large number of materials and varying areas. Sample calculations for the basic procedure described here have been performed in Mathcad and attached. In order to transform the strain profiles into stress profiles, each material's strain was multiplied by its modulus of elasticity. The basic relationship that force equals the stress multiplied by area was used to calculate the force each component provided. For the FRP and concrete, the stress profile was broken down into simple shapes whose centroids where easily found in order to calculate the moment arms. Once all forces were determined they were summed to check the internal equilibrium. Any materials who had bending moments based on curvature (the concrete arch, concrete deck, and FRP in the composite case) had their moments calculated from the curvature. To find the contribution of a component, the moment that it provided to the cross-section was divided by the total moment from all materials. An example calculation sheet is seen below as Tables A-8 and A-9.

Table A-8 Curvature Portion of Moment Calculation Sheet

Calculations Spreadsheet				Curvature			Stress Strain Integration				
Case:	NonComposite Midspan						Diagram				
Applied Moment:	1935	kip-in.		All based on 1/ρ=M/EI							
From Section Property Sheet											
EI=	31.7			Solve for EI							
FRP EI=	6.2			EI=	27.93						
Tied Arch EI=	25.5										
Concrete EI=	5.9			Solve for M							
Strain Profile				M (total)=	2199						
Material	Height	Strain (με)		M (FRP)=	430						
FRP	21	-643		M (Arch)=	251						
Concrete	20	-187		M(couple)	1303						
Concrete	18	-102									
FRP	14	120									
FRP	7	436									
Steel	0.5	741									
FRP	0	812									
Neutral Axis											
FRP											
Slope	-109	in.									
Solve for 0	-1.10										
y=	15.10										
Curvature											
1/ρ	-69.29										
Concrete											
1/ρ	-42.5										
Extrapolate Top & Bottom Strain Values											
21	-229.5										
17	-59.5										
Neutral Axis	-1.4	From Bottom of Arch									

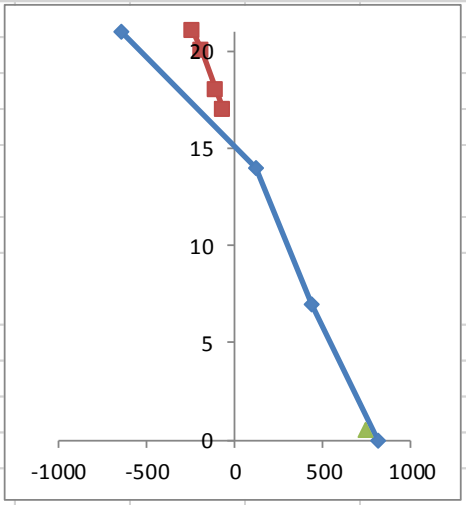

Table A-9 Force and Moment Portion of Moment Calculation Sheet

Calculate Forces						Calculate Moments			
Steel						NA=	15.10		
Stress (ksi)	Area (in^2)	Force (kips)				Force Location (in.)	Moment Arm (in.)	Moment (kip-in.)	
20.38	3.366	68.59				0.5	14.60	1001	
Concrete									
Shape	Stress (ksi)	Stress Shape Area (kip/in)	Width	Force		Force Location (in.)	Moment Arm (in.)	Moment (kip-in.)	
C Triangle	-1.03	-2.79	22	-61.35		19.20	-4.10	251	
T Triangle	-0.27	0.1874	22	4.12		16.53	-1.43	-6	
Total				-57.22				246	
FRP									
Shape	Stress (ksi)	Stress Shape Area (kip/in)	Width	Force		Force Location (in.)	Moment Arm (in.)	Moment (kip-in.)	
Top	-1.99	-0.64	24	-15.31		21	-5.90	90.31	
C Triangle	-1.99	-5.88	0.22	-1.29		19.0	-3.93	5.09	
T Triangle	0.37	0.20	0.22	0.05		14.4	0.73	0.03	
Rect 1	0.37	2.60	0.22	0.57		10.5	4.60	2.64	
Tri 1	0.98	3.43	0.22	0.75		9.33	5.77	4.35	
Rect 2	1.35	9.46	0.22	2.08		3.5	11.60	24.15	
Tri 2	1.17	4.08	0.22	0.90		2.33	12.77	11.46	
Bottom	2.52	0.63	24	15.10		0	15.10	228.07	
Wings									
Height	Strain	Stress	Area of FRP	Force=Stress*Area			Moment Arm	Moment	
21	-643	-1.99	2.54	-5.07		21	-5.90	29.91	
20	-534	-1.66	0.42	-0.70		20	-4.90	3.44	
18	-316	-0.98	2.54	-2.49		18	-2.90	7.22	
Summary									
Material	Force	Moment							
Steel	68.6	1001	0.53						
Concrete	-57.2	246	0.13						
-Bending		251	0.13						
FRP	-5.4	407	0.21						
Total	**6.0**	**1904**	**1935**						

APPENDIX B Design Procedure

B1 Proposed Design Procedure Guidelines

After examining the results of this study, the data was used to formulate a new proposed design method. It was found that the non-composite beams that must resist construction loads rely mainly on the tied arch for flexural strength, but that after the concrete bridge deck is placed the neutral axis shifts up so that the arch is in tension. Consequently, the most important element of the overall system is the tension reinforcement. The steel strands are present during every phase of loading and are farther from the neutral axis than the majority of other components, which increases their impact on flexural strength. Finally, because of their small size, the number of strands can be easily adjusted to increase or decrease the available strength in a section within some "standard" FRP and arch configurations.

B2 Limit States

The limit states for beam failure during the three stages of construction are listed below:

Stage 1: Before concrete arch placed

1. Steel ruptures
2. FRP ruptures
3. Instability of FRP web

Stage 2: Non-composite beam

1. Steel ruptures
2. FRP ruptures
3. Instability of FRP web
4. Concrete crushes

Stage 3: Composite Section

1. Steel yields
2. FRP rupture
3. Concrete crushes

Additionally, each stage must meet any deflection criteria.

The checks for these limit states are as follows:

1. Steel Rupture

The tension reinforcement is a central component during all stages of beam construction. Due to the extremely high strength of steel prestressing strands, failure is unlikely to be controlled by the strands but they do provide a great deal of the beam's strength and should still be checked. Strands will be checked by calculating the force they are required to provide from checks on the applied moment and internal equilibrium. Strain can then be calculated and compared to the ultimate strain to insure they will not be approaching failure. The ultimate strength is the ultimate stress multiplied by the area of steel.

2. FRP Rupture

FRP has very impressive tensile strength, but has an undesirable brittle failure mechanism. For this reason the maximum strains must be calculated to insure that they fall well below the maximum limit states. The bottom of the beam will have the greatest tensile strains, and should be compared to the rupture strain for the specified fiber layout. As strain compatibility with the tension strands was observed, the same strain could be taken as an estimate of the FRP strains. The AASHTO Guide for FRP Pedestrian Bridges prescribes a maximum allowable stress of just 25% of the ultimate stress (AASHTO 2008). This may be overly conservative if the FRP is generally ignored in terms of strength, but this does ensure that creep will not be an issue.

3. FRP Instability

More complicated than the strength checks are the checks for FRP stability, which occur during the non-composite stages when there will be FRP in compression, especially during the placement of the arch when the FRP must provide all of the compressive forces. Stability during this time is aided by FRP cross ties at discrete points along the length of the beam and the wing flanges on the lid. Additionally, the foam that forms the arch conduit helps to brace the web.

4. Concrete Crushing

Finally, once concrete has been placed it can fail when reaching the crushing strain of 0.003. For non-composite stages, the actual strain in the concrete can be found by using equilibrium between the concrete and steel to find a force, then transforming into a strain using the area of material and Young's modulus. A similar process can be used for the concrete deck.

Due to the overwhelming majority of brittle failure modes, a ϕ=0.65 is used in all calculations. For FRP, the strain is limited to 25% of the ultimate strain to ensure there will be no issues related to creep.

B3 Design Procedure

A sample design was performed in Mathcad and is attached. The calculation steps are numbered so commentary can be followed.

Part 1: Composite Design

The composite design is expected to control, and so the initial design will be performed for this case. Conservatively, the resisting moment is provided by the concrete deck providing the compression force and steel strand providing the tension force.

- Step 1.1: After calculating the applied moment a moment arm *d* can be assumed between the forces and the force provided by each component is calculated. The concrete force can be conservatively assumed to act at the midheight of the deck.

- Step 1.2 (Limit State 4): The concrete deck is checked to ensure that at its ultimate strength it can provide the necessary force. A Whitney stress block is assumed for the ultimate strength. The area of concrete is calculated, then divided by the effective width to give the needed height to the neutral axis. The concrete deck must be as least this thick.
- Step 1.3 (Limit State 1): The steel tension strands are checked to make sure they can provide the necessary force as well. The required area is then divided by the area of one strand to find how many strands to use.
- Step 1.4 (Limit State 2): The FRP strains in the bottom flange are checked to ensure they fall well below the ultimate strain. The allowable stress limitation set forth by AASHTO for pedestrian bridge design is 25% of the ultimate stress, and this limit will be used here as well (AASHTO, 2008). As a first check, the ultimate FRP strain is assumed to be the strain in the steel strand. If the strain is too high more strands are added until the strain is reduced to an acceptable level.
- Step 1.5 (Final Checks): Once an acceptable number of strands is found, the neutral axis for the proposed section is calculated. The strain in the steel is known from the end of Step 1.4, and similar triangles can be used to calculate the actual strains at the top of the concrete and bottom FRP to ensure they are below the failure strains.

Part 2: Non-composite design

For the construction loads, especially pouring the concrete deck, the majority of the flexural strength comes from the tied arch. In the second part of the design process the arch is sized.

- Step 2.1: Using the factored moment from dead loads, determine the moment arm between the steel strands and midpoint of the arch. To optimize the arch, the imposed moment can be taken as the ratio of the arch's flexural rigidity compared to the total beam's flexural rigidity. The force that the concrete must provide is then known.
- Step 2.2 (Limit State 4): The concrete arch is sized, assuming it has minimum bending and has a force of its area multiplied by strength.
- Step 2.3 (Limit State 1): The steel can be checked, but since the composite case includes all the dead loads the steel will be adequate.
- Step 2.4 (Limit State 2): The strain in the bottom layer of FRP is again checked to ensure it is not at critical levels. As in the composite case, the strain in the strand is calculated and geometry is used to find the FRP strain.

Additionally, the assumption that all force comes from the arch moment couple (and therefore no reduction in load) can be made to be slightly conservative. This assumption also allows the stability check in the FRP (Limit State 3) to be neglected- if it would have a stability failure the load would move into the tied arch.

Part 3: Shell Design

In order to take advantage of the light weight FRP for shipping, the first stage of construction involves the beam shell of just FRP and tension strands. This only needs to be able to support its own weight and the weight of the uncured concrete arch.

- Step 3.1: Calculate transformed section properties of the cross section with only the selected number of strands and FRP.

- Step 3.2 (Limit State 1): The stress in the steel can be calculated using $\sigma=n \cdot M \cdot y/I$. Again, since the loads are smaller than the other stages, the steel will be plenty adequate to resist just the self-weight.
- Step 3.3 (Limit State 2): The FRP flanges are checked, using $\sigma=n \cdot M \cdot y/I$, then dividing stress by Young's Modulus to find the strains.
- Step 3.4 (Limit State 3): Since the FRP is carrying load for this check, the webs must have sufficient stability. A conservative check is to assume that each web acts as a simply supported plate. The shear web buckling critical stress equation,

$$\tau_{cr} = \frac{k_v \pi^2 E t^2}{12(1-v^2)h^2}$$

can be used to find the ultimate shear load that each web can take. In this equation, k_v is a term for the support conditions of the web, E is Young's Modulus of the FRP, t is the web thickness, v is Poisson's ratio and h is the height of the web. In reality, each web is retrained by FRP ties between the webs, and are attached to the foam conduit, restricting buckling. Also, standardized FRP cross-sections predesigned to prevent stability failure would remove the need for this check as well.

Part 4: Serviceability/Deflection Checks

Final beam design is often controlled by serviceability checks for deflection, especially in FRP structures due to their low modulus of elasticity. Current HCB design is controlled by these checks, and again the best method to use will change for each stage of the beam's construction. Before the arch is placed the cross section is constant, and a transformed section can be created to find a flexural rigidity *EI*. For the composite case the cross section can again be assumed as constant by neglecting the concrete arch, and will give conservative deflections. The non-

composite beam is more difficult due to the varying cross section. Current analyses use the conjugate beam method to calculate deflections, using the *EI* value calculated at each tenth point along the span. This prediction will be approximate, but will improve if the *M/EI* value is calculated at more points. Calculations also may be required to specify camber for dead load deflections.

Ultimate Limit State

Research on the ultimate limit state is ongoing at Virginia Tech, including research on shear strength and a finite element analysis. These design guidelines can be incorporated into future research to create a full design method for ultimate beam strength.

Design Sheet: Hillman Hybrid Composite Beam

Assumed Section Properties:

User inputs highlighted in yellow

Factored Live Moment: $M_{LL} := 5300kip\cdot in$

Beam Span: $L := 50ft$

Beam Height: $h := 25in$ (Assumed as L/2)

Beam Width: $w := 24in$

Material Properties/Section Information

FRP: $E_{FRP} := 3100ksi$ $\varepsilon_u := 0.009$ $SW_{FRP} := 0.05klf$

Thickness of: Centroid:

Top Flange: $t_{top} := 0.32in$ $y_{top} := h - \frac{t_{top}}{2} = 24.84\cdot in$

Bottom Flange: $t_{bottom} := 0.25in$ $y_{bottom} := t_{bottom}\cdot 0.5 = 0.125\cdot in$

Webs: $t_{web} := 0.11in$ $y_{web} := 0.5\cdot h = 0.317\,m$

Wings:

Thickness: $t_{wing} := 0.106in$ Width: $w_{wing} := 12in$ Web Height: $h_{wwing} := 2in$

Diagonal Height: $h_d := 2in$

Total height: $h_{wing} := h_{wwing} + h_d = 4\cdot in$

Wing Centroid: $y_{wingself} := \frac{w_{wing}\cdot h_{wing} + h_{wwing}\cdot\left(h_d + 0.5\cdot h_{wwing}\right) + w_{wing}\cdot h_d\cdot 0.5}{w_{wing} + h_{wwing} + w_{wing}} = 2.538\cdot in$

Using beam coordinates: $y_{wing} := h - \left(h_{wing} - y_{wingself}\right) = 23.538\cdot in$

Moment of Inertia:

$$I_{wing} := \frac{1}{12}\cdot\left(2w_{wing}\cdot t_{wing}^{3} + t_{wing}\cdot h_{wwing}^{3}\right) + h_{wwing}\cdot t_{wing}\cdot\left(h_d + 0.5\cdot h_{wwing} - y_{wingself}\right)^2 \ldots$$
$$+ w_{wing}\cdot t_{wing}\cdot\left(y_{wingself} - h_{wing}\right)^2 + w_{wing}\cdot t_{wing}\cdot\left(0.5\cdot h_d - y_{wingself}\right)^2$$

$I_{wing} = 5.846\cdot in^4$

$A_{wing} := t_{wing}\cdot\left(2\cdot w_{wing} + h_{wwing}\right)$

Calculate total FRP centroid

$A_{FRP} := t_{top} \cdot w + 2 \cdot t_{web} \cdot h + t_{bottom} \cdot w + 2 \cdot A_{wing} = 24.692 \cdot in^2$

$$y_{FRP} := \frac{t_{top} \cdot w \cdot y_{top} + 2 \cdot t_{web} \cdot h \cdot y_{web} + t_{bottom} \cdot w \cdot y_{bottom} + 2 \cdot t_{wing} \cdot \left(2 \cdot w_{wing} + h_{wwing}\right) \cdot y_{wing}}{A_{FRP}}$$

$y_{FRP} = 15.795 \cdot in$

Calculate Moment of Area about Self

$$I_{FRP} := \frac{1}{12} \cdot \left(w \cdot t_{top}^{\ 3} + 2 \cdot t_{web} \cdot h^3 + w \cdot t_{bottom}^{\ 3}\right) + 2 \cdot I_{wing} + w \cdot t_{top} \cdot \left(y_{top} - y_{FRP}\right)^2 \ldots$$
$$+ 2 \cdot t_{web} \cdot h \cdot \left(y_{web} - y_{FRP}\right)^2 + t_{bottom} \cdot w \cdot \left(y_{bottom} - y_{FRP}\right)^2 + A_{FRP} \cdot \left(y_{wing} - y_{FRP}\right)^2$$

$I_{FRP} = 3.94 \times 10^3 \cdot in^4$

Steel: Using 1/2" diameter strands

Area of one prestressing strand: $A_{strand} := 0.153in^2$

Young's Modulus for strands: $E_s := 27500ksi$

Ultimate strength of strands: $f_{su} := 270ksi$

Centroid of steel: $y_s := 0.5in$

Modular ratio: $n_s := \frac{E_s}{E_{FRP}} = 8.871$

Concrete:

Deck:

Strength: $f_{cdeck} := 4ksi$

Young's Modulus: $E_{cdeck} := 57 \cdot \sqrt{\frac{f_{cdeck}}{psi}} \cdot ksi = 3.605 \times 10^3 \cdot ksi$

Deck thickness: $t_{deck} := 7in$

Deck centroid: $y_{deck} := h + \frac{t_{deck}}{2} = 28.5 \cdot in$

Modular ratio: $n_{deck} := \frac{E_{cdeck}}{E_{FRP}} = 1.163$

Arch:

Strength: $f_{carch} := 4ksi$

Young's Modulus: $E_{carch} := 57 \cdot \sqrt{\frac{f_{carch}}{psi}} \cdot ksi = 3.605 \times 10^{3} \cdot ksi$

Arch height: $h_{arch} := 4in$

Arch width: $w_{arch} := w - 2in = 22 \cdot in$

Arch centroid (at midspan): $y_{arch} := h - \frac{h_{arch}}{2} = 23 \cdot in$

Modular Ratio: $n_{arch} := \frac{E_{carch}}{E_{FRP}} = 1.163$

Dead Load: Assume beam DL is

Beam: $w_{DL} := 0.2klf$ Deck: $w_{DLdeck} := t_{deck} \cdot \left(w + 2 \cdot w_{wing}\right) \cdot 150pcf = 0.35 \cdot klf$

Dead Load includes beam and deck:

Factored Moment $M_{DL} := 1.2 \cdot \frac{\left(w_{DL} + w_{DLdeck}\right) \cdot L^{2}}{8} = 2.475 \times 10^{3} \cdot kip \cdot in$

Add moments to find the ultimate moment to be resisted:

$M_{uc} := M_{LL} + M_{DL} = 7.775 \times 10^{3} \cdot kip \cdot in$

Use $\phi := 0.65$ due to brittle failure modes

Step 1: Composite Design

1.1 Check force in each component

The majority of moment resistance comes from a force couple between the steel strands and concrete deck. Assume that the concrete force centroid is at 1/2 the deck height. To be conservative, the arch is neglected.

Find moment arm d: $d_{comp} := h - y_s + \frac{t_{deck}}{2} = 28 \cdot in$

Find force that each component must carry: $F := \frac{M_{uc}}{d_{comp}} = 277.679 \cdot kip$

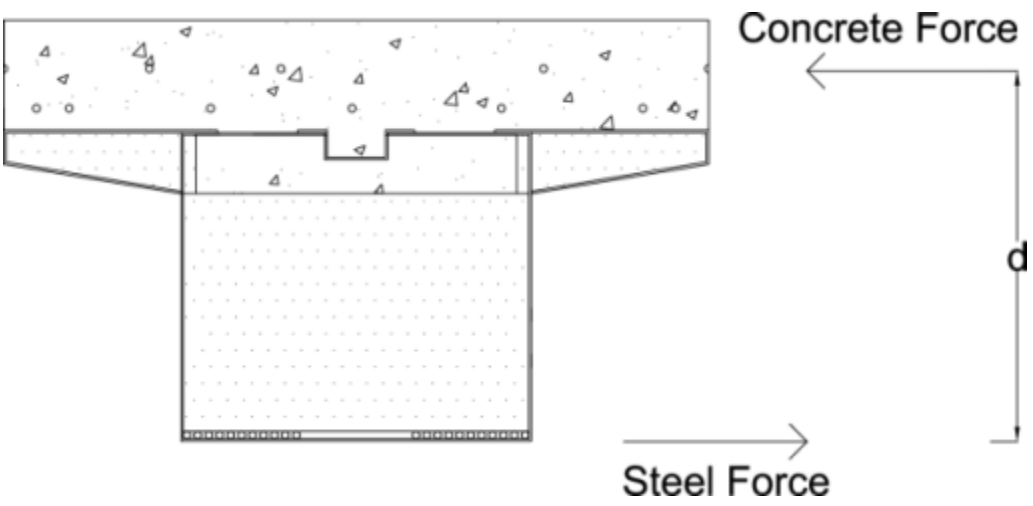

Step 1.2 Check required area of concrete with Whitney stress block:

$$A_{reqc} := \frac{F}{\phi \cdot 0.85 \cdot f_{carch}} = 125.646 \cdot in^2$$

With an effective width of $w = 24 \cdot in$

$$a_{req} := \frac{A_{reqc}}{w} = 5.235 \cdot in \qquad c_{req} := \frac{a_{req}}{0.85} = 6.159 \cdot in$$

Neutral axis is 6.16 inches from top of concrete- 7 inch deck is OK

Step 1.3 Check steel failure:

Find required area of steel

$$A_{reqs} := \frac{F}{\phi \cdot f_{su}} = 1.582 \cdot in^2$$

Strands required is $n_{strands} := \frac{A_{reqs}}{A_{strand}} = 10.341$

$n_{strands} := 11$

Step 1.4 Check FRP Rupture

Check strain in the bottom layer of FRP (which experiences most tension). According to the manufacturer, the ultimate strain of the FRP is 0.009. Modeling after AASHTO codes for pedestrian bridges, the strain should not exceed 0.25*Ultimate Strain. Making the unconservative assumption that the strand strain is equal to the bottom FRP, calculate what the strand strain is at this force.

$$\varepsilon_{max} := 0.25 \cdot \varepsilon_u = 2.25 \times 10^{-3}$$

$$\sigma_s := \frac{F}{n_{strands} \cdot A_{strand}} = 164.99 \cdot ksi$$

$$\varepsilon_s := \frac{\sigma_s}{E_s} = 6 \times 10^{-3}$$

Too high, increase to reduce strain

Try $n_{strands} := 32$

$$\sigma_s := \frac{F}{n_{strands} \cdot A_{strand}} = 56.715 \cdot ksi \qquad \varepsilon_s := \frac{\sigma_s}{E_s} = 2.062 \times 10^{-3}$$

Proceed with 32 strands

Step 1.5 Final Checks

Calculate neutral axis location

$$y_{bar} := \frac{A_{FRP} \cdot y_{FRP} + n_{strands} \cdot A_{strand} \cdot n_s \cdot y_s + w \cdot t_{deck} \cdot n_{deck} \cdot y_{deck}}{A_{FRP} + n_{strands} \cdot A_{strand} \cdot n_s + w \cdot t_{deck} \cdot n_{deck}} = 22.694 \cdot in$$

Check that strain at top of deck is within limit

$$\varepsilon_c := \left(h + t_{deck} - y_{bar}\right) \cdot \frac{\varepsilon_s}{y_{bar} - y_s} = 8.647 \times 10^{-4}$$

Is below crushing limit of 0.003

Check that strain in FRP is acceptable

$$\varepsilon_{FRP} := y_{bar} \cdot \frac{\varepsilon_s}{y_{bar} - y_s} = 2.109 \times 10^{-3}$$

Within acceptable limit

Check Deflections

$$I := I_{FRP} + A_{FRP} \cdot \left(y_{FRP} - y_{bar}\right)^2 + n_{strands} \cdot A_{strand} \cdot n_s \cdot \left(y_s - y_{bar}\right)^2 + \frac{n_{deck} \cdot w \cdot t_{deck}^3}{12} \ldots$$

$$+ n_{deck} \cdot w \cdot t_{deck} \cdot \left(y_{bar} - y_{deck}\right)^2$$

$$I = 3.389 \times 10^4 \cdot in^4$$

Calculate Deflection due to Design Truck

Loads at Midspan, Midspan+14ft, Midspan +28ft

Deflection Equation for Simply Supported Beam:

$$\Delta_x(P, b, x) := \frac{P \cdot b \cdot x}{6 \cdot E_{FRP} \cdot I \cdot L} \cdot \left(L^2 - b^2 - x^2\right)$$

Concentrated Load P, Load distance b from right support deflection at location x from left support

Use superposition

Midspan: $P_1 := 11kip$ $b_1 := \frac{L}{2}$ $\Delta_1 := \Delta_x\left(P_1, b_1, \frac{L}{2}\right) = 0.471 \cdot in$

Second Axle: $P_2 := P_1$ $b_2 := \frac{L}{2} + 14ft$ $\Delta_2 := \Delta_x\left(P_2, b_2, \frac{L}{2}\right) = 0.208 \cdot in$

Cab Axle: $P_3 := 3kip$ $b_3 := \min(0.5 \cdot L + 28ft, L) = 50 \cdot ft$ Axle off span

Total Deflection: $\Delta_1 + \Delta_2 = 0.679 \cdot in$ Limit: $\frac{L}{800} = 0.75 \cdot in$ Good!

Design works for all components in composite section

Part 2: Noncomposite Design

We now have a deck design that works. Use these dead loads to ensure that the arch is capable of supporting these loads.

$M_{unc} := M_{DL} = 2.475 \times 10^{3} \cdot kip \cdot in$ Design arch for 80% of moment $M_{arch} := 0.8 \cdot M_{unc}$

$M_{arch} = 1.98 \times 10^{3} \cdot kip \cdot in$

Step 2.1 Determine moment arm

Use a similar moment couple concept to before, with assumed arch height of 4 inches

$d_{nc} := h - \frac{h_{arch}}{2} - y_s = 22.5 \cdot in$ $F_{nc} := \frac{M_{arch}}{d_{nc}} = 88 \cdot kip$

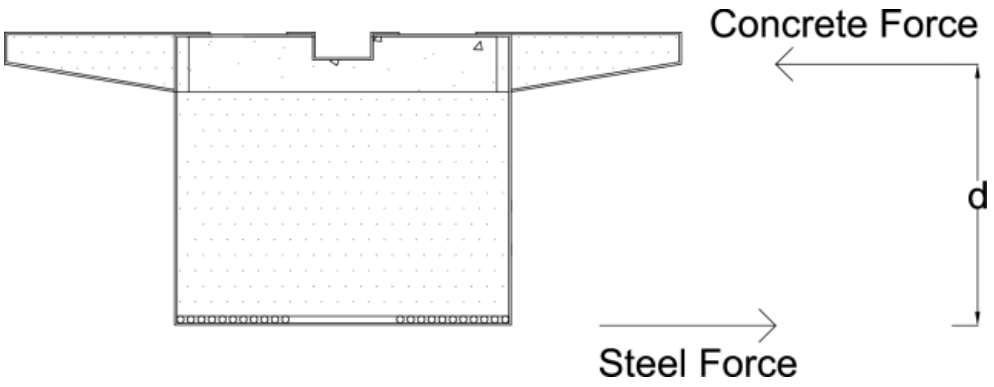

Step 2.2- Size concrete arch

Concrete: Ultimate force in arch is $h_{arch} \cdot w_{arch} \cdot f_{carch} = 352 \cdot kip$

$\phi \cdot h_{arch} \cdot w_{arch} \cdot f_{carch} = 228.8 \cdot kip$

Capable of withstanding force- try smaller

$h_{arch} := 3in$ $y_{arch} := h - 0.5 \cdot h_{arch} = 23.5 \cdot in$

$h_{arch} \cdot w_{arch} \cdot f_{carch} = 264 \cdot kip$ $\phi \cdot h_{arch} \cdot w_{arch} \cdot f_{carch} = 171.6 \cdot kip$

Step 2.3- Check steel strands

By inspection, steel strands is OK (since strong enough to resist heavier composite loads), but check gives

$\sigma_s := \frac{F_{nc}}{n_{strands} \cdot A_{strand}} = 17.974 \cdot ksi$ $\varepsilon_s := \frac{\sigma_s}{E_s} = 6.536 \times 10^{-4}$ Good

Step 2.4- Check strain in FRP:

Calculate neutral axis for noncomposite section:

$$y_{bar} := \frac{A_{FRP} \cdot y_{FRP} + n_{strands} \cdot A_{strand} \cdot n_s \cdot y_s + w_{arch} \cdot h_{arch} \cdot n_{arch} \cdot y_{arch}}{A_{FRP} + n_{strands} \cdot A_{strand} \cdot n_s + w_{arch} \cdot h_{arch} \cdot n_{arch}} = 15.292 \cdot in$$

FRP has strain compatibility with steel strand

$$\varepsilon_{FRP} := y_{bar} \cdot \frac{\varepsilon_s}{y_{bar} - y_s} = 6.757 \times 10^{-4}$$

Well below max allowable strain in FRP- Design is good for noncomposite strength

Part 3: Shell Design Check:

Step 3.1: Calculate section properties

Without arch

$$y_{bar} := \frac{A_{FRP} \cdot y_{FRP} + n_{strands} \cdot A_{strand} \cdot n_s \cdot y_s}{A_{FRP} + n_{strands} \cdot A_{strand} \cdot n_s} = 6.044 \cdot in$$

$$I_{shell} := I_{FRP} + A_{FRP} \cdot \left(y_{FRP} - y_{bar}\right)^2 + n_{strands} \cdot A_{strand} \cdot n_s \cdot \left(y_s - y_{bar}\right)^2 = 7.623 \times 10^3 \cdot in^4$$

Dead load for beam and arch loads only

$$M_D := \frac{w_{DL} \cdot L^2}{8} = 750 \cdot kip \cdot in$$

Step 3.2: Calculate stress in steel

$$\sigma_s := n_s \cdot \frac{M_D \cdot \left(y_{bar} - y_s\right)}{I_{shell}} = 4.839 \cdot ksi$$

Well below capacity

Step 3.3: Calculate stress in FRP flanges

$$\sigma_{FRPbottom} := \frac{M_D \cdot \left(y_{bar}\right)}{I_{shell}} = 0.595 \cdot ksi \qquad \varepsilon_{bottom} := \frac{\sigma_{FRPbottom}}{E_{FRP}} = 1.918 \times 10^{-4}$$

$$\sigma_{FRPtop} := \frac{M_D \cdot \left(h - y_{bar}\right)}{I_{shell}} = 1.865 \cdot ksi \qquad \varepsilon_{top} := \frac{\sigma_{FRPtop}}{E_{FRP}} = 6.016 \times 10^{-4}$$

Below limiting strains- good

Step 3.4: Stability of FRP webs:

Use web shear buckling equation for simply supported plate

$t_w := 0.11in \qquad v := 0.3$

$\tau_{cr} := 8.98 \cdot \frac{\pi^2 \cdot E_{FRP} \cdot t_w^2}{12 \cdot (1 - v)^2 \cdot h^2} = 0.905 \cdot ksi \qquad V_n := 2 \cdot \tau_{cr} \cdot h \cdot t_w = 4.975 \cdot kip \quad V_u := \frac{50ft}{2} \cdot w_{DL} = 5 \cdot kip$

Also have bracing from cross ties and connection to foam, so close enough!

Find deflection from beam self weight for camber:

$\Delta_{SW} := \frac{5 w_{DL} \cdot L^4}{384 \cdot E_{FRP} \cdot I_{shell}} = 1.19 \cdot in$

Calculate deflection due to deck for camber:

$w_{deck} := t_{deck} \cdot 24in \cdot 150pcf = 0.175 \cdot klf$

Incorporate varying cross-section: $WP := h_{arch} \cdot 0.5 = 1.5 \cdot in$

Arch Centerline Equation: Coefficients:

$c := \frac{-4 \cdot \left(h - t_{top} - \frac{h_{arch}}{2} - WP \right)}{L^2} \qquad d := 4 \cdot \frac{\left(h - t_{top} - h_{arch} \cdot .5 - WP \right)}{L} \qquad e := WP$

$y_{arch}(x) := c \cdot x^2 + d \cdot x + e$

Shear Fin Properties

$w_{SF} := 4in$

$h_{SF}(x) := h - y_{arch}(x) - 0.5 \cdot h_{arch} \qquad A_{SF}(x) := h_{SF}(x) \cdot w_{SF}$

$y_{SF}(x) := h - h_{SF}(x) \cdot .5 \qquad I_{SF}(x) := \frac{1}{12} \cdot \left(w_{SF} \cdot h_{SF}(x)^3 \right)$

$y_{bar}(x) := \frac{A_{FRP} \cdot y_{FRP} + n_{strands} \cdot A_{strand} \cdot n_s \cdot y_s + n_{arch} \cdot \left(w_{arch} \cdot h_{arch} \cdot y_{arch}(x) + A_{SF}(x) \cdot y_{SF}(x) \right)}{A_{FRP} + n_{strands} \cdot A_{strand} \cdot n_s + n_{arch} \cdot \left(w_{arch} \cdot h_{arch} + A_{SF}(x) \right)}$

$I(x) := I_{FRP} + A_{FRP} \cdot \left(y_{FRP} - y_{bar}(x) \right)^2 + n_{strands} \cdot A_{strand} \cdot n_s \cdot \left(y_s - y_{bar}(x) \right)^2 + I_{SF}(x) \ ...$

$+ n_{arch} A_{SF}(x) \cdot \left(y_{bar}(x) - y_{SF}(x) \right)^2 + \frac{n_{arch} \cdot w_{arch} \cdot h_{arch}^3}{12} + w_{arch} \cdot h_{arch} \cdot \left(y_{bar}(x) - y_{arch}(x) \right)^2$

Moment as a function of x is $M(x) := \frac{w_{deck} \cdot x}{2} \cdot (L - x)$

$I_{FRP} = 3.94 \times 10^3 \cdot in^4$ $\frac{I_{FRP}}{I(0.5L)} = 0.222$ Non-composite assumption that arch takes 20% of load is OK

Load on conjugate beam is equal to M/EI- calculate at tenth points (use variable C)

$C(x) := \frac{M(x)}{E_{FRP} \cdot I(x)}$

$C_1 := C(0.1L) = 5.586 \times 10^{-6} \cdot \frac{1}{in}$ $C_4 := C(0.4L) = 1.184 \times 10^{-5} \cdot \frac{1}{in}$

$C_2 := C(0.2L) = 9.739 \times 10^{-6} \cdot \frac{1}{in}$ $C_5 := C(0.5L) = 1.194 \times 10^{-5} \cdot \frac{1}{in}$

$C_3 := C(0.3L) = 1.136 \times 10^{-5} \cdot \frac{1}{in}$

Approximate Midspan Moment in Conjugate Beam

$$M_m := \frac{L^2}{200} \cdot \left(3 \cdot C_1 + 5 \cdot C_2 + 7 \cdot C_3 + 9 \cdot C_4\right) ... + \frac{L^2}{600} \cdot \left[2 \cdot C_1 + 5 \cdot \left(C_2 - C_1\right) + 8 \cdot \left(C_3 - C_2\right) + 11 \cdot \left(C_4 - C_3\right) + 13 \cdot \left(C_5 - C_4\right)\right] = 0.484 \cdot in$$

Camber for deck deflection of 0.5 in.

Check that self-weight assumption OK

$w_{DL} = 0.2 \cdot klf$ $SW_{FRP} = 0.05 \cdot klf$ $SW_s := n_{strands} \cdot 0.52plf = 0.017 \cdot klf$

Treating arch as distributed load: $SW_{arch} := \left(h_{arch} \cdot w_{arch} + A_{SF}(0.25L)\right) \cdot 150pcf = 0.093 \cdot klf$

$w_{DLreal} := SW_{FRP} + SW_s + SW_{arch} = 0.159 \cdot klf$ Assumption is conservative- good

Sample Calculations- Non-composite Case

Stress Integration Analysis
Part 1- FRP
Strain Profile

Test with loads applied at quarter points

$M_{app} := 1612kip \cdot in$

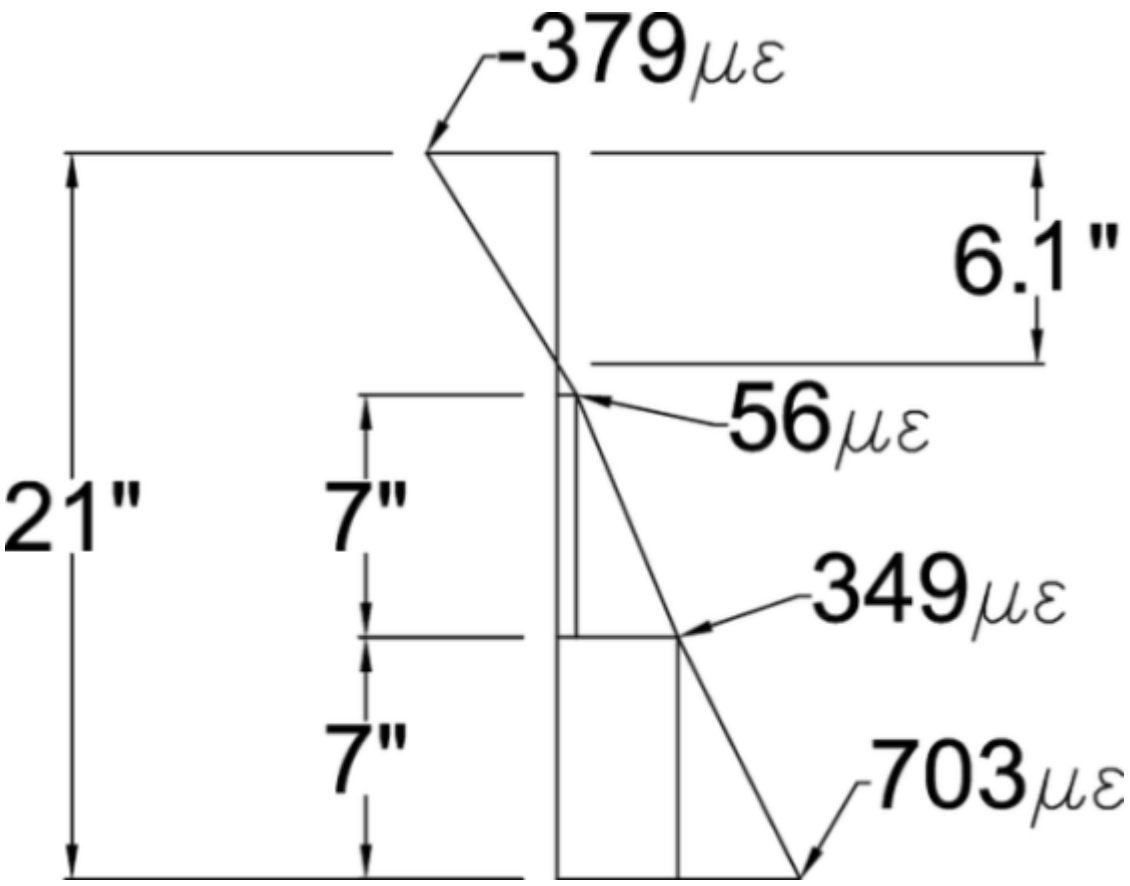

Material Properties

$E_{FRP} := 3100ksi$

Thicknesses:

$t_{top} := 0.32in$ $t_{bottom} := 0.25in$ $t_{web} := 0.11in$

Beam dimensions

$w := 24in$ $h := 21in$

First step: Transform strains into stresses

$\varepsilon_{21} := -379$ $\sigma_{21} := \varepsilon_{21} \cdot 10^{-6} \cdot E_{FRP} = -1.175 \cdot ksi$

$\varepsilon_{14} := 56$ $\sigma_{14} := \varepsilon_{14} \cdot 10^{-6} \cdot E_{FRP} = 0.174 \cdot ksi$

Neutral Axis Location:

$\varepsilon_{7} := 349$ $\sigma_{7} := \varepsilon_{7} \cdot 10^{-6} \cdot E_{FRP} = 1.082 \cdot ksi$

$y_{bar} := 14.9in$

$\varepsilon_{0} := 703$ $\sigma_{0} := \varepsilon_{0} \cdot 10^{-6} \cdot E_{FRP} = 2.179 \cdot ksi$

Calculate Forces, working from top down

Force 1: Top Plate- No shape (all at one height)

$y_1 := 21in$ $A_{top} := t_{top} \cdot w = 7.68 \cdot in^2$ $F_1 := A_{top} \cdot \sigma_{21} = -9.023 \cdot kip$

Force 2: Compressive Triangle

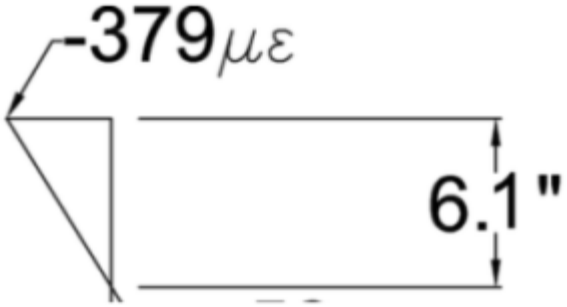

Triangle Centroid is at 2/3 of height

Triangle Height

$h_2 := 6.1in$

Shape Area $A_2 := h_2 \cdot \sigma_{21} \cdot 0.5 = -3.583 \cdot \frac{kip}{in}$

Multiply Shape Area by Material Thickness- Factor of 2 due to 2 webs

$F_2 := A_2 \cdot 2 \cdot t_{web} = -0.788 \cdot kip$ $y_2 := h - \frac{h_2}{3} = 18.967 \cdot in$

Force 3: Tiny Tensile Triangle

Triangle Height

$h_3 := 7in - h_2 = 0.9 \cdot in$

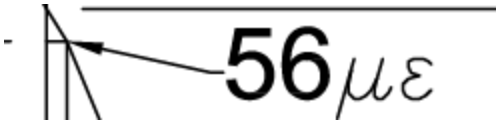

Shape Area $A_3 := h_3 \cdot \sigma_{14} \cdot 0.50 = 0.078 \cdot \frac{kip}{in}$

Multiply Shape Area by Material Thickness- Factor of 2 due to 2 webs

$F_3 := A_3 \cdot 2 \cdot t_{web} = 0.017 \cdot kip$ $y_3 := 14in + \frac{h_3}{3} = 14.3 \cdot in$

Forces 4 and 5: Rectangle and Triangle between 7" and 14"

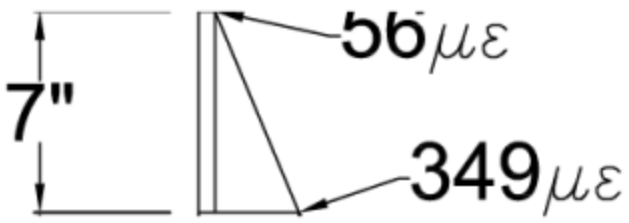

Rectangle:

$h_4 := 7in$ Shape Area: $A_4 := h_4 \cdot \sigma_{14} = 1.215 \cdot \frac{kip}{in}$

Multiply Shape Area by Material Thickness- Factor of 2 due to 2 webs

$F_4 := A_4 \cdot 2 \cdot t_{web} = 0.267 \cdot kip$ $y_4 := 14in - \frac{h_4}{2} = 10.5 \cdot in$

Triangle:

$h_5 := h_4 = 7 \cdot in$ Shape Area: $A_5 := h_5 \cdot (\sigma_7 - \sigma_{14}) \cdot 0.5 = 3.179 \cdot \frac{kip}{in}$

Multiply Shape Area by Material Thickness- Factor of 2 due to 2 webs

$F_5 := A_5 \cdot 2 \cdot t_{web} = 0.699 \cdot kip$ $y_5 := 14in - \frac{2h_5}{3} = 9.333 \cdot in$

Forces 6 and 7: Recatangle and Triangle between 0" and 7"

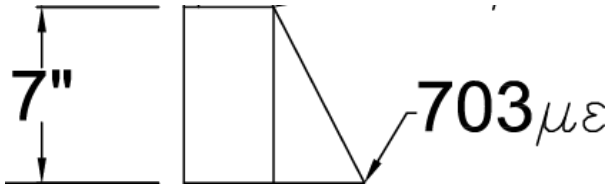

Rectangle:

$h_6 := 7in$ Shape Area: $A_6 := h_6 \cdot \sigma_7 = 7.573 \cdot \frac{kip}{in}$

Multiply Shape Area by Material Thickness- Factor of 2 due to 2 webs

$F_6 := A_6 \cdot 2 \cdot t_{web} = 1.666 \cdot kip$ $y_6 := \frac{h_6}{2} = 3.5 \cdot in$

Triangle:

$h_7 := h_6 = 7 \cdot in$ Shape Area: $A_7 := h_7 \cdot (\sigma_0 - \sigma_7) \cdot 0.5 = 3.841 \cdot \frac{kip}{in}$

Multiply Shape Area by Material Thickness- Factor of 2 due to 2 webs

$F_7 := A_7 \cdot 2 \cdot t_{web} = 0.845 \cdot kip$ $y_7 := \frac{h_7}{3} = 2.333 \cdot in$

Force 8: Bottom Web- No Shape

$y_8 := 0in$ $A_{bottom} := w \cdot t_{bottom} = 6 \cdot in^2$

$F_8 := \sigma_0 \cdot A_{bottom} = 13.076 \cdot kip$

Summary of Main FRP:

Force:	Centroid:	Distance from NA:	Moment:
$F_1 = -9.023 \cdot kip$	$y_1 = 21 \cdot in$	$d_1 := y_{bar} - y_1 = -6.1 \cdot in$	$M_1 := F_1 \cdot d_1 = 55.042 \cdot kip \cdot in$
$F_2 = -0.788 \cdot kip$	$y_2 = 18.967 \cdot in$	$d_2 := y_{bar} - y_2 = -4.067 \cdot in$	$M_2 := F_2 \cdot d_2 = 3.206 \cdot kip \cdot in$
$F_3 = 0.017 \cdot kip$	$y_3 = 14.3 \cdot in$	$d_3 := y_{bar} - y_3 = 0.6 \cdot in$	$M_3 := F_3 \cdot d_3 = 0.01 \cdot kip \cdot in$
$F_4 = 0.267 \cdot kip$	$y_4 = 10.5 \cdot in$	$d_4 := y_{bar} - y_4 = 4.4 \cdot in$	$M_4 := F_4 \cdot d_4 = 1.176 \cdot kip \cdot in$
$F_5 = 0.699 \cdot kip$	$y_5 = 9.333 \cdot in$	$d_5 := y_{bar} - y_5 = 5.567 \cdot in$	$M_5 := F_5 \cdot d_5 = 3.893 \cdot kip \cdot in$
$F_6 = 1.666 \cdot kip$	$y_6 = 3.5 \cdot in$	$d_6 := y_{bar} - y_6 = 11.4 \cdot in$	$M_6 := F_6 \cdot d_6 = 18.994 \cdot kip \cdot in$
$F_7 = 0.845 \cdot kip$	$y_7 = 2.333 \cdot in$	$d_7 := y_{bar} - y_7 = 12.567 \cdot in$	$M_7 := F_7 \cdot d_7 = 10.619 \cdot kip \cdot in$
$F_8 = 13.076 \cdot kip$	$y_8 = 0 \cdot in$	$d_8 := y_{bar} - y_8 = 14.9 \cdot in$	$M_8 := F_8 \cdot d_8 = 194.829 \cdot kip \cdot in$

FRP Wings

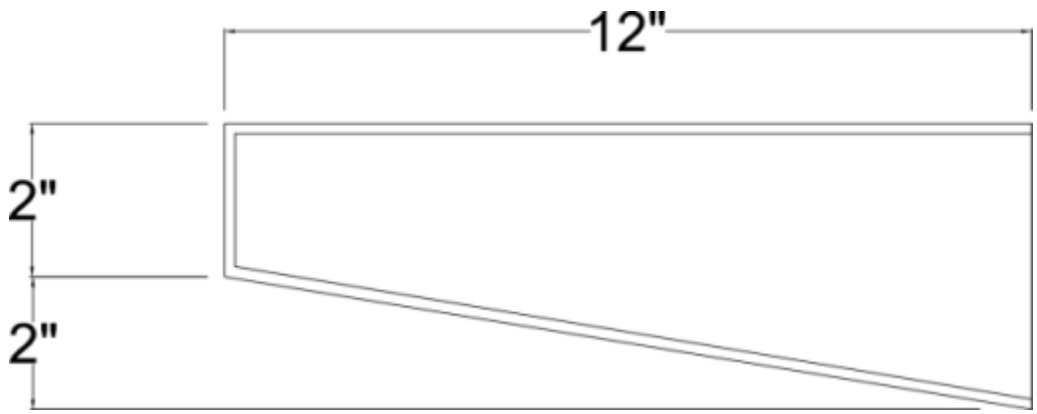

Approximate as 3 forces: Top layer, web, and treat bottom layer as horizontal layer at midheight

Slope: $Slope := \frac{\sigma_{21} - \sigma_{14}}{7in} = -0.193 \cdot \frac{ksi}{in}$ $\sigma_{20} := \sigma_{14} + 6in \cdot Slope = -0.982 \cdot ksi$

$t_{wing} := .106in$ $\sigma_{18} := \sigma_{14} + 4in \cdot Slope = -0.597 \cdot ksi$

Top Layer:

$y_{w1} := 21in$ $A_{w1} := 2 \cdot t_{wing} \cdot 12in = 2.544 \cdot in^2$ $F_{w1} := \sigma_{21} \cdot A_{w1} = -2.989 \cdot kip$

Web: Take average stress at height 20 inches

$y_{w2} := 20in$ $h_{w2} := 2in$ $A_{w2} := 2h_{w2} \cdot t_{wing} = 0.424 \cdot in^2$ $F_{w2} := \sigma_{20} \cdot A_{w2} = -0.416 \cdot kip$

Bottom Layer:

$y_{w3} := 18in$ $A_{w3} := 2 \cdot t_{wing} \cdot 12in = 2.544 \cdot in^2$ $F_{w3} := \sigma_{18} \cdot A_{w1} = -1.519 \cdot kip$

Wing Summary:

Force:	Centroid:	Distance from NA:	Moment:
$F_{w1} = -2.989 \cdot kip$	$y_{w1} = 21 \cdot in$	$d_{w1} := y_{bar} - y_{w1} = -6.1 \cdot in$	$M_{w1} := F_{w1} \cdot d_{w1} = 18.233 \cdot kip \cdot in$
$F_{w2} = -0.416 \cdot kip$	$y_{w2} = 20 \cdot in$	$d_{w2} := y_{bar} - y_{w2} = -5.1 \cdot in$	$M_{w2} := F_{w2} \cdot d_{w2} = 2.124 \cdot kip \cdot in$
$F_{w3} = -1.519 \cdot kip$	$y_{w3} = 18 \cdot in$	$d_{w3} := y_{bar} - y_{w3} = -3.1 \cdot in$	$M_{w3} := F_{w3} \cdot d_{w3} = 4.708 \cdot kip \cdot in$

FRP Total Forces

Internal Equilibrium:

$\Sigma F_{FRP} := F_1 + F_2 + F_3 + F_4 + F_5 + F_6 + F_7 + F_8 + F_{w1} + F_{w2} + F_{w3} = 1.835 \cdot kip$

Almost in equilibrium with self

Moment Provided:

$\Sigma M_{FRP} := M_1 + M_2 + M_3 + M_4 + M_5 + M_6 + M_7 + M_8 + M_{w1} + M_{w2} + M_{w3} = 312.834 \cdot kip \cdot in$

Concrete Arch Forces

$E_c := 4500ksi$ Width $w_c := 22in$ Height $h_c := 4in$

Strain Profile- extrapolated values

$\varepsilon_{c21} := -159.5$ $\sigma_{c21} := E_c \cdot \varepsilon_{c21} \cdot 10^{-6} = -0.718 \cdot ksi$

$\varepsilon_{c17} := -109.5$ $\sigma_{c17} := E_c \cdot \varepsilon_{c17} \cdot 10^{-6} = -0.493 \cdot ksi$

Have shapes that are a triangle and a rectangle

Rectangle: $y_{c1} := 19in$ $A_{c1} := \sigma_{c17} \cdot h_c = -1.971 \cdot \frac{kip}{in}$ $F_{c1} := A_{c1} \cdot w_c = -43.362 \cdot kip$

Triangle:

$y_{c2} := 21in - \frac{h_c}{3} = 19.667 \cdot in$ $A_{c2} := 0.5 \cdot h_c \cdot (\sigma_{c21} - \sigma_{c17}) = -0.45 \cdot \frac{kip}{in}$

$F_{c2} := A_{c2} \cdot w_c = -9.9 \cdot kip$

Concrete Totals

Force:	Centroid:	Distance from NA:	Moment:
$F_{c1} = -43.362 \cdot kip$	$y_{c1} = 19 \cdot in$	$d_{c1} := y_{bar} - y_{c1} = -4.1 \cdot in$	$M_{c1} := F_{c1} \cdot d_{c1} = 177.784 \cdot kip \cdot in$
$F_{c2} = -9.9 \cdot kip$	$y_{c2} = 19.667 \cdot in$	$d_{c2} := y_{bar} - y_{c2} = -4.767 \cdot in$	$M_{c2} := F_{c2} \cdot d_{c2} = 47.19 \cdot kip \cdot in$

Internal Force:

$\Sigma F_c := F_{c1} + F_{c2} = -53.262 \cdot kip$

Moment Provided:

$\Sigma M_c := M_{c1} + M_{c2} = 224.974 \cdot kip \cdot in$

Steel Strand

$E_s := 27500ksi$ $\varepsilon_s := 656$ $\sigma_s := \varepsilon_s \cdot 10^{-6} \cdot E_s = 18.04 \cdot ksi$

$A_s := 3.366in^2$ $y_s := 0.5in$

$F_s := A_s \cdot \sigma_s = 60.723 \cdot kip$ $M_s := F_s \cdot (y_{bar} - y_s) = 874.406 \cdot kip \cdot in$

Bending of Concrete Arch

$EI_{concrete} := 5.9kip \cdot in^2$ $\rho_c := \frac{h_c}{\varepsilon_{c21} - \varepsilon_{c17}}$ $M_{arch} := \frac{EI_{concrete}}{-\rho_c} = 73.75 \cdot kip \cdot in$

Sum Totals

Force Equilibrium:

$\Sigma F := \Sigma F_{FRP} + \Sigma F_c + F_s = 9.296 \cdot kip$

Total Moment:

$\Sigma M := \Sigma M_{FRP} + \Sigma M_c + M_s + M_{arch} = 1.486 \times 10^3 \cdot kip \cdot in$

Proportion of total moment:

Tied Arch: $\frac{\Sigma M_c + M_s}{\Sigma M} = 0.74$

Arch Bending: $\frac{M_{arch}}{\Sigma M} = 0.05$

FRP Shell: $\frac{\Sigma M_{FRP}}{\Sigma M} = 0.211$

Arch responsible for 80% of moment

$\Sigma M = 1.486 \times 10^3 \cdot kip \cdot in$ $M_{app} = 1.612 \times 10^3 \cdot kip \cdot in$ $\frac{\Sigma M}{M_{app}} = 0.922$

Attempt to locate unrecovered moment from foam:

$E_{foam} := 1.2ksi$

$\sigma_{14F} := \varepsilon_{14} \cdot 10^{-6} \cdot E_{foam} = 6.72 \times 10^{-5} \cdot ksi$

$\sigma_{7F} := \varepsilon_7 \cdot 10^{-6} \cdot E_{foam} = 4.188 \times 10^{-4} \cdot ksi$

$\sigma_{0F} := \varepsilon_0 \cdot 10^{-6} \cdot E_{foam} = 8.436 \times 10^{-4} \cdot ksi$

$F_{foam} := \sigma_{0F} \cdot w \cdot (h - y_{bar}) \cdot 0.5 = 0.062 \cdot kip$

Curvature Calculations

Curvature 1/ρ is equal to slope of strain profile

$\rho := \frac{21in}{\varepsilon_{21} - \varepsilon_0}$ $\frac{1}{\rho} = -51.524 \cdot \frac{1}{in}$

First: Plug in applied moment, calculate actual moment

$M_{test} := 1612kip \cdot in$

$\frac{1}{\rho} = \frac{M}{EI}$ $EI_{test} := M_{test} \cdot -\rho = 31.287 \cdot kip \cdot in^2$

Second: Plug in transformed section theoretical EI values, find resisting moment

$EI_{shell} := 6.21kip \cdot in^2$ $EI_{tiedarch} := 25.53kip \cdot in^2$ $EI_{concrete} := 5.9kip \cdot in^2$

All x10^6

$EI_{total} := EI_{shell} + EI_{tiedarch} = 31.74 \cdot kip \cdot in^2$ Very close to value calculated!

$M_{total} := \frac{EI_{total}}{-\rho} = 1.635 \times 10^3 \cdot kip \cdot in$ Very close to applied moment

Individual Pieces:

$M_{shell} := \frac{EI_{shell}}{-\rho} = 319.963 \cdot kip \cdot in$

Concrete arch has different curvature- not strain compatible

$\rho_c := \frac{h_c}{\varepsilon_{c21} - \varepsilon_{c17}}$

$\frac{1}{\rho_c} = -12.5 \cdot \frac{1}{in}$

$M_{arch} := \frac{EI_{concrete}}{-\rho_c} = 73.75 \cdot kip \cdot in$

just bending of concrete- strand has no moment capacity on own

Moment couple between concrete arch and steel strand- use steel strand force (calculation shown below as the force, moment arm of 19 in.

$F_s = 60.723 \cdot kip \quad d := 19in$

$M_{couple} := F_s \cdot d = 1.154 \times 10^3 \cdot kip \cdot in$

$\Sigma M := M_{shell} + M_{arch} + M_{couple} = 1.547 \times 10^3 \cdot kip \cdot in$

Arch component: $\frac{M_{arch} + M_{couple}}{\Sigma M} = 0.793$ Shell: $\frac{M_{shell}}{\Sigma M} = 0.207$

Sample Calculations- Composite Case

Stress Integration Analysis
Part 1- FRP
Strain Profile created from test to 150 kips total Applied moment: $M_{app} := 4524kip \cdot in$

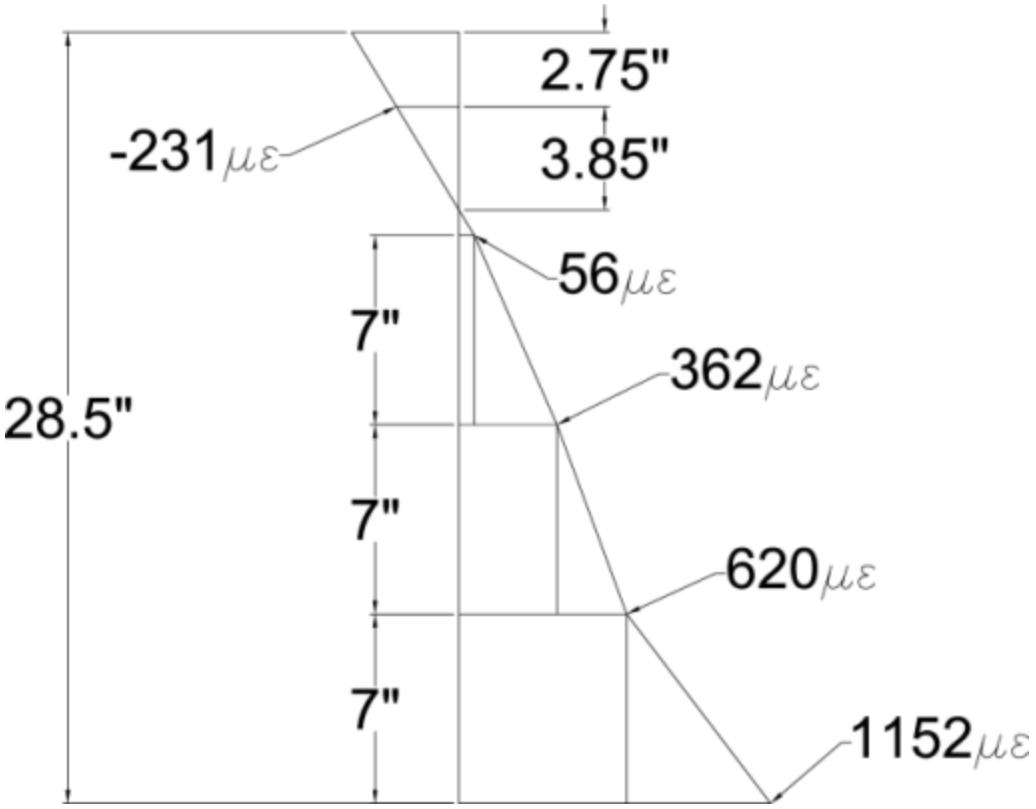

Material Properties

$E_{FRP} := 3100ksi$

Thicknesses:

$t_{top} := 0.32in$ $t_{bottom} := 0.25in$ $t_{web} := 0.11in$

Beam dimensions

$w := 24in$ $h := 21in$

First step: Transform strains into stresses

$\varepsilon_{21} := 56$ $\sigma_{21} := \varepsilon_{21} \cdot 10^{-6} \cdot E_{FRP} = 0.174 \cdot ksi$

$\varepsilon_{14} := 362$ $\sigma_{14} := \varepsilon_{14} \cdot 10^{-6} \cdot E_{FRP} = 1.122 \cdot ksi$

$\varepsilon_{7} := 620$ $\sigma_{7} := \varepsilon_{7} \cdot 10^{-6} \cdot E_{FRP} = 1.922 \cdot ksi$

$\varepsilon_{0} := 1152$ $\sigma_{0} := \varepsilon_{0} \cdot 10^{-6} \cdot E_{FRP} = 3.571 \cdot ksi$

Neutral Axis Location:

$y_{bar} := 21.9in$

Calculate Forces, working from top down

Force 1: Top Plate- No shape (all at one height)

$y_1 := 21in \qquad A_{top} := t_{top} \cdot w = 7.68 \cdot in^2 \qquad F_1 := A_{top} \cdot \sigma_{21} = 1.333 \cdot kip$

Force 2: Compressive Triangle and Rectangle

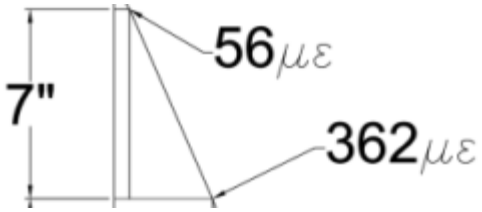

Triangle Centroid is at 2/3 of height

Triangle Height

$h_2 := 7in$

Shape Area $\qquad A_2 := h_2 \cdot (\sigma_{14} - \sigma_{21}) \cdot 0.5 = 3.32 \cdot \frac{kip}{in}$

Multiply Shape Area by Material Thickness- Factor of 2 due to 2 webs

$F_2 := A_2 \cdot 2 \cdot t_{web} = 0.73 \cdot kip \qquad y_2 := 14in + \frac{h_2}{3} = 16.333 \cdot in$

Force 3: Rectangle

Triangle Height

$h_3 := h_2 = 7 \cdot in$

Shape Area $\qquad A_3 := h_3 \cdot \sigma_{21} = 1.215 \cdot \frac{kip}{in}$

Multiply Shape Area by Material Thickness- Factor of 2 due to 2 webs

$F_3 := A_3 \cdot 2 \cdot t_{web} = 0.267 \cdot kip \qquad y_3 := 14in + \frac{h_3}{2} = 17.5 \cdot in$

Forces 4 and 5: Rectangle and Triangle between 7" and 14"

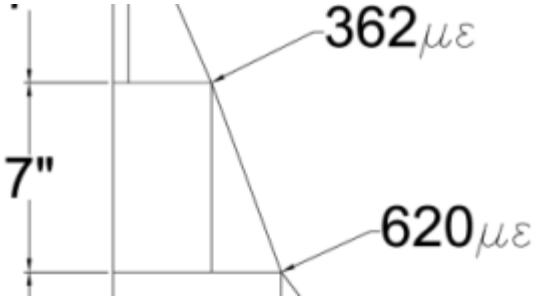

Rectangle:

$h_4 := 7in$ Shape Area: $A_4 := h_4 \cdot \sigma_{14} = 7.855 \cdot \frac{kip}{in}$

Multiply Shape Area by Material Thickness- Factor of 2 due to 2 webs

$F_4 := A_4 \cdot 2 \cdot t_{web} = 1.728 \cdot kip$ $y_4 := 14in - \frac{h_4}{2} = 10.5 \cdot in$

Triangle:

$h_5 := h_4 = 7 \cdot in$ Shape Area: $A_5 := h_5 \cdot (\sigma_7 - \sigma_{14}) \cdot 0.5 = 2.799 \cdot \frac{kip}{in}$

Multiply Shape Area by Material Thickness- Factor of 2 due to 2 webs

$F_5 := A_5 \cdot 2 \cdot t_{web} = 0.616 \cdot kip$ $y_5 := 14in - \frac{2h_5}{3} = 9.333 \cdot in$

Forces 6 and 7: Recatangle and Triangle between 0" and 7"

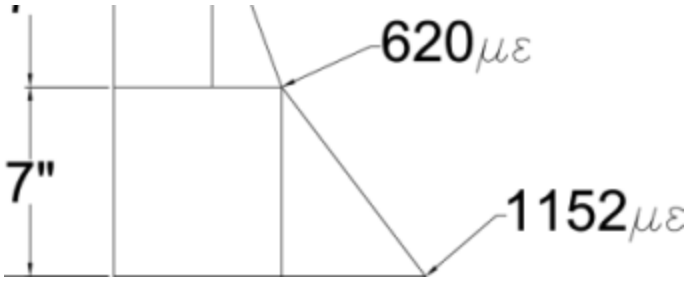

Rectangle:

$h_6 := 7in$ Shape Area: $A_6 := h_6 \cdot \sigma_7 = 13.454 \cdot \frac{kip}{in}$

Multiply Shape Area by Material Thickness- Factor of 2 due to 2 webs

$F_6 := A_6 \cdot 2 \cdot t_{web} = 2.96 \cdot kip$ $y_6 := \frac{h_6}{2} = 3.5 \cdot in$

Triangle:

$h_7 := h_6 = 7 \cdot in$ Shape Area: $A_7 := h_7 \cdot (\sigma_0 - \sigma_7) \cdot 0.5 = 5.772 \cdot \frac{kip}{in}$

Multiply Shape Area by Material Thickness- Factor of 2 due to 2 webs

$F_7 := A_7 \cdot 2 \cdot t_{web} = 1.27 \cdot kip$ $y_7 := \frac{h_7}{3} = 2.333 \cdot in$

Force 8: Bottom Web- No Shape

$y_8 := 0in$ $A_{bottom} := w \cdot t_{bottom} = 6 \cdot in^2$

$F_8 := \sigma_0 \cdot A_{bottom} = 21.427 \cdot kip$

Summary of Main FRP:

Force:	Centroid:	Distance from NA:	Moment:
$F_1 = 1.333 \cdot kip$	$y_1 = 21 \cdot in$	$d_1 := y_{bar} - y_1 = 0.9 \cdot in$	$M_1 := F_1 \cdot d_1 = 1.2 \cdot kip \cdot in$
$F_2 = 0.73 \cdot kip$	$y_2 = 16.333 \cdot in$	$d_2 := y_{bar} - y_2 = 5.567 \cdot in$	$M_2 := F_2 \cdot d_2 = 4.066 \cdot kip \cdot in$
$F_3 = 0.267 \cdot kip$	$y_3 = 17.5 \cdot in$	$d_3 := y_{bar} - y_3 = 4.4 \cdot in$	$M_3 := F_3 \cdot d_3 = 1.176 \cdot kip \cdot in$
$F_4 = 1.728 \cdot kip$	$y_4 = 10.5 \cdot in$	$d_4 := y_{bar} - y_4 = 11.4 \cdot in$	$M_4 := F_4 \cdot d_4 = 19.701 \cdot kip \cdot in$
$F_5 = 0.616 \cdot kip$	$y_5 = 9.333 \cdot in$	$d_5 := y_{bar} - y_5 = 12.567 \cdot in$	$M_5 := F_5 \cdot d_5 = 7.739 \cdot kip \cdot in$
$F_6 = 2.96 \cdot kip$	$y_6 = 3.5 \cdot in$	$d_6 := y_{bar} - y_6 = 18.4 \cdot in$	$M_6 := F_6 \cdot d_6 = 54.462 \cdot kip \cdot in$
$F_7 = 1.27 \cdot kip$	$y_7 = 2.333 \cdot in$	$d_7 := y_{bar} - y_7 = 19.567 \cdot in$	$M_7 := F_7 \cdot d_7 = 24.847 \cdot kip \cdot in$
$F_8 = 21.427 \cdot kip$	$y_8 = 0 \cdot in$	$d_8 := y_{bar} - y_8 = 21.9 \cdot in$	$M_8 := F_8 \cdot d_8 = 469.256 \cdot kip \cdot in$

FRP Wings

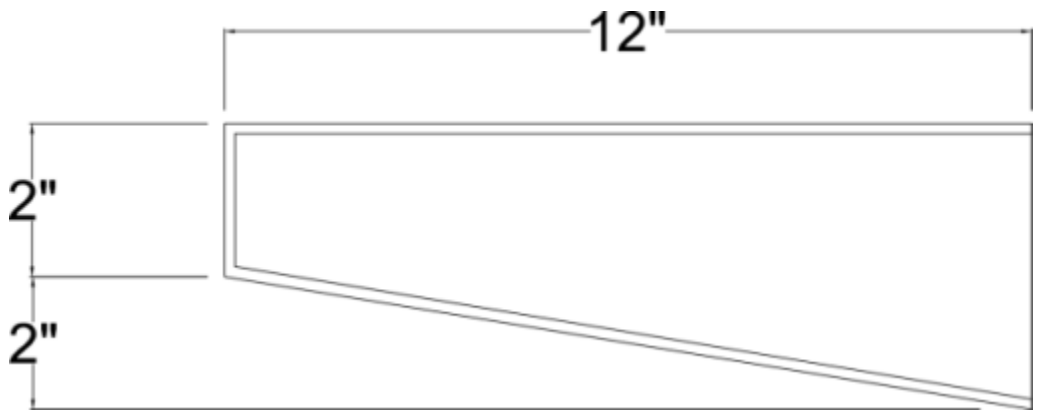

Approximate as 3 forces: Top layer, web, and treat bottom layer as horizontal layer at midheight

Slope: $\text{Slope} := \frac{\sigma_{21} - \sigma_{14}}{7\text{in}} = -0.136 \cdot \frac{\text{ksi}}{\text{in}}$ $\sigma_{20} := \sigma_{14} + 6\text{in} \cdot \text{Slope} = 0.309 \cdot \text{ksi}$

$t_{wing} := .106\text{in}$ $\sigma_{18} := \sigma_{14} + 4\text{in} \cdot \text{Slope} = 0.58 \cdot \text{ksi}$

Top Layer:

$y_{w1} := 21\text{in}$ $A_{w1} := 2 \cdot t_{wing} \cdot 12\text{in} = 2.544 \cdot \text{in}^2$ $F_{w1} := \sigma_{21} \cdot A_{w1} = 0.442 \cdot \text{kip}$

Web: Take average stress at height 20 inches

$y_{w2} := 20\text{in}$ $h_{w2} := 2\text{in}$ $A_{w2} := 2h_{w2} \cdot t_{wing} = 0.424 \cdot \text{in}^2$ $F_{w2} := \sigma_{20} \cdot A_{w2} = 0.131 \cdot \text{kip}$

Bottom Layer:

$y_{w3} := 18\text{in}$ $A_{w3} := 2 \cdot t_{wing} \cdot 12\text{in} = 2.544 \cdot \text{in}^2$ $F_{w3} := \sigma_{18} \cdot A_{w1} = 1.476 \cdot \text{kip}$

Wing Summary:

Force:	Centroid:	Distance from NA:	Moment:
$F_{w1} = 0.442 \cdot \text{kip}$	$y_{w1} = 21 \cdot \text{in}$	$d_{w1} := y_{bar} - y_{w1} = 0.9 \cdot \text{in}$	$M_{w1} := F_{w1} \cdot d_{w1} = 0.397 \cdot \text{kip} \cdot \text{in}$
$F_{w2} = 0.131 \cdot \text{kip}$	$y_{w2} = 20 \cdot \text{in}$	$d_{w2} := y_{bar} - y_{w2} = 1.9 \cdot \text{in}$	$M_{w2} := F_{w2} \cdot d_{w2} = 0.249 \cdot \text{kip} \cdot \text{in}$
$F_{w3} = 1.476 \cdot \text{kip}$	$y_{w3} = 18 \cdot \text{in}$	$d_{w3} := y_{bar} - y_{w3} = 3.9 \cdot \text{in}$	$M_{w3} := F_{w3} \cdot d_{w3} = 5.756 \cdot \text{kip} \cdot \text{in}$

FRP Total Forces

Internal Equilibrium:

$\Sigma F_{FRP} := F_1 + F_2 + F_3 + F_4 + F_5 + F_6 + F_7 + F_8 + F_{w1} + F_{w2} + F_{w3} = 32.381 \cdot kip$

Moment Provided:

$\Sigma M_{FRP} := M_1 + M_2 + M_3 + M_4 + M_5 + M_6 + M_7 + M_8 + M_{w1} + M_{w2} + M_{w3} = 588.85 \cdot kip \cdot in$

Concrete Deck Forces

$E_c := 4670ksi$ Width $w_c := 24in$ Height $h_c := 7.5in$

Strain Profile- extrapolated values

$\varepsilon_{c2575} := -231 \quad \varepsilon_{c21} := \varepsilon_{21} = 56 \quad slope := \frac{\varepsilon_{c2575} - \varepsilon_{c21}}{4.75in} = -60.421 \cdot \frac{1}{in}$

$\varepsilon_{c28.5} := \varepsilon_{c21} + 7.5in \cdot slope = -397.158$

$\sigma_{c21} := E_c \cdot \varepsilon_{c21} \cdot 10^{-6} = 0.262 \cdot ksi \quad \sigma_{c28.5} := E_c \cdot \varepsilon_{c28.5} \cdot 10^{-6} = -1.855 \cdot ksi$

Have two triangles: 1 tension, 1 compression

Tension:

$y_{c1} := 21in + \frac{y_{bar} - 21in}{3} = 21.3 \cdot in \quad h_{c1} := y_{bar} - 21in = 0.9 \cdot in \quad A_{c1} := 0.5 \sigma_{c21} \cdot h_{c1} = 0.118 \cdot \frac{kip}{in}$

$F_{c1} := A_{c1} \cdot w_c = 2.824 \cdot kip$

Compression:

$h_{c2} := 28.5in - y_{bar} = 6.6 \cdot in \quad A_{c2} := 0.5 \cdot h_{c2} \cdot (\sigma_{c28.5}) = -6.121 \cdot \frac{kip}{in}$

$y_{c2} := y_{bar} + \frac{2}{3} \cdot h_{c2} = 26.3 \cdot in \quad F_{c2} := A_{c2} \cdot w_c = -146.894 \cdot kip$

Concrete Totals

Force:	Centroid:	Distance from NA:	Moment:
$F_{c1} = 2.824 \cdot kip$	$y_{c1} = 21.3 \cdot in$	$d_{c1} := y_{bar} - y_{c1} = 0.6 \cdot in$	$M_{c1} := F_{c1} \cdot d_{c1} = 1.695 \cdot kip \cdot in$
$F_{c2} = -146.894 \cdot kip$	$y_{c2} = 26.3 \cdot in$	$d_{c2} := y_{bar} - y_{c2} = -4.4 \cdot in$	$M_{c2} := F_{c2} \cdot d_{c2} = 646.335 \cdot kip \cdot in$

Internal Force:

$\Sigma F_c := F_{c1} + F_{c2} = -144.07 \cdot kip$

Moment Provided:

$\Sigma M_c := M_{c1} + M_{c2} = 648.03 \cdot kip \cdot in$

Deck rebar: Use geometry to determine strain at lower bars

Lower bar height: $\varepsilon_{22.5} := \varepsilon_{c21} + slope \cdot 1.5in = -34.632$

$E_{rebar} := 29000ksi$

Top Row

$y_{r1} := 25.75in$

$\sigma_{r25.75} := E_{rebar} \cdot \varepsilon_{c2575} \cdot 10^{-6} = -6.699 \cdot ksi$

$A_{25.75} := 0.4in^2$ 2 bars

$F_{r1} := \sigma_{r25.75} \cdot A_{25.75} = -2.68 \cdot kip$

$d_{r1} := y_{r1} - y_{bar} = 3.85 \cdot in$

$M_{r1} := F_{r1} \cdot d_{r1} = -10.316 \cdot kip \cdot in$

$y_{r2} := 22.5in$

$\sigma_{r22.5} := \varepsilon_{22.5} \cdot E_{rebar} \cdot 10^{-6} = -1.004 \cdot ksi$

$A_{22.5} := 0.6in^2$ 3 bars

$F_{r2} := \sigma_{r22.5} \cdot A_{22.5} = -0.603 \cdot kip$

$d_{r2} := y_{r2} - y_{bar} = 0.6 \cdot in$

$M_{r2} := F_{r2} \cdot d_{r2} = -0.362 \cdot kip \cdot in$

Deck Totals:

Internal Force:

$\Sigma F_d := \Sigma F_c + F_{r1} + F_{r2} = -147.352 \cdot kip$

Moment Provided:

$\Sigma M_d := \Sigma M_c + M_{r1} + M_{r2} = 637.352 \cdot kip \cdot in$

Steel Strand

$E_s := 27500ksi$ $\varepsilon_s := 1039$ $\sigma_s := \varepsilon_s \cdot 10^{-6} \cdot E_s = 28.573 \cdot ksi$

$A_s := 3.366in^2$ $y_s := 0.5in$

$d_s := y_{bar} - y_s = 21.4 \cdot in$

$F_s := A_s \cdot \sigma_s = 96.175 \cdot kip$ $M_s := F_s \cdot d_s = 2.058 \times 10^3 \cdot kip \cdot in$

Sum Totals

Force Equilibrium:

$\Sigma F := \Sigma F_{FRP} + \Sigma F_d + F_s = -18.797 \cdot kip$

Total Moment:

$\Sigma M := \Sigma M_{FRP} + \Sigma M_d + M_s = 3.284 \times 10^3 \cdot kip \cdot in$

Proportion of total moment:

Strand: $\frac{M_s}{\Sigma M} = 0.627$

FRP Shell: $\frac{\Sigma M_{FRP}}{\Sigma M} = 0.179$

Deck: $\frac{\Sigma M_d}{\Sigma M} = 0.194$

Kind of odd to think of this way- rather, separate into moment couples between deck and steel/FRP

Find location of force by using centroid like equation

$y = \frac{\text{Force}\cdot\text{Distance}}{\text{Force}}$ Can use moments already found to get location of force with respect to neutral axis.

Location of deck force: $d_d := \frac{\Sigma M_d}{\Sigma F_d} = -4.325\cdot in$ Location of FRP Force: $d_{FRP} := \frac{\Sigma M_{FRP}}{\Sigma F_{FRP}} = 18.185\cdot in$

Steel couple contribution: $M_{steel} := F_s\cdot(d_s - d_d) = 2.474 \times 10^3\cdot kip\cdot in$

FRP couple contribution: $M_{FRP} := \Sigma F_{FRP}\cdot(d_{FRP} - d_d) = 728.908\cdot kip\cdot in$

$\Sigma M := M_{steel} + M_{FRP} = 3.203 \times 10^3\cdot kip\cdot in$

Also have bending of deck and FRP

Determine using curvature-

From spreadsheet $EI_{FRP} := 11.1 kip\cdot in^2$ $EI_d := 10.6 kip\cdot in^2$

Deck Component:
Curvature 1/ρ is equal to slope of strain profile

$\rho := \frac{4.75in}{\varepsilon_{c2575} - \varepsilon_{21}}$ $\frac{1}{\rho} = -60.421\cdot\frac{1}{in}$

$\frac{1}{\rho} = \frac{M}{EI}$ $M_{deck} := -EI_d\cdot\frac{1}{\rho} = 640.463\cdot kip\cdot in$

FRP Component:

$\rho := \frac{21in}{\varepsilon_{21} - \varepsilon_0}$ $\frac{1}{\rho} = -52.19\cdot\frac{1}{in}$

$M_{FRPb} := -EI_{FRP}\cdot\frac{1}{\rho} = 579.314\cdot kip\cdot in$

Total moment recovered from beam:

$M_{total} := \Sigma M + M_{deck} + M_{FRPb} = 4.423 \times 10^3\cdot kip\cdot in$ $\frac{M_{total}}{M_{app}} = 0.978$

$M_{app} = 4.524 \times 10^3\cdot kip\cdot in$ Good moment recovery

Proportions:

Beam: $\frac{\Sigma M + M_{FRPb}}{M_{total}} = 0.855$ Deck: $\frac{M_{deck}}{M_{total}} = 0.145$ Deck carries 15% of applied in bending and must provide axial force for internal equilibrium

Of which: Steel: $\frac{M_{steel}}{M_{total}} = 0.559$

FRP: $\frac{M_{FRP} + M_{FRPb}}{M_{total}} = 0.296$

Curvature Calculations

Curvature 1/ρ is equal to slope of strain profile

$$\rho := \frac{4.75in}{\varepsilon_{c2575} - \varepsilon_{21}} \qquad \frac{1}{\rho} = -60.421 \cdot \frac{1}{in}$$

First: Plug in applied moment, calculate actual moment

$$M_{test} := 4524kip \cdot in$$

$$\frac{1}{\rho} = \frac{M}{EI} \qquad EI_{test} := M_{test} \cdot -\rho = 74.875 \cdot kip \cdot in^2$$

Second: Plug in transformed section theoretical EI values, find resisting moment

$$EI_{total} := 63.17kip \cdot in^2$$

$$M_{total} := \frac{EI_{total}}{-\rho} = 3.817 \times 10^3 \cdot kip \cdot in \qquad M_{app} = 4.524 \times 10^3 \cdot kip \cdot in$$

Not as accurate as during noncomposite case